2006

Experimental and Analytical Investigation of Inertial Propulsion Mechanisms and Motion Simulation of Rigid-Multi-Body Mechanical Systems

Mohammed Almesallmy
University of Rhode Island

EXPERIMENTAL AND ANALYTICAL INVESTIGATION OF INERTIAL PROPULSION MECHANISMS AND MOTION SIMULATION OF RIGID-MULTI-BODY MECHANICAL SYSTEMS.

BY

MOHAMMED ALMESALLMY

A DISSERTATION SUBMITTED IN PARTIAL FULFILLMENT OF THE REQUIREMENTS FOR THE DEGREE OF

DOCTOR OF PHILOSOPHY

IN

MECHANICAL ENGINEERING AND APPLIED MECHANICS

UNIVERSITY OF RHODE ISLAND

2006

DOCTOR OF PHILOSOPHY DISSERTATION

OF

MOHAMMED ALMESALLMY

APPROVED:

Dissertation Committee:

Major Professor

DEAN OF THE GRADUATE SCHOOL

UNIVERSITY OF RHODE ISALND

2006

ABSTRACT

Methodologies are developed for dynamic analysis of mechanical systems with emphasis on inertial propulsion systems. This work adopted the Lagrangian methodology. Lagrangian methodology is the most efficient classical computational technique, which we call Equations of Motion Code (EOMC). The EOMC is applied to several simple dynamic mechanical systems for easier understanding of the method and to aid other investigators in developing equations of motion of any dynamic system. In addition, it is applied to a rigid multibody system, such as Thornson IPS [Thornson 1986]. Furthermore, a simple symbolic algorithm is developed using Maple software, which can be used to convert any nonlinear n-order ordinary differential equation (ODE) systems into 1^{st}-order ODE system in ready format to be used in Matlab software.

A side issue, but equally important, we have started corresponding with the U.S. Patent office to persuade them that patent applications, claiming gross linear motion based on inertial propulsion systems should be automatically rejected. The precedent is rejection of patent applications involving perpetual motion machines.

ACKNOWLEDGMENTS

Professor Philip Datseris, with unlimited appreciation and respect, I would like to let you know that I will miss you. When you are tired and rest on the leather chair in your office, please ask yourself 'why was Mohammed so good to me!!' Thank you dear doctor forever.

I am indebted to my friends and colleagues in Mechanical Engineering and Applied Mechanics department. Thank you to Ahmed Fadl for his unlimited support. Thank you to Deborah Osborn for her guidance while teaching my first course. Thank you to all students in Dr. Shukla's Lab. for their kindness, and friendly support.

I would like to thank Jim Byrnes on his electronic circuitry, and his humble, supportive and friendly personality. Jim, thank you so much.

The assistance and inspiration I received from Donna and, Kathy is greatly acknowledged. Thank you, you make our department lovely.

I extend great gratitude to the faculty at URI with whom I have interacted throughout the years.

To Mom, and Dad, no words reward your love, care, and prayers for me.

To my lovely wife and children: Ahmed, Shrief, and Mustafa, I greatly appreciate your patience, love, and support during the years of my study toward this Ph.D. Degree.

Mohammed Almesallmy

PREFACE

Since the beginning of the last century and until the present time, almost all the patented devices in the inertia propulsion field were built with the belief that centrifugal forces can cause "Gross Motion" (the system center of mass is in unidirectional motion). Chapter 1 reviews some of the previous work since 1912. Over fifty patents have been granted to inventors in the inertial propulsion field, but unfortunately, this technology has not yet been exploited for commercial use [Thomas Valone 1993]. This was one of the initial reasons of this study. Chapter 1 includes experimental work, measurement techniques, and devices, developed to investigate the existence of the inertia forces due to rotating bodies. In addition, chapter 1 includes the experimental technique, which is used to define the phase angle between the angular position of a body, and the corresponding position of its inertial force. Where, the position of a body is the line passing by both of the center of rotation and the center mass of this body. It concludes that the rotational arm and the angular displacement are the two parameters influencing both the magnitude and direction of the dynamic system's linear motion respectively. However, this conclusion is modified in Chapter 2.

In the design field, dynamic simulations are required to answer many questions with regard to motion and joint forces between components of a mechanical system. Dynamic simulation requires either developing the mathematical model for the system under investigation or knowledge of one of the commercial mechanical analysis software.

In Chapter 2, an algorithm (EOMC) is developed in Maple software based on 'Lagrange's equations,' to develop the equations of motion of mechanical systems. In addition, three examples are included to show the use of this algorithm. Therefore, any investigator can use the EOMC to develop the mathematical model (equations of motion) of a mechanism under investigation. Furthermore, examples of the code, which is used to simulate the motion are also provided. This code is numerically solved (integrated) with Runge-Kutta method in Matlab software.

In Chapter 3, we simulate and analyze in detail one of the most promising new inertial propulsion systems (IPS), which is Thornson IPS [Thornson 1986].

The computational method used in this work is systematic and reliable, once the four parameters (T, V, F, Q) of the mechanical system are defined, where, T, and V, are the kinetic and the potential energies of the system respectively, F is the dissipative forces (i.e Rayleigh function) of the system, and Q represents external forces on the system. Furthermore, this method enables the investigators to develop the equations of motion symbolically. It is a good tool to verify the correctness of commercial dynamic analysis software. The only drawback of this computational method (versus the virtual commercial dynamic analysis software) is that one must provide the correct four parameters T, V, F, Q as they are explained in Chapters 2, and 3.

TABLE OF CONTENTS

LIST OF FIGURES

CHAPTER I: EXPERIMENTAL AND ANALYTICAL INVESTIGATION OF INERTIAL PROPULSION SYSTEMS

I.1. Introduction to Rotating Devices

Engines, shafts, propellers, testing machines, CNC machines, washing machines, tires, and many toys all are examples of applications that include rotating masses. With the exception of some toys, rotating masses are not the direct cause of motion. For example, balanced spinning tires of a car placed on a lift will never cause the car to leave the lift. What could happen if the tires are not balanced?

Almost all rotating parts are designed to be inherently balanced in a dynamic system by applying the dynamic balance ($\sum F = 0$, and $\sum M = 0$) Figure 1 [Norton 1999]. Balancing procedures are well established and when they are applied correctly all shaking forces (static balance) and shaking moments are eliminated [Wilson 1967]. A balanced system results in high performance and reasonable life service. Balancing procedures involve measuring accurately the amount and location of any imbalance and compensating by adding or removing material in or from the correct location(s) respectively.

Unfortunately, the service life can be terminated prematurely due to any unbalanced condition. Some examples of these unbalanced conditions could be changes of the weight distribution along the rotating shaft, firing disorder in the engine, twisted or damaged blades in the propeller or the turbine, etc.

Most research in this area involves elimination of the unbalanced masses and unbalanced service conditions from rotating machines. Sometimes it is impossible to eliminate these shaking forces and the design must account for them. For example, these shaking forces exist when the space ship takes off. Therefore, Vibrating Shaking Tables Figures 2, 3 [Victor 1995] were developed to simulate the effects of shaking forces on space ships.

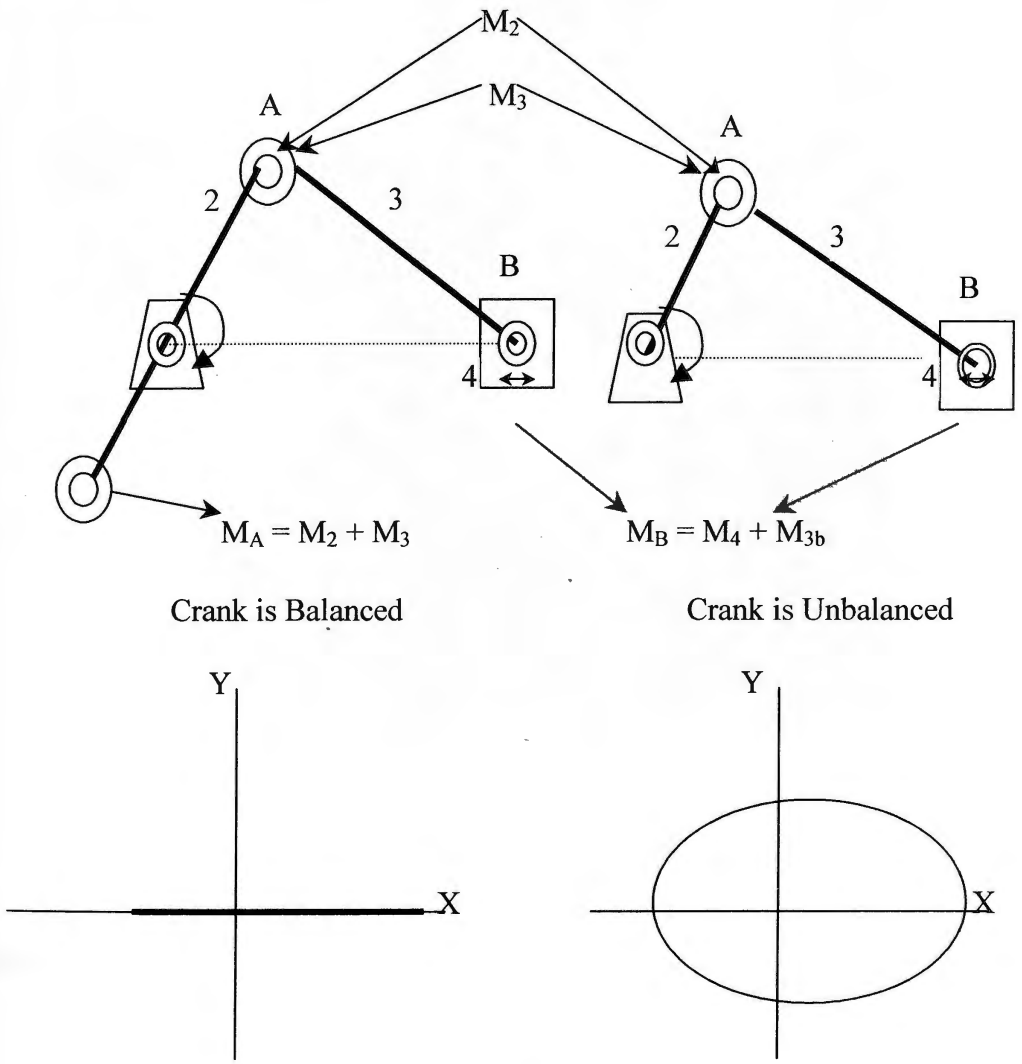

Figure 1 – Two Balanced Conditions of the Slider Crank Assembly

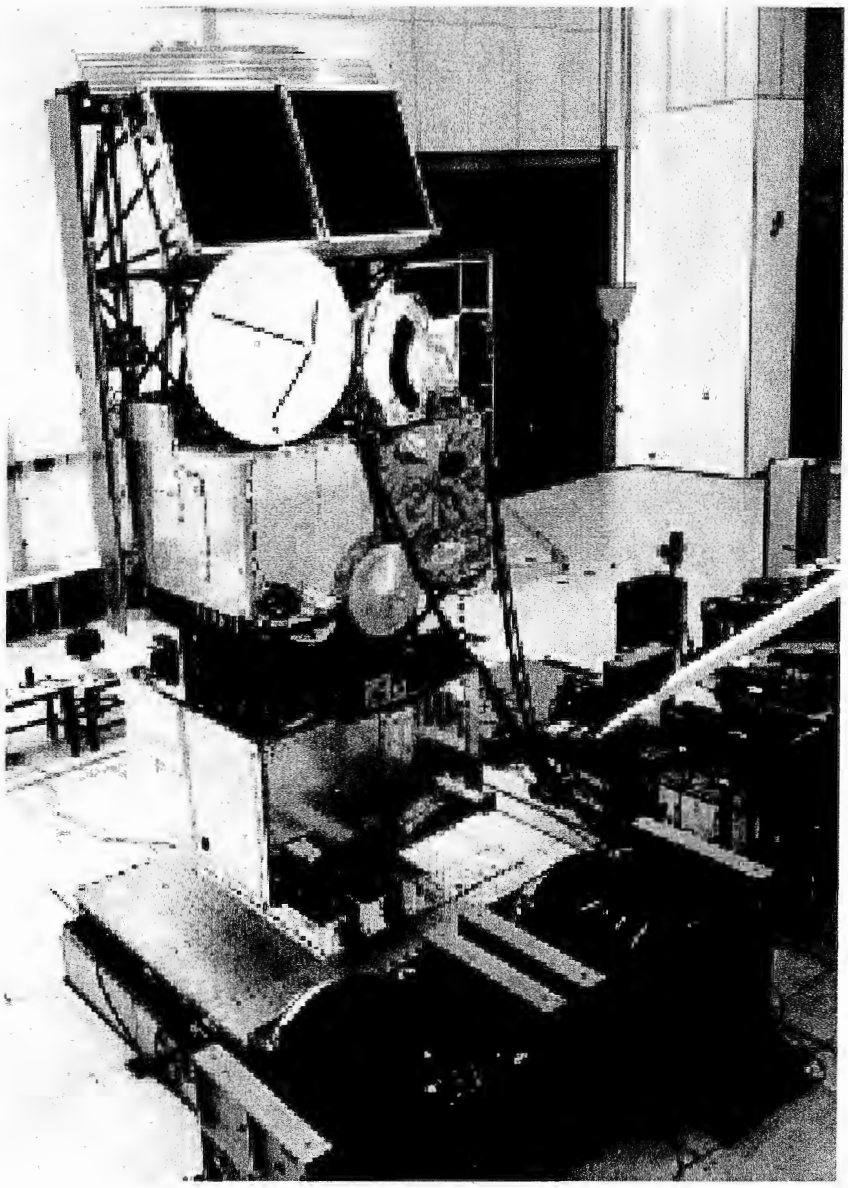

Figure 2 – Structural model of the ERS-I spacecraft undergoing lateral vibration tests on the electro-dynamic multi-shaker, see website (1)

Double head expander

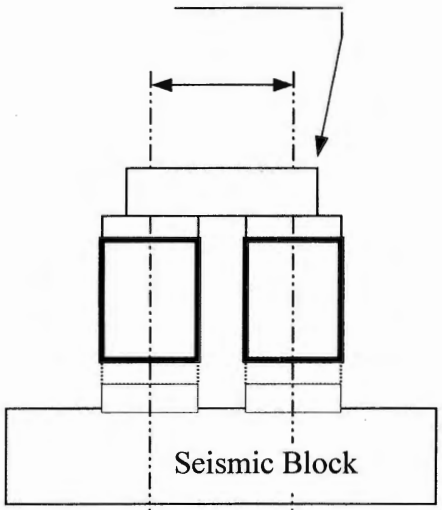

Vertical configuration with the dual head expander, side view

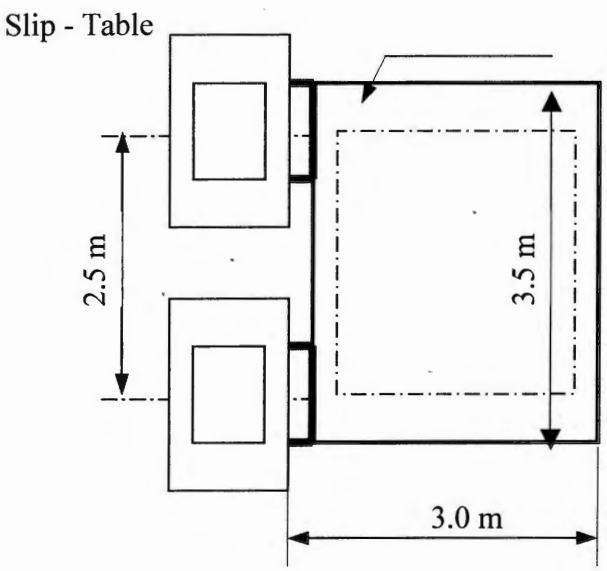

Horizontal configuration with slip table, top view

Figure 3- Multi-Shaker Configuration, see website (1)

In this work, investigations are conducted to find out if these types of forces can be utilized to provide useful work. Review of previous work shows that since 1912, over fifty patents have been granted to inventors in the inertial propulsion field. Unfortunately, this technology has not yet been exploited for commercial use [Thomas Valone 1993]. The mechanisms of patents by Cuff C (1976), by Thornson (1983), by Bristow (1992) are investigated in chapter two of this work. Simulations showed that these mechanisms could deliver] vibratory motion only.

Since the beginning of the last century, almost all the patented devices in the inertia propulsion field were built with the belief that centrifugal forces can cause linear motion. Therefore, one of the goals of this work is to define the dynamic term(s), which can cause unidirectional linear motion in rotating devices. In order to accomplish this, three main tasks will be completed:

The first task is to design a simple mass-rotating device that is shown in Figure 4 in order to investigate the generated forces associated with the rotating unbalanced masses from a novel viewpoint to determine if these forces can be utilized for propulsion or unidirectional linear motion. Also, this device is used to accomplish two other major tasks.

The second task is composed of two steps. The first step is to generate and to quantify forces generated by eccentric rotation of masses. The second step is to determine the exact direction of these generated forces as function of the angular position of these masses with respect to the testing machine's loading train axis.

The third task is to test the interactions and effects of these forces on the device's motion.

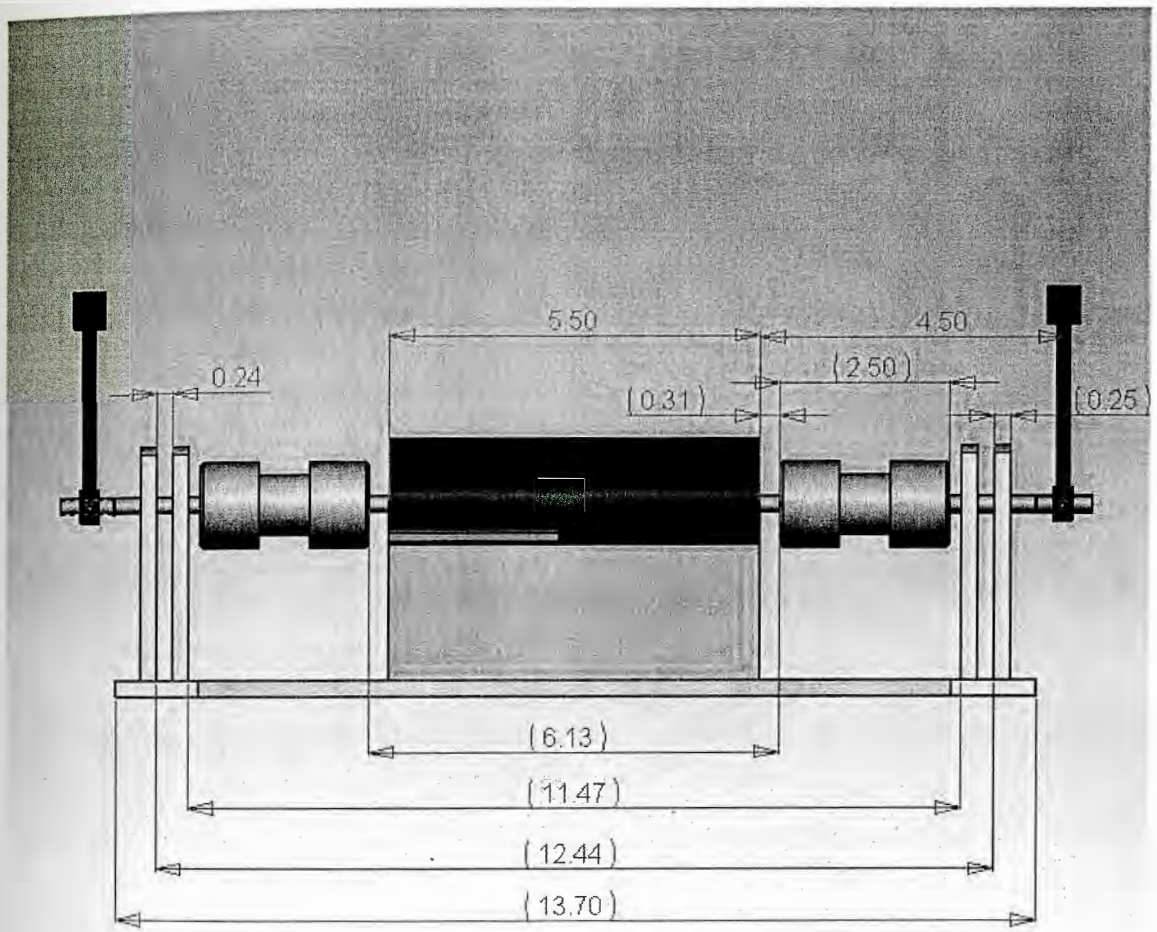

Figure 4 – Eccentric mass device is composed of an electric motor, motor shaft, two couplings, two rotating arms with one mass on each, and the supporting structure. Supporting structure is composed of two longitudinal beams, four transverse brackets, one motor mounting plate, and the base plate. All dimensions are in inches.

ITEM NO.	QTY.	PART NO.	DESCRIPTION
1	1	Base_Plate	Aluminum # 6061
2	2	Beam	Aluminum # 6061
3	1	Motor_Mounting	Done
4	1	Motor	Done
5	2	Loaded_Shaft	Carbon Steel 1035 cold rolled
6	2	Coupling	A 5C 5-1808
7	4	Bearing_Bracket	Aluminum # 6061
8	4	AFBMA 12,2 - 0.2500 - 0.5000 - 0.1250 - 12,DE,NC,12	S9912Y - E2550 PS1G
9	1	Shaft	Done
10	2	Arm	(Aluminum), with a 1 lb Weight
11	2	LW 0.25	Regular L W
12	4	HNUT 0.2500-20-D-S	Steel

Item Number
Quantity

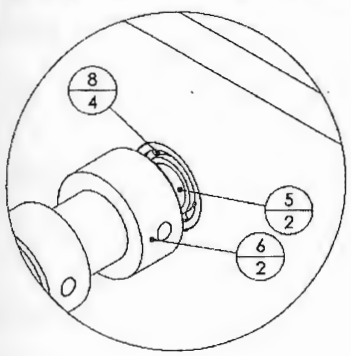

A (2 : 1)

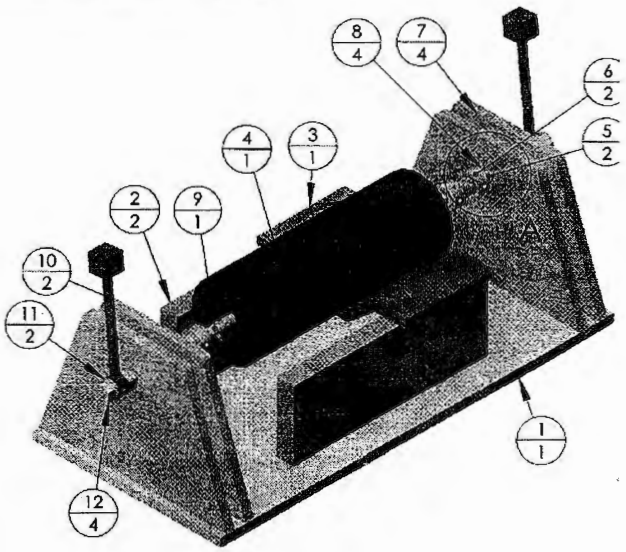

Figure 5 – Shows the Eccentric Mass Rotating Device with its Material Table. It is composed of an electric motor 4, motor shaft 9, two couplings 6, two rotating arms (radius of rotation) 10 with one mass on each, and the supporting structure. Supporting structure is composed of two longitudinal beams 2, four transverse brackets 7, motor's mounting plate 3, and the base plate 1.

I.1.1. Specifications of the Rotating Device

To investigate the exerted forces due to the rotation of masses, the 'eccentric mass device' shown in Figure 4 is designed to provide rotational motion of eccentric masses. This device consists of one motor, two couplings, two rotating shafts, two adjustable arms, two weights, four transverse brackets with ball bearings each, two longitudinal brackets, and the base plate. Upon running the electric motor, a rotational motion is transferred to the two rotating shafts through the two couplings. The two rotating shafts in turn drive the two masses, where the center gravity of these masses have radius of rotation 'r' from the axis of rotation of the rotating shaft.

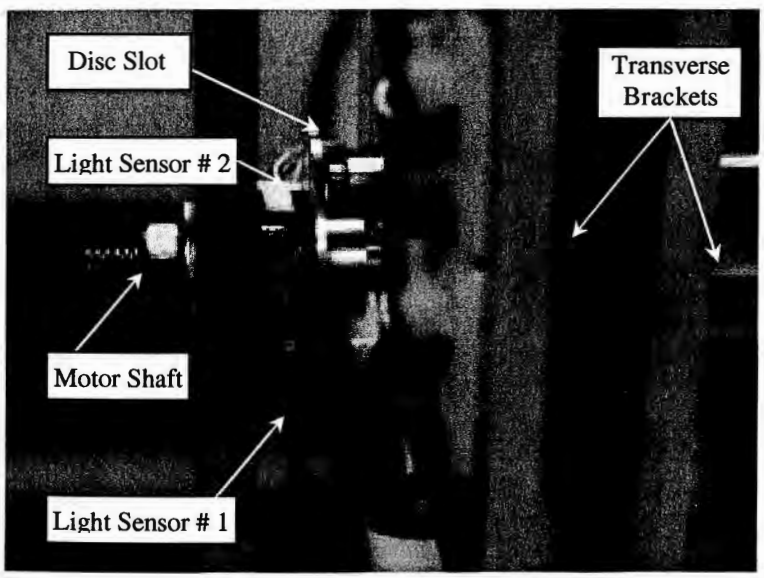

Figure 6 – Shows Two Light Sensors with U-shape; One is Mounted to be Parallel to the Machine Loading Train Centerline while the Other One is at 90° in the Vertical Plane from the First Sensor; a Circular Disc with a Rectangular Slot along its Radial Line is Mounted on the Motor Shaft.

To determine the exact position of the generated forces, a sensor-system shown in Figure 6 is mounted on the device shown in Figure 4. This system is composed of two infrared sensors, a disc with a slot, and an electronic circuit (see Figure 22). The slotted disc is mounted on the free end of one of the two rotating shafts where the slot was aligned with both masses. The two infrared sensors are mounted at 90° from each other on the transverse bracket where the slotted disc is free to run across the sensors' infrared light beam. One of the two sensors is positioned parallel to the axis of the testing machine's loading train. This position permits the sensor to send its signal when the rotating masses are parallel to the axis of this loading train. However, each sensor is in a U shape where the light beam can travel from the emitter side to the receiver side. The receiver converts the light beam into voltage signal. This voltage signal will be permitted only when the slot in the slotted disc reaches the infrared beam. Furthermore, the voltage electronic signals coming out of the two sensors are sent to the electronic circuit. The electronic circuit in turn amplifies and shapes the signal respectively (see III.3.2). The output signals are displayed on and recorded through one channel with an oscilloscope (Tektronix TDS 340A). The oscilloscope's adding channel is adjusted to show and record two signals. The first signal is from the light sensors and the second signal is from a load transducer.

The rotation of the eccentric masses will cause a repeated dynamic loading on each of the rotating shafts. Therefore, a reasonable service life of the rotating shaft, which could carry the effects of these eccentric masses, is a crucial matter.

It is felt that this issue should be addressed to insure that a system which has eccentric masses can be designed for infinite life under expected cyclic loading. Therefore, this work will provide design procedures of the structure, which supports the shafts and the eccentric rotating masses.

I.1.2 Design Procedures of the Rotating Device

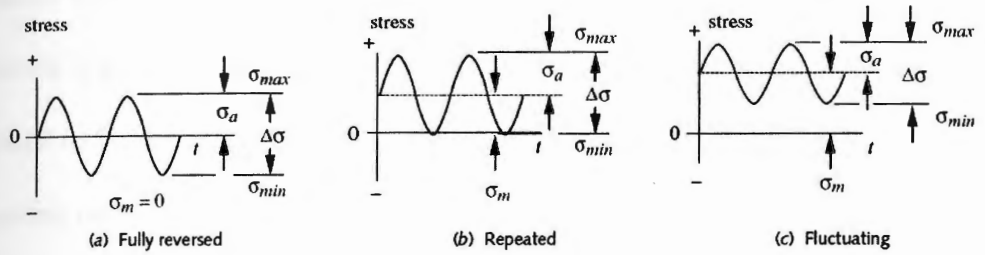

Figure 7 – Shows the three sinusoidal stress-time functions rotating machinery can experience [Norton 2000].

The device to be designed can be classified as one of the rotating machinery type, where the characters of the loading-time functions, waveform, are always defined as sinusoidal – or sawtooth wave and not random. Sinusoidal loading can be classified as fully reversed, repeated, and fluctuating, Figure 7 [Norton 2000]. Therefore, upon defining a specific sinusoidal loading and during the early stage of designing this type of machinery, the prediction of the service life will be always close to the actual service life.

Design procedures of the rotating device follow four major steps. The first step is to choose the proper preventive fatigue criteria model. The second step is to estimate the maximum possible dynamic load, which a ¼ inch diameter motor shaft can carry. The third step is to select a motor. The fourth step is to design a frame structure. This structure should be able to support both of the dead weights of the motor and the eccentric masses, and the life load of the exerted dynamic load due to the mass rotation. Furthermore, deflection should be maintained below 0.001 inch. The importance of the deflection minimization is not only to assure a proper mechanical running operation but also to assure that the rotation plane of the eccentric load is approximately parallel to the loading train axis of the testing machine.

I.2. Previous Work

A number of rotating devices will be investigated to determine if claims of unidirectional motion can be proven. These devices have been patented. In addition, other researchers in the field have investigated the motion of these patented devices. Some of these patents are listed below and in the reference section.

I.2.1. Summary of Patents

1. Laskowitze Device (U.S. Patent No. 1,953,964) on Apr. 10 1934.

2. Laskowitze Device (U.S. Patent No. 2,009,780) on July 30, 1935.
3. Halvorson et al Davice (U.S. Patent No. 3,530,617) on Sept. 29, 1970.
4. Cuff Device (U.S. Patent No. 3,968,700) on July 13, 1976.
5. Cook Device (U.S. Patent No. 4,238,968) on Dec. 16, 1980.
6. Thornson Device (U.S. Patent No. 4,631,971) on Dec. 30, 1986.
7. T. Valone papers in 1991, 1993, and 1994.
8. Bristow Device (U.S. Patent No. 5,156,058) on Oct. 20, 1992

I.2.2. Brief Review of Several Patents

I.2.2.1 Laskowitz (U.S. Patent No. 1,953,964)

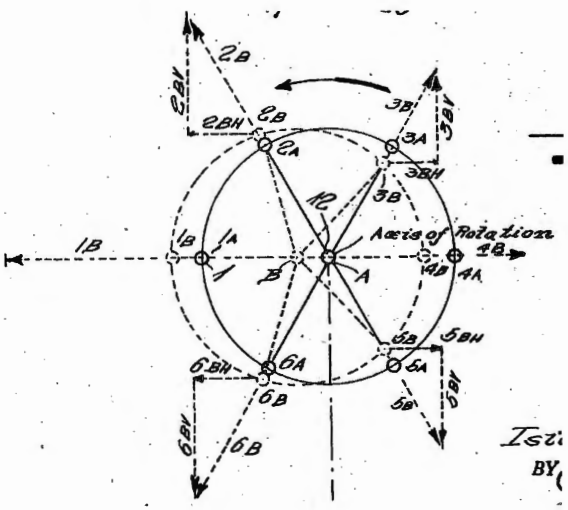

Figure 8 – A diagrammatic view shows the normal and displaced positions of the six weights 1A to 6A with its generated force components, which in turn provide the predicted thrust in the direction of arrow 1B.

Laskowitz invented a centrifugal variable thrust mechanism wherein the principle of centrifugal force is utilized and which is capable of developing a thrust, as he claimed. However, the centrifugal or propelling driving force will be *entirely independent* of the medium upon or through which the vehicle travels.

Figure 8 shows when the axis of rotation of the equal six weights positioned in 1A to 6A is positioned at "A", the weights are all spaced at equal distances from the axis of rotation "A" and consequently, the centrifugal force set up in each weight is the same. The forces are all in equilibrium and no unbalanced resultant thrust is set up. However, by shifting the axis of the rotation from position "A" to position "B", it will be observed that the weights have assumed new positions as indicated by the dotted lines and when in this last mentioned position, the radial distances of the weights from the axis of rotation "A" vary. The result is that when the weights are rotated, different centrifugal forces are set up in the weights and an unbalanced resultant thrust "R" in the direction shown by the arrows in Figure 8 is set up, tending to move the mechanism and which resultant may be utilized as a propelling force.

I.2.2.2. Halvorson (U.S. Patent No. 3,530,617)

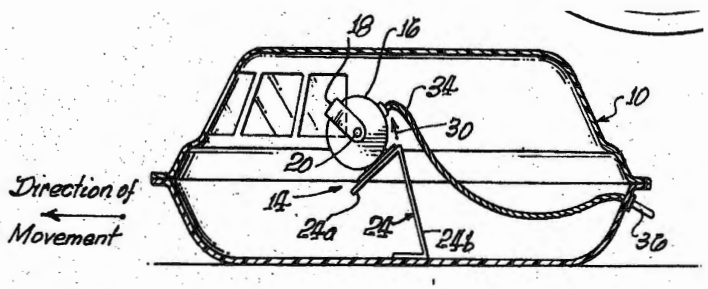

Figure 9– The vehicle where a drive means is enclosed therein

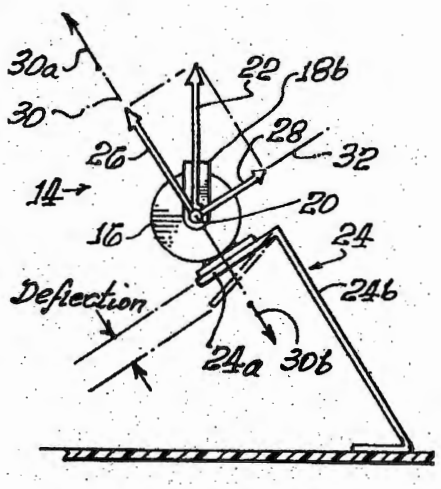

Figure 10 – The Drive Means Consists of Motor 16, Unbalanced Rotational Weight 18b, Short Spring 24a with a Natural Frequency Close to the Motor Rotating Frequency, and Long Spring 24b with Natural Frequency far from the Motor's Operating Frequency.

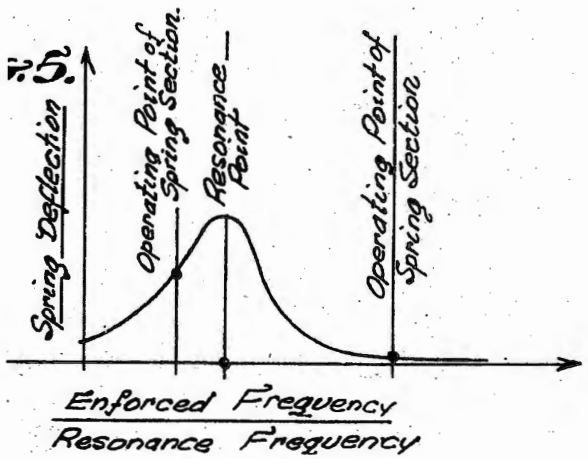

Figure 11 – Deflection response of the spring to the enforced normalized springs frequency (motor frequency / spring natural frequency)

Halvorson designed a toy vehicle shown in Figures 9, and 10 which includes an upper disk housing 10 rigidly attached to a lower disk-shaped housing 12, having a flat bottom surface and a drive means 14 totally enclosed therein and rigidly attached to the floor of housing 12. The drive means 14 comprises a DC motor 16, with two unbalanced weights 18a and 18b eccentrically mounted on both ends of its horizontal drive shaft 20 for symmetry. When the drive shaft 20 rotates, weights 18a and 18b rotate in a vertical plane and due to their rotation, produce a centrifugal force 22 as shown in Figure 10 also rotating in a vertical plane. The DC motor 16 is rigidly attached to the short section 24a of an L-shaped leaf spring 24 and is forward-downward inclined in direction 32a-32b, whereas the base of the long section 24b is rigidly attached to the floor of the vehicle structure in a forward-upward inclined direction 30a – 30b.

Referring to Figure 10, section 24a and 24b of spring 24 are shown to be perpendicular to each other. As indicated in Figure 10, force vector 22 rotating at motor frequency, can be divided into two oscillating force components, in this case in a force component 26 perpendicular to spring section 24a and a force component 28 perpendicular to spring section 24b. The force components acting upon the respective spring sections tend to deflect them in a reciprocating motion at the oscillating frequency of the component, which is also the motor frequency, enforced vibration frequency. Thus, the vibrating system has two principal directions of vibration. In this invention, each spring section has its own resonance frequency.

Figure 11 shows that if the enforced frequency is below or close to resonance frequency, very large spring deflection results. Whereas, if the enforced frequency is above and far removed from the resonance frequency, very small or nearly zero deflection occurs. Therefore, the short sections 24a and 24a are designed to operate at the points indicated in Figure 11. It shows that the motor frequency, enforced frequency, is close to the resonance frequency of spring 24a, and too large compared to the resonance frequency of spring 24b.

However, considerable force is imposed upon the vehicle structure by the vibration of spring section 24a. The vertically pulsating force in direction 30a produced by spring 24a, is the propulsive force. Vehicle weight and friction force between the vehicle bottom surface and the ground overcome the force in other direction during the weight's rotation.

I.2.2.3. Cuff's Device (U.S. Patent No. 3,968,700)

Cuff believed that the shown device is able to produce motion in the shown direction 13 in Figure 12. The invention converts the centrifugal forces produced by the rotating masses 8a, 8b,.., 8h into a propulsive force acting in one direction which is perpendicular to the plane of rotating masses. Propulsive force is due to the continuously variation of the radius of gyration of each mass during its cycle of revolution. Cuff's invention produces an unbalanced centrifugal force by varying the radius of rotation of rotating masses at predetermined moments in their cycle of revolution by means of an eccentrically disposed circular member.

The path of rotation of the rotating masses contains certain predetermined sectors in which each rotating mass attains a maximum radial distance and then, after 180° more of rotation, a minimum radial of distance.

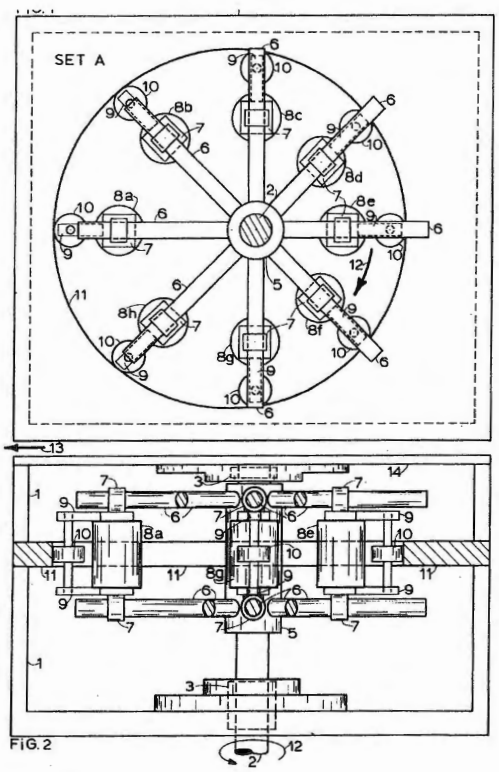

Figure 12 – The top drawing shows the top plan of eight identical sets of revolving masses and their components. The lower drawing is a cross section of the device showing its side view, the motor rotational direction, and the direction of motion due to the predicted thrust in arrow 13.

The position of that predetermined sector in which the rotating masses attain their maximum radial distance corresponds to the direction of travel and that predetermined sector in which the rotating masses attain their minimum

radial distance corresponds to the direction that is opposed to the desired direction of travel. The rotating masses and the eccentrically disposed circular members are arranged in such a manner that those rotating masses which, at a given moment are producing centrifugal-force components in the direction opposed to the desired direction of travel are either positioned at, or just approaching, or just leaving the minimum-radial-distance predetermined sector, and those rotating masses which, at a given moment, are producing centrifugal-force components in the desired direction of travel are either positioned at or just approaching, or just leaving the maximum-radial distance predetermined sector; this results in an unbalanced centrifugal force in the direction of the maximum-radial-distance predetermined sector.

I.2.2.4. Thornson's Device (U.S. Patent No.4,631,971):

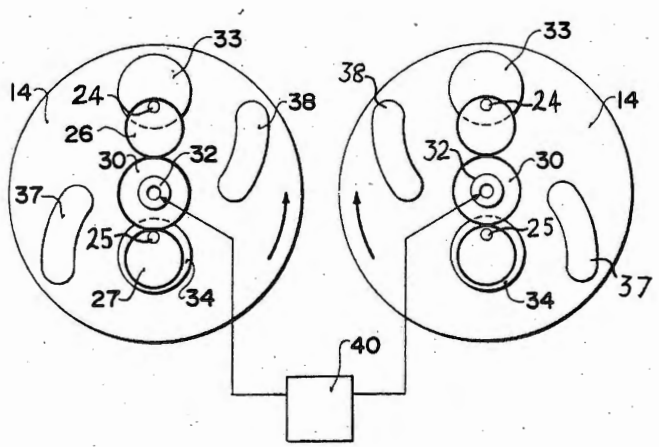

Figure 13– Thornson's device; cross sectional view along the line 1-1 of Figure 14 showing two rotateble bodies associated into a complete apparatus.

The device shown in Figure 13 from US Patent Number 4,631,971 is symmetric with the exception of two masses 33, and 34 which are free to rotate about pivot points 24, and 25, respectively. Thornson claims that the eccentric masses (33, and 34) will provide a propulsion force as described below from his patent. It comprises two symmetrical wheels 14 mounted in the same plane for rotation about parallel axes at right angles to the plane and driven synchronously

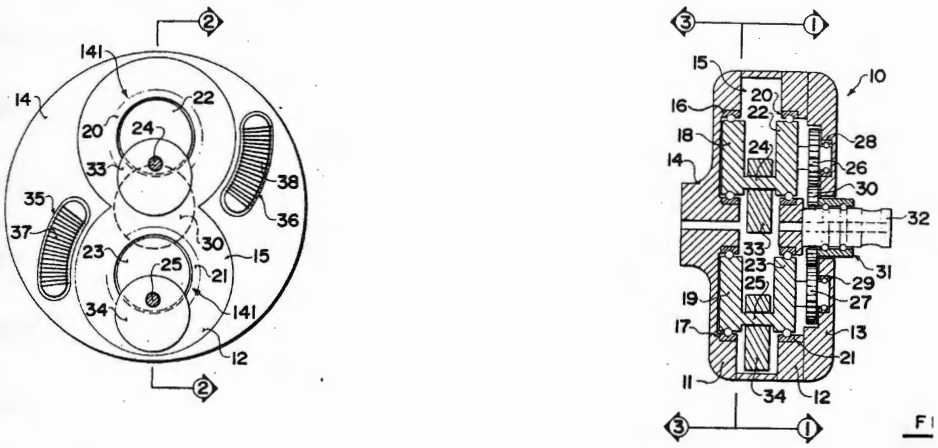

Figure 14 – The left hand side is one rotateble body. The right hand side is the cross section along the lines 2 – 2.

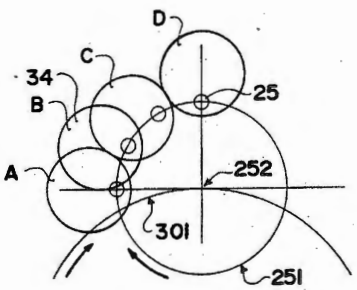

Figure 15 – Thornson's device; schematic illustration of the motion of one of the planet masses 34 delayed due to magnetic action at position A, at position C it is free to swing outwardly about the pin 25. The whip-like motion of the planet mass, mass 34, when it becomes free from the magnet produces the pulling force.

in opposite directions. Figure 14 shows that each wheel carries a pair of gearwheels 26, and 27, which rotate around the axis of the wheel with the wheel and support eccentrically a pair of planet masses 33, and 34. The masses are arranged such that their distance from the axis of rotation of the wheel increases and decreases under control of the gearwheels. At a position immediately prior to the maximum distance of the planet from the axis, electromagnetic devices 37, and 38 restrain outward movement of the planet mass so that when released the planet mass provides whip-like action inducing a resultant force in a direction at a right angles to the plane containing the axes of the wheel, according to Thornson. For example, Figure 14 shows four positions of mass 34 indicated respectively at "A", which is the immediate position prior to the maximum distance through "D". Where D is the position of mass 34 at the maximum spacing distance. It should be noted that the positions "B" and "C" are inhibited inwardly of their normal positions so that the center of mass of the planet 34 in the positions "B" and "C" are no longer on the radius joining the rotation axis and the pivot axis 25. In addition, the inhibiting means preferably is arranged on the body for rotation therewith and uses electromagnetic forces to restrain the movement of the planet mass. In addition the positioning of the electromagnetic restraining device is such that the planet mass is released immediately prior to its position of maximum spacing from the first axis so that it provides a whip-like action while traveling at its maximum velocity.

I.3. Inertia Force Measurement and Its Effects on the Device's Motion

In this section, the dynamic inertia force will be measured experimentally. This measure is accomplished with the shown layout In Figure 16. It shows the device with the two eccentric rotating masses attached to an Instron machine. In addition, the effects of this dynamic force on the device motion will be experimentally tested with the layout shown in Figure 25.

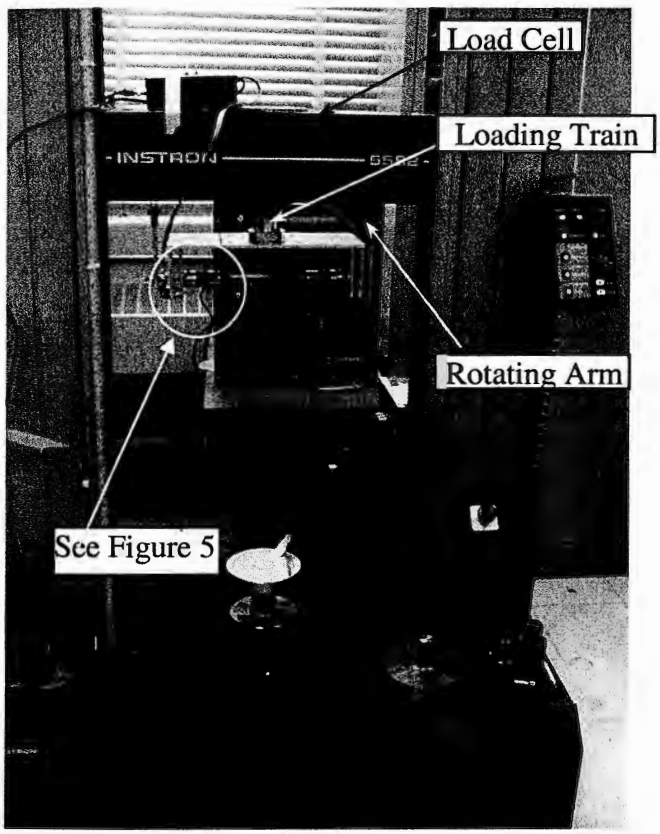

Figure 16 – The Eccentric Mass Rotating Device is Mounted along the Centerline of the Loading Train of the Automated Testing Machine. The Rotating Arms are Positioned Parallel to the Centerline of the Loading Train.

I.3.1 Testing Procedures

Testing procedures involve three steps, which are:

1- Mounting the rotating mechanism on the automated testing machine as shown in Figure 16. Zeroing the system of the Instron machine so that the weights of the loading train and the rotating mechanism are ignored when the data acquisition records the load cell output signals to a file.

2- Writing a simple 'dynamic load program' to utilize the data acquisition of the testing machine to collect data from the load cell in a file. Instantaneously, this data also will be sent through one of the external channels located in the automated testing machine to an oscilloscope.

3- The oscilloscope is prepared to add and record data signals from the testing machine and light sensors instantaneously. The oscilloscope adding signal feature channel is activated to add the two signals. The save and record procedures are followed to record them in a numerical file.

I.3.2 Measuring the Centrifugal Force (CF)

This section investigates the measurement of CF in two different conditions. The first condition is when the point of application of the CF is stationary and the second when the point of application of the CF is permitted to move.

I.3.2.1 Condition # 1: Measuring the Centrifugal Force – No Linear Motion

In this test the device is attached to the Instron machine, and therefore the device does not move, no linear motion.

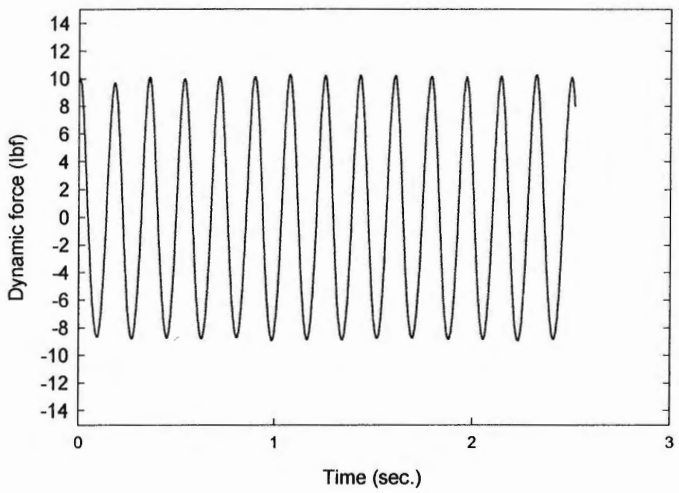

Figure 17 – The exerted dynamic load in (Ib) measured with the automated testing machine's load cell versus the testing time increments in seconds

The two eccentric masses are machined of four thin discs with a centered hole in each. The weight of each set of discs is obtained with a sensitive digital scale and is found to be about 0.15 Ib. Each set of discs is mounted on an arm with a distance of 6.5 inches between the geometry centers of the discs to the geometry centerline of the motor shaft. The weight of each arm is found to be about 0.125 Ib.

The load cell in the automated testing machine measures the magnitudes or the components of forces acting in or parallel to the centerline of the loading train axis (see Figure 16). Therefore, The load cell will sense and read the maximum magnitude of the exerted forces by the rotating masses when the angle between the rotating arms and the loading train axis is zero or a multiple of 180°. The testing machine is programmed to run in displacement mode and the displacement magnitude is programmed to be very small. This will provide no linear motion of the device during the dynamic test. The output file is programmed to obtain load signals versus the time increments every 2.0 milliseconds. Figure 17 shows that the dynamic load, F_m , fluctuate between '-9' and '+10' Ib with 5.5 cycles per second or 330.0 rpm.

The Measured Force, F_m , output results are then, as follows:

$\omega = 5.5$ rps

$F_m = (-9.0)$ to $(+10.0)$ Ib.

The Estimated Force, F_c , is calculated using the well-known centrifugal force equation, as follows:

$$F_c = \sum_1^{Ns} (m_i * r_i * \omega_i^2)$$

$$= ((W_1/g) * r_1 * \omega_1^2 + (W_2/g) * r_2 * \omega_2^2) * N_s$$

$$= ([\omega_1 / g] * [(W_1 * r_1 + W_2 * r_2)]) * N_s \quad (\text{where, } \omega_1 = \omega_2)$$

$$= [(5.5 * 2pi)^2 / (32*12)] * [(0.152 * (7.25/2) + 0.15 * 6.5)] * 2$$

$$\approx 9.45 \text{ Ib.}$$

Where

$m_i \equiv$ the rotating element mass in slugs

$_i \equiv$ an index to indicate the rotating element number

$W_1 \equiv$ the weight of each aluminum arm in Ib.

$W_2 \equiv$ the weight of each two thin discs in Ib.

$r_1 \equiv$ distance between the mass center of the arm and the centerline of the motor shaft in inch.

$r_2 \equiv$ distance between the mass center of the discs and the centerline of the motor shaft in inch

$g \equiv$ gravitational acceleration = 32 ft/sec^2

$N_s \equiv$ the number of rotating sets, one arm and two discs

Results show that *the exerted dynamic force is the centrifugal force*, when the device is mounted on the Instron machine and has no linear motion.

I.3.2.2 Condition # 2: Measuring the Centrifugal Force – With Linear motion.

It has been concluded that the rotating eccentric devices exert centrifugal forces on the stationary testing machine, but *if the machine becomes free to move what will be the exerted force on it by a rotating eccentric device*? A model shown in Figure 18 is developed using Working Model (WM) software to perform the simulation. The test performed on the Instron machine is simulated and forces should be the same as those along the X-axis. Forces measured along

the Y-axis, when the carriage is permitted to move, have not been obtained experimentally.

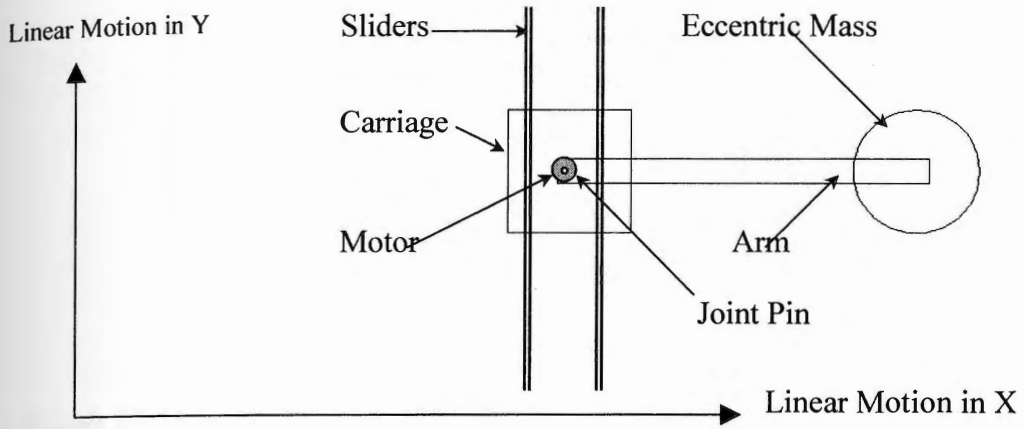

Figure 18 – In Working Model, a model of a rotating mass is developed to investigate the force on the joint pin due to the rotating eccentric mass. Forces are measured at the pin joint in both X and Y -axis; the carriage cannot not move along the X-axis but guides permit the carriage to move along the Y-axis

Parameters are chosen to be the same in both experimental and computer simulations, as follows:

(a) a weight of 0.3 Ibs to simulate the weight of the four eccentric discs

(b) one rotating arm of 7.4 in length and 0.302 Ibs weight to simulate the two rotating arms in the device.

(c) a motor which rotates with 5.5 rps (330 rpm)

Figure 19 shows the maximum WM's output force of 9.3 Ib is almost equal to the experimentally measured force of 9.5 Ibs. when using an Instron

testing machine. This small error of 2% is possibly due to speed variation during testing. Therefore, WM is sufficiently accurate.

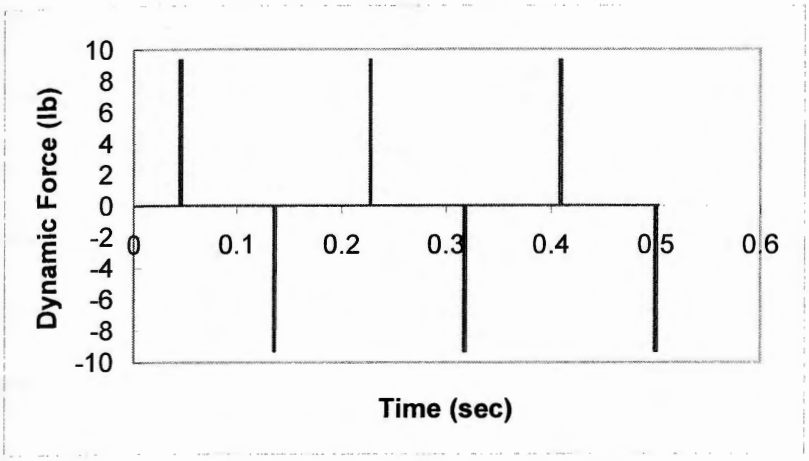

Figure 19 – Exerted dynamic force along the X-axis; measurement is made only when the center of gravity of eccentric mass is in the horizontal plane.

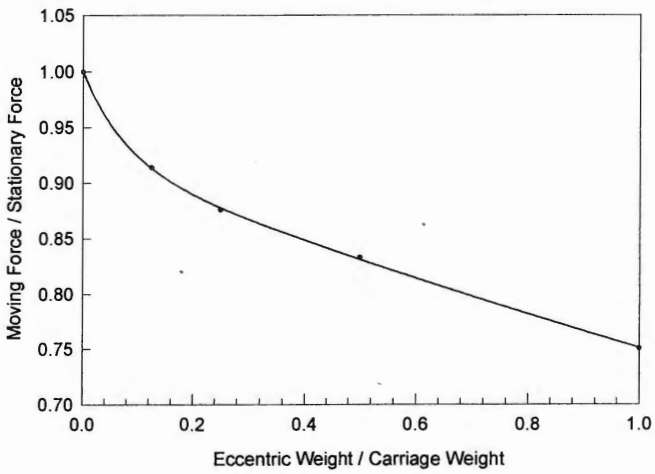

Figure 20 –The normalized eccentric weight – Y- force relationship at pin joint shows that the force along the Y-axis at the pin is varying between 100 to 75 % of the stationary force as function of the normalized weight.

The rotating device is now permitted to have linear motion along the Y-axis. The goal of this simulation is to find out the effects of the rotating device on the

movable machine. This is done by measuring the forces at the joint, see pin joint in Figure 18. For different rotational speeds, the model in Figure 18 is used to find out the corresponding exerted dynamic force on the pin joint as a function of different weight ratios of the eccentric weight to the carriage weight. Figure 20 shows the relationship plot of the ratio of the eccentric weight to the carriage weight versus the normalized measured applied force along the Y-axis, along which the carriage is free to move.

The output result in Figure 20 shows that the force at the joint pin decreases as the ratio of the eccentric weight to the carriage weight decreases and vice versa. This can be also interpreted as follows; as the carriage weight increases then the required force to move it from a stationary mode to a motion mode will be higher until it reaches its maximum which is the stationary CF.

It should be mentioned that eccentric weight is normally very small compared to the carriage weight. Then in Figure 20, a machine based on the principle of unbalanced rotating masses should operate at weight ratios magnitudes close to zero and take almost full advantage of CF. It is also important to note that a the load at the pin joint has a sinusoidal profile, see *Figure 17.* In other words, in these systems, *the force at the pin joint fully reverses and its magnitude corresponds to the weight ratio, eccentric weight to carriage weight, as shown in Figure 20.*

I.3.3 Identifying the Angular position of the Exerted Inertia Forces

The angular position of the maximum exerted inertia force, centrifugal force, with respect to the initial angular position of the eccentric mass is determined by using the sensors shown in Figures 6, and 16. Figure 21 shows the schematic diagram of the device components with respect to the Instron machine. It shows that the arms of the rotating eccentric masses and one of the two light sensors are placed in line with the loading train while the second sensor is placed with 90^{o} from the first sensor.

The first signal is from the load cell in the testing machine, and the second signal is from the infrared sensors. These signals are sent to an oscilloscope as shown in Figure 22. However, the test preparation to achieve these two signals is composed of the following three steps:

Step #1: Automated Testing Machine Signal Preparation.

Step # 2: The Infrared Sensor's Signal preparation.

Step # 3: The Oscilloscope Preparation.

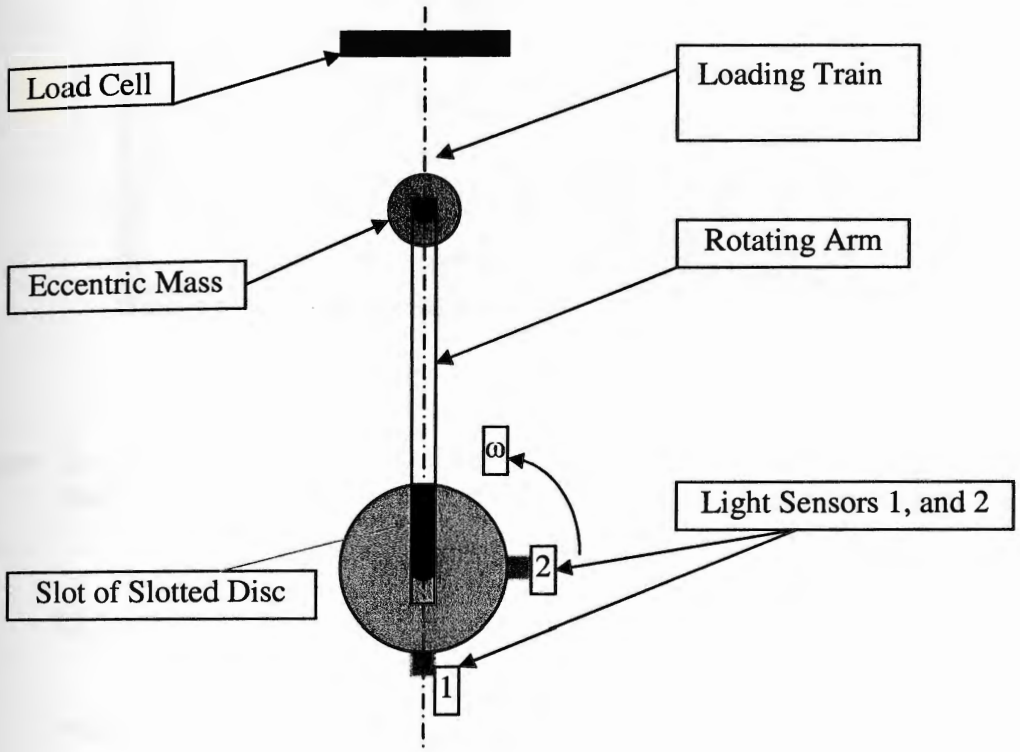

Figure 21 – Schematic diagram showing the layout of the slotted disk, light sensors, and the eccentric mass with respect to the machine loading train centerline at the initial condition. The eccentric mass, the slotted disc and the arm rotate in the arrow direction; the load cell, the loading train centerline, and the two sensors are stationary.

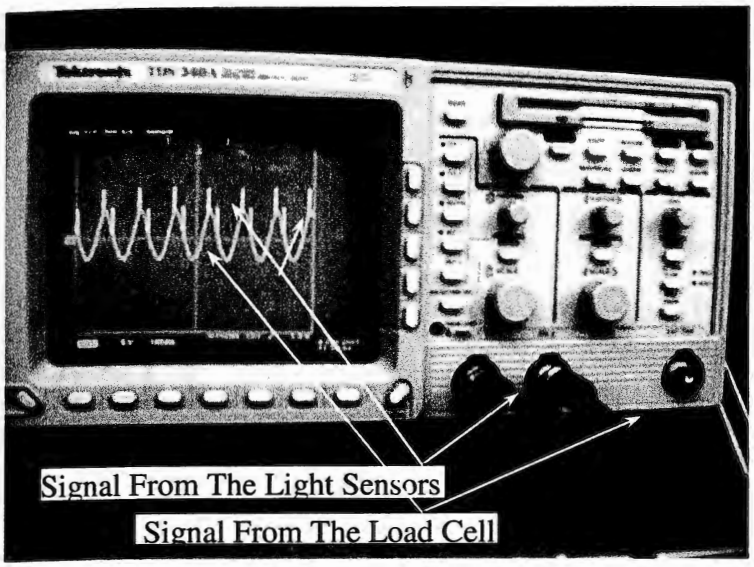

Figure 22 – The Oscilloscope receives the Two Signals from the Loading Cell and the Light Sensors. The screen shows the sum of the Two Signals.

I.3.3.1 Step #1: Automated Testing Machine Signal Preparation

The automated testing machine is programmed to perform as follows:

1. Its movable head moves under the displacement control with 0.1 in/hr.
2. Its data acquisition collects one sample every 2.0 millisecond.
3. The sample is composed of the outputs of the load cell and the computer registrar clock.
4. One of its analog output channel (Y1 or number 3) is activated to receive the load cell output signal.
5. After attaching the rotating device in the automated testing machine, the load cell reads the weight of the attached device. Therefore, before running the test

to measure only the force due to the rotating eccentric mass, the load cell is zeroed.

I.3.3.2 Step # 2: The Infrared Sensor's Signal preparation

As mentioned earlier that the two U-shape, see Figure, infrared sensors are positioned 90^{o} apart, as shown in Figure 21. The circular plate with a rectangular slot is mounted on the motor shaft to run through the two sensors. In addition, this slot is *aligned* with the rotating arm, which carries the unbalanced masses as shown in Figure 21.

In this arrangement, a sensor signal exits only in two positions during every one full cycle of the eccentric masses as shown in Figure 21. One position is when the eccentric masses are in the vertical position and the disc's slot reaches 'sensor 1'. The other position is when the eccentric masses are in the horizontal position and the disc's slot reaches 'sensor 2'. The magnitude and the duration of the output signal of these sensors are also preconditioned with an electronic circuit shown in Figure 23. It shows an amplifier LM348, A/D converter C4093, and Multivibrator (CD4047BC) are connected to the light sensors outputs to provide a usable signal to the oscilloscope. The amplifier is used to increase the output voltage of the sensors to 5.0 V. The 5.0 volt analog signal is send to the A/D converter to change the analog signal to digital signal. The Monostable/Unstable Multivibrator is used to shape the digital signal. The original shape of the sensors' output signal which is converted to Analog signal is a step function with a period of time equal to the elapsed period of time which required to pass the gab

in the disc through the sensors. However, the Multivibrator is operated in a Monostable mode where the step signal width shape can be decreased to a spike shape, see Figure 22, to represent the start at which the gap reaches the light sensors.

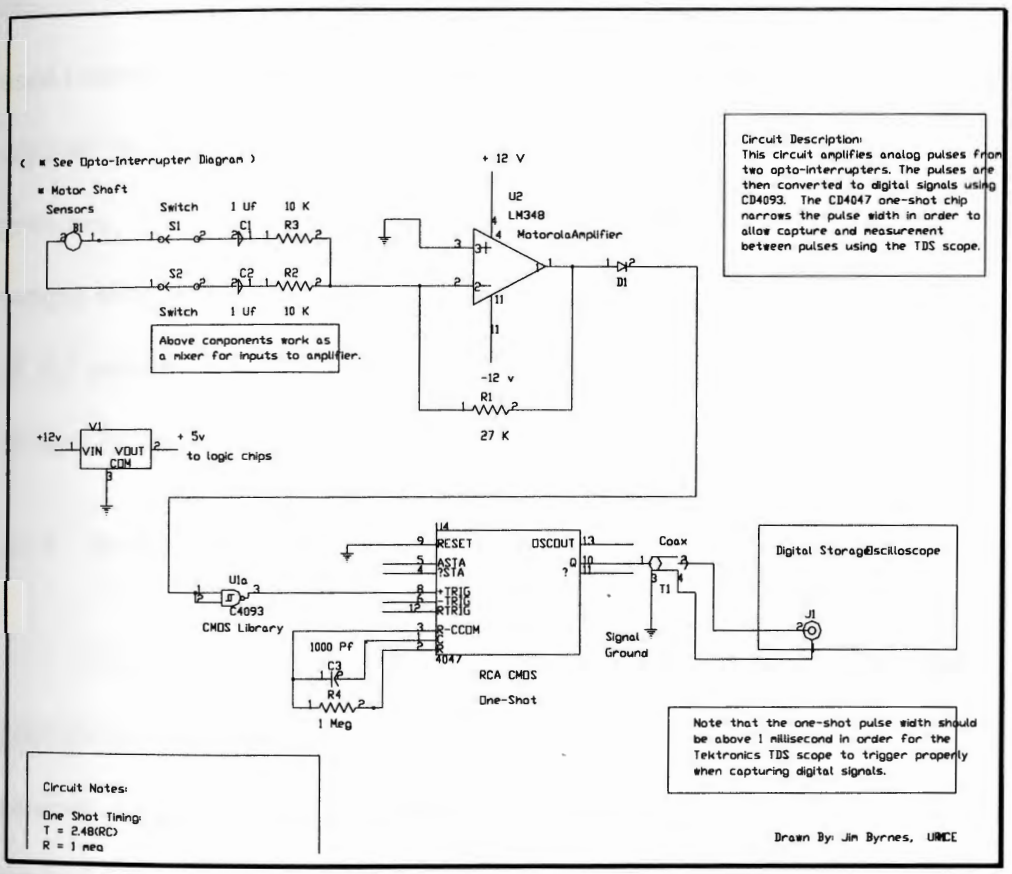

Figure 23 – Electronic Circuit Amplifies the magnitude and Changes the Shape of the output signal of the light sensors from a step to a spike shape signal.

I.3.3.3 Step #3: The Oscilloscope Preparation

The TekTronix TDS 340A oscilloscope has two input channels, one math channel, and two reference channels waveform. The two oscilloscope's input channels are connected to the two output digital signals which are coming from the testing machine, and the output signals of the infrared sensors. The math channel is used to add the two incoming signals. One of the reference channels is used to store the "live" math waveform. The magnitude scale of all the channels is adjusted to 5-voltage in the y-axis between every two consecutive horizontal gridlines. The horizontal scale is adjusted to sample 500 points per second, 1.0 sample every 2 milliseconds, for a maximum period of 2.0 seconds in the x-axis of the screen. The stored reference channel is saved on a floppy disc and re-plotted, as shown in Figure 24.

I.3.4 Inertia Force and Sensor Signals

The test involves turning on the motor of the unbalanced masses device to generate the oscillating centrifugal force, turning on the infrared sensors to generate a signal, turning on the automated testing machine, Instron, to activate the load cell, and turning on the oscilloscope to receive and record signals from the load cell and the light sensors.

The rotating arms are aligned with the open gap in the rotating disc as shown in Figure 21, which in turn allows the light sensors to send a signal. One

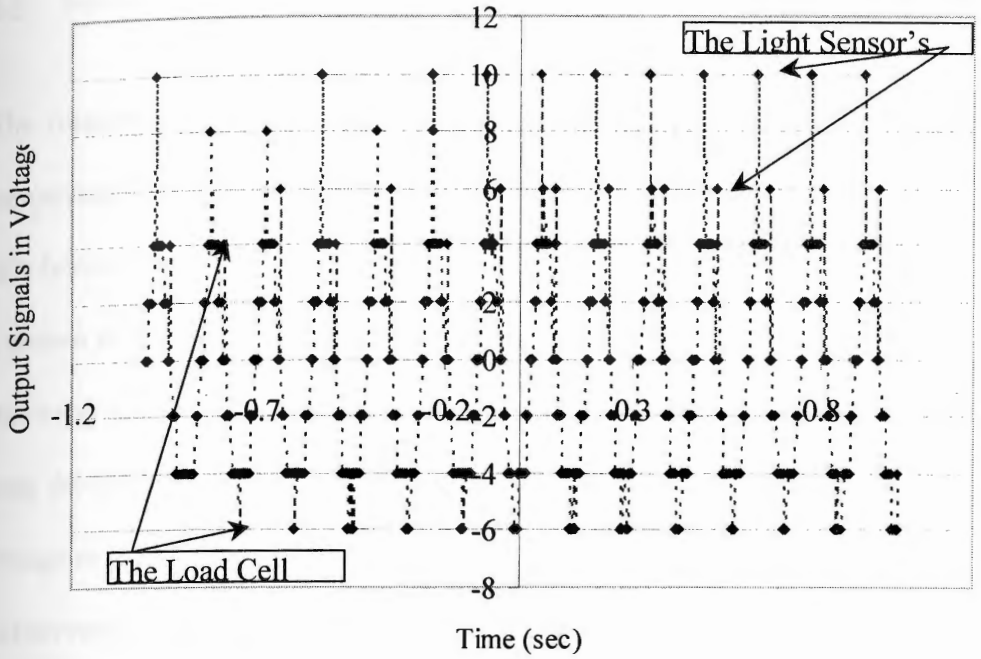

Figure 24 – Voltage – Time; Signals From the Load Cell and the Two Light Sensors as Captured on the Oscilloscope's Screen. The Output Signals of the Load Cell Ranges Between ± 6 V. and the Light Sensors Signals Range Between 0 to 10 V. and 0 to 6 V.

of the two light sensors is positioned parallel to the machine loading train centerline, and the second sensor is positioned at 90° from that centerline. The test output results shown in Figure 22, or 24 show that the two spike signals, which have been sent by the two light sensors positioned themselves on the peak and the zero of the load cell signal. The light sensor 2 is turned off and the test is performed again to verify results. The spike signal from sensor 1 is found on the peak of the load signal. As expected, this proves that the peak of the load occurs when the rotating arm with its eccentric mass are parallel to the loading train centerline.

I.3.5 Motion Due to Inertia Forces

The rotating eccentric mass device is mounted on a carriage with two screws. The carriage has free rolling motion on a slide rail as shown in Figure 25. The rail's horizontal elevation is adjusted to be even by utilizing a bubble level scale as shown in the right hand side of the figure. The motor in the rotating device rotates the eccentric masses, which in turn induce the linear motion of the carriage along the rail. Three tests are performed. The first test involves motion of the carriage as a function of two different angular velocities of the rotating masses. It is observed that increasing the angular velocity of the masses is not coupled with any increase in the magnitude of the displacement of the system.

The second test involves motion of the carriage as function of the radius of rotation of the eccentric mass. It is observed that increasing the radius of rotation is coupled with an increase in the magnitude of the system displacement.

As expected, in the previous two cases, system motion after one full rotation of the eccentric mass, is such that the carriage moves to the right direction with certain displacement then moves back to the left with exactly the same displacement. Therefore, there is no net linear motion since at the end of each cycle the carriage returns to its initial position.

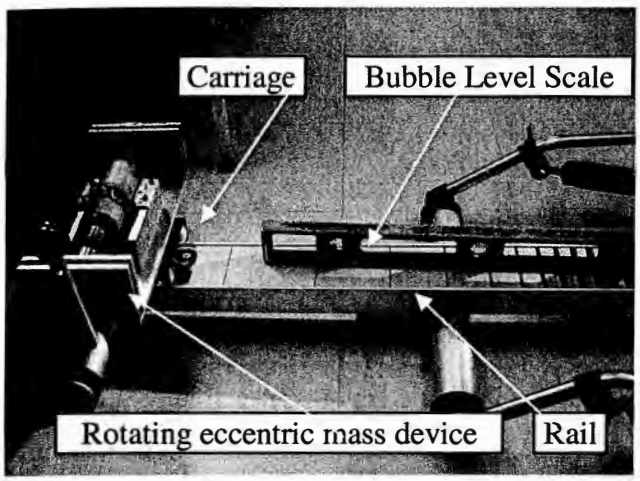

Figure 25 – The rotating device with its unbalanced masses is mounted on a carriage with rolling wheels. The wheels are free to rotate along the right and left directions on the rail. To the right hand side a bubble level scale is placed to show the even horizontal elevation of the rail.

The third test involves the same mechanism but the carriage is restrained by a physical stop and cannot move in one direction. It is observed that the carriage reaches a certain amount of net linear displacement in the opposite direction of the physical stop and after a period of time only the oscillating motion remains. Figure 26 shows this motion in a qualitative fashion since no measurements are made in this test. However, this experiment is video taped.

The net linear motion is due to the impact force between the carriage and the stop and it vanishes due to friction. The oscillation motion, which the system maintains is due to the rotation of the unbalanced masses.

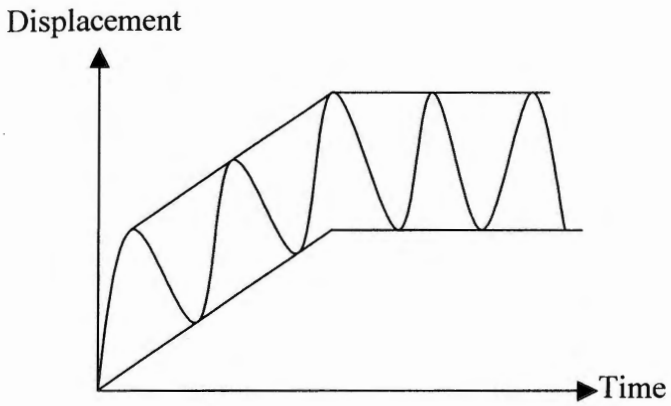

Figure 26 – Schematic plot shows the resultant motion of the device shown in Figure 25 when a physical stop is used to prevent motion of the carriage in x-direction. The resultant motion is oscillating with certain unidirectional linear displacement but after a certain amount of time only oscillating motion remains

I.4. Results and Conclusions

I.4.1. Results:

1. The eccentric rotational masses generate centrifugal force effects at the pin joint and the carriage. These forces act outward and are collinear with the radius of rotation.
2. The centrifugal force is a function of the weight ratio of the rotating eccentric masses to the weight of the carriage.
3. The eccentric rotating mass exerts a fully reversed loading profile at the pin joint, which attaches the arm of eccentric mass to the carriage.
4. In the dynamic system, the magnitude of the force at the pin joint is determined as function of the weight ratio, eccentric weight to the carriage weight.
5. The rotational motion of the eccentric masses causes oscillating motion.
6. An increase of the angular velocity of the rotating mass does not affect the magnitude of the motion but increases the frequency.
7. The magnitude of the linear displacement has a proportional relationship to the radius of rotation.

I.4.2. Conclusions:

These results show that the magnitude of motion is dependent on two factors. The first factor is the radius of rotation at which the eccentric masses are located and the second factor is the angular position of the arm that holds the eccentric masses, which changes the direction of the linear motion every half cycle. Therefore, additional work will investigate the possibility of manipulating the two factors to achieve unidirectional linear displacement.

In addition, an in-depth study of the patents in this field will be done to choose the most promising Rotating Inertial device for further improvements. Specifically, the aim is to invert a geared system such that eccentric masses do not make full rotations in the plane of motion as shown in the Figure 27.

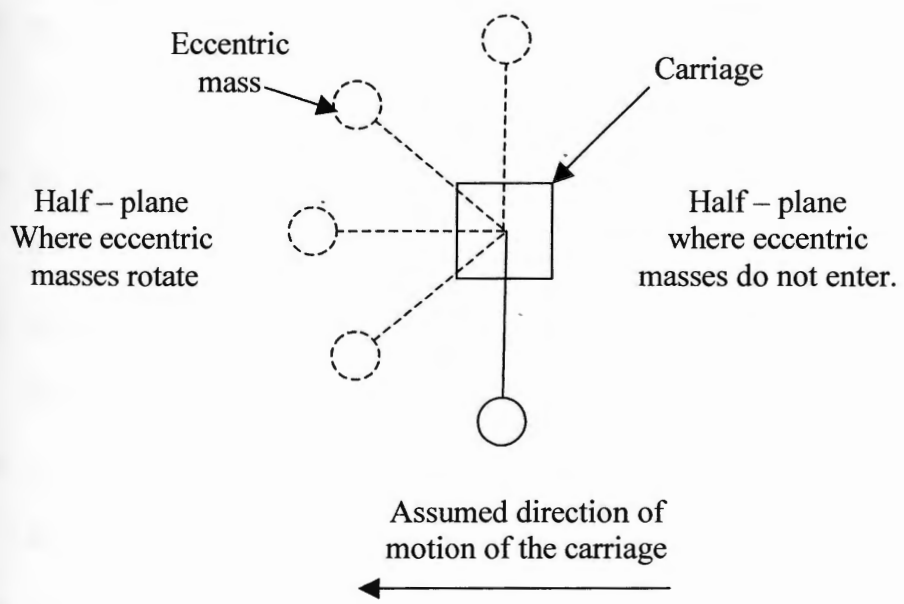

Figure 27 – Schematic shows the aim to confined the eccentric mass rotational motion in one half of the motion plane (the plane of the carriage motion)

I.5. References and Websites

1. Valone, Thomas. "Inertial Propulsion: concept and experiment, part 1" proceedings of the intersociety Energy Conversion Engineering conference, Aug. 1993, v2, p 303-308.
2. Valone, Thomas. "Inertial Propulsion: concept and experiment, part 2" proceedings of the intersociety Energy Conversion Engineering conference, Aug. 1994, v3, p 1484-1489.
3. Foster, R.E. Converting Rotary Motion Into Unidirectional Motion, U.S. Patent # 3,653,269, Issued May 15, 1970.
4. Young Jr., H.W., et al. Directional Force Generator, U.S. Patent # 3,555,915, Issued Jan. 19, 1971.
5. Kellogg Jr., H.D. Gyroscopic Inertial Space Drive, U.S. Patent # 3,203,644, Issued Aug. 31, 1965.
6. Dean, N.L. System for Converting Rotary Motion into Unidirectional Motion, U.S. Patent # 2,886,976. Issued May 19, 1959.
7. Goldschmidt, R. Propulsion of Vehicles, U.S. Patent # 1,512,960, Issued Oct. 14, 1924.
8. Halverson, E.M., et al. Vibration Drive Vehicle, U.S. Patent # 3,530,617, Issued Sept. 29, 1970.
9. Laskowitz, I.B. Centrifugal Variable Thrust Mechanism, U.S. Patent # 1,953,964, Issued April 10, 1934.

10. Laskowitz, I.B. Centrifugal Variable Thrust Mechanism, U.S. Patent # 2,009,780, Issued July 30, 1935.

11. Cuff, C. Device for Converting Rotary Motion into a Unidirectional Linear Motion, U.S. Patent # 3,968,700, Issued July 13, 1976.

12. Thornson, B.R. Apparatus for Developing a Propulsion Force, U.S. Patent # 4,631,971, Issued Dec. 30, 1986.

13. Bristow Jr. Method and Apparatus for Converting Motion to Lineal Motion, U.S. Patent # 5,156,058, Issued Oct. 20, 1992.

14. Cook, R.L. Device for Conversion of Centrifugal Force to Linear Force and Motion, U.S. Patent # 4,238,968, Issued Dec. 16, 1980.

15. Farrall, A.W. Inertial Propulsion Device, U.S. Patent # 3,266,233, Issued Aug. 15, 1966.

16. Matyas, L.B. Propulsion Apparatus, U.S. Patent # 3,584,515, Issued June 15, 1971.

17. Novak, L.J. Centrifugal Mechanical device, U.S. Patent # 3,810,394, Issued May 15, 1974.

18. Holwerda, M. "Unidentified Flying Object with Unusual Propulsive Techniques: Generation of Antigravity by the Absorbtion of Gravitational Vortices." Journal of new energy, v 6, n 1, Summer, 2001, p 169-178.

19. Kammash, T., and Galbraith, D.L. "Novel Fusion Approach to Space power and propulsion." Proceeding of the 24th Intersociety Energy Conversion Engineering Conference, v 5, 1989, p 2531-2534.

20. Kagiwada, T. "Propulsion Mechanism Based on Inertial Force." Proceedings of the IASTED International Conference on Robatics and Applications, 2003, p 148-153.

21. Langman, H. Vehicle and Steering Apparatus Therefore, U.S. Patent # 3,006,581, Issued Oct. 31 1961.

22. Geyer, H.M. Vibration Driven Actuator, U.S. Patent # 2,700,542, Issued Jan. 25, 1955.

23. Nowlin, A.C. Device for Obtaining Directional Force from Rotary Motion, U.S Patent # 2,350,248, Issued Nov. 30, 1942.

24. Robert L. Norton. "Design of Machinery." PP. 620 – 633, 1999.

25. Robert L. Norton. "Machine Design." PP. 328, 2000.

26. J.B. Wilson. "Dynamic Balancing og Rotating Machinery." PP. 144 – 180, 1967.

27. Victor Wowk. "Machinery Vibration: Balancing." PP. 125 – 147, 1995.

28. Websites :

    1. www.estec.esa.nl.
    2. www.howstuffworks.com
    3. www.uspto.gov
    4. www.sdp-si.com

CHAPTER II: SIMULATION OF MODELED MECHANICAL SYSTEMS BASED ON LAGRANGIAN MECHANICS

II.1 Abstract:

The objective of this work is to develop an integrated computer tool to automatically develop equations of motion in symbolic form, simulate, and analyze any dynamic system.

Many virtual software such as Working Model, Pro/Engineer, ADAMS, DADS, PAM-VEF, etc. are available, that can be used to simulate systems but they do not provide details or display the equations of motion.

In this work, the Lagrangian expression is coded in Maple, a symbolic software. This developed symbolic equations of motion code (EOMC) automatically generates the equations of motion in a symbolic form for any dynamic system.

Furthermore, procedures such as the TSC, (the transformation symbolic code), which transform the n-order ODE system to 1^{st} order ODE and Matlab code, which are used to numerically simulate a dynamic motion of a mechanical model are also presented and discussed. Three text-book examples are given to demonstrate the use of this code.

The developed procedures will also greatly aid in teaching advanced courses in dynamics and enhance knowledge and experience of students.

II.2 Introduction:

The objective of this work is to develop a simple computer tool to effectively simulate and analyze the dynamic motion of n-D systems. Therefore, Maple software is used to develop a symbolic code EOMC (equation of motion code), which in turn can be used to develop the equations of motion of any dynamic system. Simply, it performs the derivatives of the Lagrangian expression, shown in equation 1.

$$d/dt\,(\partial\, Lag / \partial\, \dot{q}) - \partial\, Lag / \partial q = - \partial\, F / \partial\, \dot{q} + Q \qquad (1)$$

where

$$Lag = T - V \qquad (2)$$

$\dot{q}$ = time derivative of the generalized coordinate.

T = kinetic energy of the system

V = potential energy of the system

F = dissipative forces of the system (Rayleigh function in this case)

Q = external forces on the system

Dissipative forces include all forces where energy is dissipated from the system when motion takes place, i.e frictional, viscous, and proportional forces, see [Walls 1967].

In general, the Lagrangian technique is extensively used to develop the equations of motion, especially for multiple-degree-of freedom systems with distributed masses [Saeed, 2001, Paul 1981, Asada 1986, Sciavicco, 1996, Fu 1987, Featherstone 1983, Shahinpoor 1988]. The Lagrangian method is based on energy terms only and, thus, is easy to use it and results in the least number of equations of motion. The Lagrangian method is chosen for its simplicity instead of matrix methods, see [Vibet 1994, Richard 1993, Paul 1981].

Therefore, the developed symbolic EOMC based Lagrangian mechanics is demonstrated on two textbook examples and the invention work of Thornson [Thornson 1986]. The first example is particle motion in a uniform gravitational field expressed in spherical coordinates, see example 6-3 [Greenwood 1988] Figure 28. For clarification, the first example demonstrates the use of the EOMC in developing the equations of motion without going into details of defining variables T, V, F, and Q. The second example [Datseris] shows a one-dimensional 'lumbed-parameter mechanical system' (LPMS) in Figure 29. Example 2 explains the use of Lagrange's methodology where all the parameters (T, V, F, and Q) are identified, then the EOMC is used to develop the equations of motion of the LPMS. Furthermore, the 'Transform Symbolic Code' (TSC), which is used to reduce the n-order equations of motion to 1^{st} order, and rewriting the symbolic 1^{st} order equations of motion is provided in the Appendices.

Finally, the third example simulates the dynamics of the model shown in Figure 35. This example is chosen because the mechanical system it represents is the building block for many IPS.

However, the simulation results of the third example show clearly that the Gross motion of a mechanical system depends on the motion of the system's center mass. This fact will be used in a subsequent paper to investigate the motion capabilities of inertial propulsion systems, especially Thornson's Mechanism, see [Almesallmy, et. al 2006].

II.3 Example 1: A Body in a Uniform Gravitational Environment.

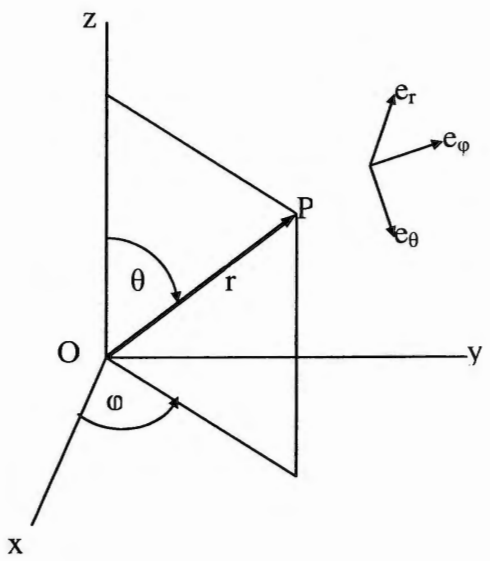

Figure 28 – Body P is located at distance r in the spherical coordinate system r, θ, and φ. The unit vector triad represents the instantaneous motion direction of P in this coordinate system.

This example demonstrates the development of the equations of motion in spherical coordinates r, θ, and φ for body P in a uniform gravitational environment using the EOMC. However, to use the EOMC, one shall define the four variables T, V, F, and Q in Maple software. These variables are copied from example 6 – 3 [Greenwood 1988] and re-written in Maple as follows;

T:= ½ m (d/dt (r(t))^2 + r(t)^2 (d/dt (θ(t)))^2 + r(t)^2 sin (θ(t))^2 d/dt (φ(t))^2):

V:= m g r(t) cos (θ(t)):

F:= 0:

Q_r:= 0: Q_ θ:= 0: Q_: φ = 0:

II.3.1 The Equation of Motion Code (EOMC)

Then continue by pasting the following code (EOMC) in Maple software. Note, make sure that there is no space between the semicolon and the equal sign, i.e. '**Lag:= T – V:**' and not like 'Lag: =T - V:'

```
Lag:          = T - V:
F_dq:         = subs(diff(q(t),t)=dq,F):
D_F_dq:       = value(Diff(F_dq,dq)):
D_F_dq:       = subs(dq=diff(q(t),t),%):
Lag_dq:       = subs(diff(q(t),t)=dq,Lag):
D_Lag_dq:     = value(Diff(Lag_dq,dq)):
D_Lag_dq:     = subs(dq=diff(q(t),t),%):
d_D_Lag_dq_t: = diff(%,t):
Lag_q:        = subs(q(t)=q,Lag_dq):
D_Lag_q:      = value(Diff(Lag_q,q)):
D_Lag_q:      = subs({q=q(t),dq=diff(q(t),t)},%):
EQ1:          = collect(d_D_Lag_dq_t - D_Lag_q = -
                D_F_dq + Q_q,{diff(r(t), `$`
                (t,2)),diff(θ
                (t),`$`(t,2)),diff(φ(t),`$`(t,2))});
```

To get the equations of motion for the generalized coordinates r, θ, and φ, simply substitute for q in the previous EOMC with each one of the general coordinates, one at a time. For example, to get the equation of motion in r – coordinate, just substitute for each 'q' with 'r' as follows;

```
> Lag:          = T - V:
> F_dr:         = subs (diff (r (t), t) = dr, F):
> D_F_dr:       = value (Diff(F_dr, dr)):
> D_F_dr:       = subs (dr = diff(r (t), t), %):
>Lag_dr:        = subs (diff(r (t), t) = dr, Lag):
>D_Lag_dr:      = value (Diff (Lag_dr,dr)):
>D_Lag_dr:      = subs (dr = diff(r (t), t),%):
>d_D_Lag_dr_t:  = diff(%,t):
>Lag_r:         = subs(r (t) = r,Lag_dr):
>D_Lag_r:       = value (Diff (%,r)):
>D_Lag_r:       =   subs ({r = r (t), dr = diff(r
                    (t),t)},%):
>EQ1:           = collect (d_D_Lag_dr_t-D_Lag_r = -
                  D_F_dX + Q_r,
                  {diff(r(t), `$`(t,2)),diff(θ
                  (t),`$`(t,2)),diff(φ(t),`$`(t,2))})
                  ;
```

$$EQ1 :=$$

$$-m\,r(t)\left(\frac{\partial}{\partial t}\theta(t)\right)^2 + m\left(\frac{\partial^2}{\partial t^2} r(t)\right) - m\,r(t)\sin(\theta(t))^2\left(\frac{\partial}{\partial t}\phi(t)\right)^2 + m\,g\cos(\theta(t)) = 0 \qquad (3)$$

Again, to get the equation of motion in θ – coordinate just substitute in the EOMC for 'q' with 'θ' as follows,

```
> Lag:          = T - V:

> F_dθ:         = subs (diff (θ (t), t) = dθ, F):

> D_F_dθ:       = value (Diff(F_dθ, dθ)):

> D_F_dθ:       = subs (dθ = diff(θ (t), t), %):

>Lag_dθ:        =  subs (diff(θ (t), t) = dθ, Lag):

>D_Lag_dθ:      =  value (Diff (Lag_dθ,dθ)):

>D_Lag_dθ:      =  subs (dθ = diff(θ (t), t),%):

>d_D_Lag_dθ_t: =  diff(%,t):

>Lag_θ:         =  subs(r (t) = θ,Lag_dθ):

>D_Lag_θ:       =  value (Diff (%, θ)):

>D_Lag_θ:       =  subs ({θ = θ (t), dθ = diff(θ
                   (t),t)},%):

>EQ2:           =  collect (d_D_Lag_dθ_t-D_Lag_θ = -
                   D_F_dX + Q_θ,{diff(r(t), `$`
                   (t,2)),diff(θ
                   (t),`$`(t,2)),diff(φ(t),`$`(t,2))});
```

$$EQ2 := 2\,m\,\mathrm{r}(t)\left(\frac{\partial}{\partial t}\theta(t)\right)\left(\frac{\partial}{\partial t}\mathrm{r}(t)\right) + m\,\mathrm{r}(t)^2\left(\frac{\partial^2}{\partial t^2}\theta(t)\right)$$
$$- m\,\mathrm{r}(t)^2 \sin(\theta(t))\left(\frac{\partial}{\partial t}\phi(t)\right)^2 \cos(\theta(t)) - m\,g\,\mathrm{r}(t)\sin(\theta(t)) = 0 \qquad (4)$$

Finally, for the third equation of motion in the φ – coordinate substitute in the EOMC for 'q' with 'φ' as follows,

```
> Lag:          = T - V:

> F_dφ:         = subs(diff(φ(t),t)=dφ,F):

> D_F_dφ:       = value(Diff(F_dφ,dφ)):

> D_F_dφ:       = subs(dφ=diff(φ(t),t),%):

>Lag_dφ:        =  subs (diff(φ (t), t)= dφ,Lag):

>D_Lag_dφ:      =  value (Diff (Lag_dφ,dφ)):

>D_Lag_dφ:      =  subs (dφ=diff(φ (t), t),%):

>d_D_Lag_dφ_t:  =  diff(%,t):

>Lag_φ:         =  subs(φ(t)=φ,Lag_dφ):

>D_Lag_φ:       =  value (Diff (%, φ)):

>D_Lag_φ:       =  subs ({φ=φ(t),dφ=diff(φ(t),t)},%):

>EQ3:           =  collect (d_D_Lag_dφ_t-D_Lag_φ=-
                   D_F_φ + Q_φ , {diff(r(t), `$`
                  (t,2)),diff(θ
                  (t),`$`(t,2)),diff(φ(t),`$`(t,2))});
```

$$EQ3 := 2\,m\,r(t)\sin(\theta(t))^2\left(\frac{\partial}{\partial t}\phi(t)\right)\left(\frac{\partial}{\partial t}r(t)\right) + 2\,m\,r(t)^2\sin(\theta(t))\left(\frac{\partial}{\partial t}\phi(t)\right)\cos(\theta(t))\left(\frac{\partial}{\partial t}\theta(t)\right) + m\,r(t)^2\sin(\theta(t))^2\left(\frac{\partial^2}{\partial t^2}\phi(t)\right) = 0 \quad \textbf{(5)}$$

Note that equations (3), (4), and (5) are identical to the three equations developed in Example 6-3 in [Greenwood 1988], which are shown below for verifications.

$$\mathbf{m\,\ddot{r} - m\,r\,\dot{\theta}^2 - m\,r\,\dot{\varphi}^2\sin^2\theta + m\,g\cos\theta = 0}$$

$$\mathbf{m\,r^2\,\ddot{\theta} - 2\,m\,r\,\dot{r}\,\dot{\theta} - m\,r^2\,\dot{\varphi}^2\sin\theta\cos\theta - m\,g\,r\sin\theta = 0}$$

$$\mathbf{m\,r^2\,\ddot{\varphi}\sin^2\theta + 2\,m\,r\,\dot{r}\,\dot{\varphi}\sin^2\theta + 2\,m\,r^2\,\dot{\theta}\,\dot{\varphi}\sin\theta\cos\theta = 0}$$

EQ1, EQ2, and EQ3 are the developed equations of motion in r, θ, and φ coordinates respectively. The mathematical model, which is composed of equations (3), (4), and (5) are coupled nonlinear second order and non-homogeneous ODE, cannot be simulated in Matlab. To make the mathematical model ready for simulation, the three equations must be modified as follows,

1. Reduce its order to 1st order system.
2. Substitute for all the coordinate variables r, θ, and φ and first derivatives with y(1), y(2), y(3), y(4), y(5), and y(6) respectively
3. Separate the second derivatives dy(4), dy(5), and dy(6) in one side.

However, these steps are discussed in detail in the example 2.

II.4 Example 2: One Dimensional Lumbed-Parameter Mechanical System

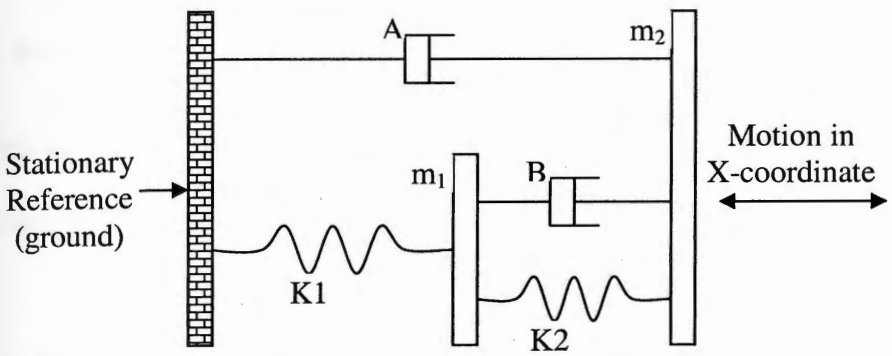

Figure 29 – The system includes two masses m1, and m2, two springs with stiffness K1, and K2, and two dashpots with damping coefficients A, and B. Its motion is in a horizontal frictionless plan

The example shown in Figure 29 demonstrates the use of the developed integrated tool to solve and simulate the motion of the dynamic systems. There are four major steps:

1. Development of T, V, F, and Q expressions to form the Lag expression
2. Development of the equations of motion utilizing the EOMC (see example 1)
3. Converting the n–order differential equations of motion to a first order differential equations
4. Simulation.

At this stage, an investigator must define the T, V, F, and Q expressions in step 1, while the other steps are automated systematic procedures.

II.4.1 Step 1: Developing the expression of the four variables T, V, F, and Q.

Lagrangian (Lag) is a function of T and V, Lag = T – V, where, T, and V are the system kinetic energy and the non-dissipative potential energy of a system respectively. The existence of V is due to the masses being exposed to gravitational, magnetic, spring effects, etc.

Before developing T, V, F, and Q generalized coordinates must be established. Two differential sets of generalized coordinates are provided in Figures

30, and 31 to show that the dynamic response of a system is independent of the chosen reference as long as the initial conditions are expressed correctly; These two sets of generalized coordinates also show that the process requires some attention to avoid errors.

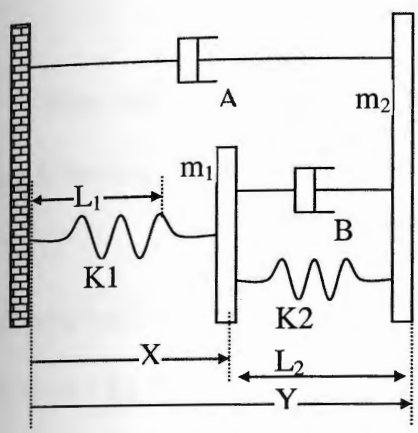

Figure 30 – Case # 1, shows two chosen generalized coordinates X, and Y to express the motion responses of the two masses m_1, and m_2 respectively; they are both absolute generalized coordinates measured from the ground

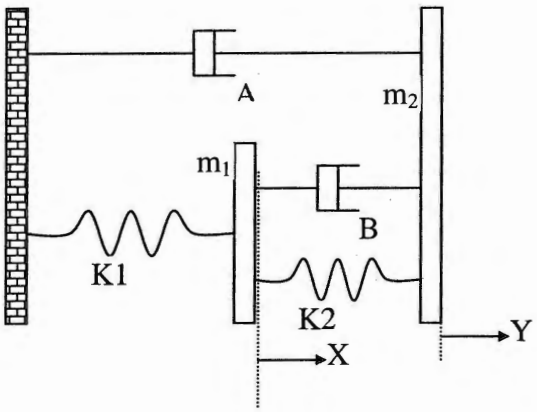

Figure 31 – Case # 2, shows X, and Y are the two chosen generalized coordinates to express the motion response of the two masses m_1, and m_2; they are both measured from the undeformed position of the springs.

Case # 1

Defining kinetic energy and other key parameters is straight forward because generalized coordinates X, and Y are measured from a stationary reference, see Figure 30.

$T = \frac{1}{2}\, m1\, \dot{X}^2 + \frac{1}{2}\, m2\, \dot{Y}^2$ (where $\dot{X}$, and $\dot{Y}$ are dX/dt, and dY/dt respectively)

$V = \frac{1}{2}\, K1\, (X - L_1)^2 + \frac{1}{2}\, K2\, [(Y - X) - L_2]^2$

$F = \frac{1}{2}\, B\, (\dot{Y} - \dot{X})^2 + \frac{1}{2}\, A\, \dot{Y}^2$

Q_q = 0: (where q is replaced with X, Y respectively, see below)

Note, that rewriting the previous four equations in Maple software will take the following formats,

T := ½ *m1* (diff(X(t),t))^2 + ½ *m2 * (diff(Y(t),t))^2

V := ½ * K1 * (X(t) – L1) ^ 2 + ½ * K2 [(Y(t) – X(t)) – L2] ^ 2

F := ½ * B * (diff(Y(t),t)) – diff(X(t),t))) ^ 2 + ½ * A * (diff(Y(t),t))^2

Q_X: = 0: Q_Y:= 0:

Case # 2

Defining kinetic energy and other key parameters in this case (Figure 31) requires a little care. By inspection in Figure 31, assume that m1 is displaced in X-coordinate , one can realize that the force elements B2, and K2 to the right hand side of m1 are displaced without deformation. In other words the motion in X – coordinate affects the model's components m2, K1, and A only, where both of the spring with stiffness K1, and the dashpot with damping coefficient A are

deformed. Again, assume that m2 is displaced in Y – coordinate, one can realize that the mechanical components A, K2, and B shall only be affected. In other words, mass m1 does not move, and spring K1 in turn shall not have any changes. Therefore, the four variables can be defined as follows:

$T = \frac{1}{2}\, m1\, \dot{X}^2 + \frac{1}{2}\, m2\, (\dot{Y} + \dot{X})^2$

$V = \frac{1}{2}\, K1\, X^2 + \frac{1}{2}\, K2\, Y^2$

$F = \frac{1}{2}\, B\, \dot{Y}^2 + \frac{1}{2}\, A\, (\dot{Y} + \dot{X})^2$ (for dashpot has Rayleigh's dissipation behavior)

$Q\_X = 0,\ Q\_Y = 0$ (in X, and Y coordinates respectively)

Where,

$X, Y, \dot{X}, \dot{Y}$ = the displacements and its derivatives w.r.t time (velocity) in X and Y coordinates.

K1, K2 = the stiffness of the springs shown in Figures 30, and 31.

A, B = the damping coefficients as shown in Figures 30, and 31.

II.4.2 Step 2: Developing the equations of motion

Figure 30 shows that the general coordinates are X, and Y. Therefore, for each case, the EOMC is used twice to develop two equations of motion. This is done by substituting for the q in the EOMC with X, and Y respectively. For

example, to develop the equation of motion 6 in X-coordinate, which is shown below, the EOMC becomes as follows,

```
Lag:          = T - V:
F_dX:         = subs(diff(X(t),t)=dX,F):
D_F_dX:       = value(Diff(F_dX,dX)):
D_F_dX:       = subs(dX=diff(X(t),t),%):
Lag_dX:       = subs(diff(X(t),t)=dX,Lag):
D_Lag_dX:     = value(Diff(Lag_dX,dX)):
D_Lag_dX:     = subs(dX=diff(X(t),t),%):
d_D_Lag_dX_t: = diff(%,t):
Lag_X:        = subs(X(t)=X,Lag_dX):
D_Lag_X:      = value(Diff(Lag_X,X)):
D_Lag_X:      = subs({X=X(t),dX=diff(X(t),t)},%):
EQ1:          = collect(simplify(d_D_Lag_dX_t-
                D_Lag_X=- D_F_dX + Q_X),diff);
```

EQ1:=

$$=(m1+m2)\left(\frac{\partial^2}{\partial t^2}\mathrm{X}(t)\right)+m2\left(\frac{\partial^2}{\partial t^2}\mathrm{Y}(t)\right)+K1\mathrm{X}(t)=-A\left(\left(\frac{\partial}{\partial t}\mathrm{Y}(t)\right)+\left(\frac{\partial}{\partial t}\mathrm{X}(t)\right)\right) \quad \textbf{(6)}$$

Again to develop the equation of motion in Y-coordinate, all what one has to do is to substitute Y for q in the EOMC. This provides the second equation of motion (7) in the Y-coordinate as shown below,

EQ2:=

$$\left(\frac{\partial^2}{\partial t^2}X(t)\right)m2+m2\left(\frac{\partial^2}{\partial t^2}Y(t)\right)+K2Y(t)=-A\left(\frac{\partial}{\partial t}Y(t)\right)-A\left(\frac{\partial}{\partial t}X(t)\right)-B\left(\frac{\partial}{\partial t}Y(t)\right) \quad (7)$$

Note that all the procedure in step 2 should be repeated again for case 2 to develop the corresponding equations of motion as those of equations 6, and 7 for case 1.

II.4.3 Step 3: Rewriting the 2nd order equations of motion for Matlab simulation

The mathematical system, which is composed of equations 6, and 7, must be solved numerically to simulate the motion of the mechanism shown in Figure 30. In order to simulate this system, which is composed of two coupled 2nd order nonlinear, non-homogeneous deferential equations 6, and 7 with Matlab software, this 2nd order system is automatically converted to 1st order system. Also, the variables in coordinates X, Y and its first derivatives must be assigned as y(#), i.e y(1), y(2), etc. This is to make the equations of motion in Maple software ready to be sent to Matlab. Therefore, an example of the Transform Symbolic Code (TSC) is provided and explained in the Appendix A. However, the TSC develops the following two equations 8, and 9 from equations 6, and 7 respectively which shall be solved in Matlab numerically.

$$PP3 := Y4 = -(y(4)\,m1\,B + y(4)\,m2\,B + y(4)\,A\,m1 + A\,y(3)\,m1 + m1\,K2\,y(2) + m2\,K2\,y(2) - m2\,K1\,y(1))/(m2\,m1) \quad (8)$$

$$PP4 := Y3 = \frac{B\,y(4) + K2\,y(2) - K1\,y(1)}{m1} \qquad \textbf{(9)}$$

II.4.4 Step 4: Simulation #1

Some arbitrary system parameters are assumed for the two cases to obtain simulation results. These parameters are assumed as follows:

L1=2.35 inch; L2=2 in; K1=50 Ib/in; K2=50 Ib/in; A=1.0 Ib-sec/in; B=1.0 Ib-sec/in; m1=0.72 Ib; m2=1.36 Ib (see Figures 30, and 31)

Initial conditions will be assumed the same for both cases as follows:

IC_{math} of case 1:

X_In_Disp =2.35 in; Y_In_Disp = L1+L2+0.5 = 4.85 in;

IC_{math} of case 2:

X_In_Disp =0.0 in; Y_In_Disp =0.5 in;

Where; X_In_Disp, and Y_In_Disp are the initial position of masses m1, and m2 respectively. The two conditions appear different but they are actually identical for the defined generalized coordinates, see Figures 30, and 31.

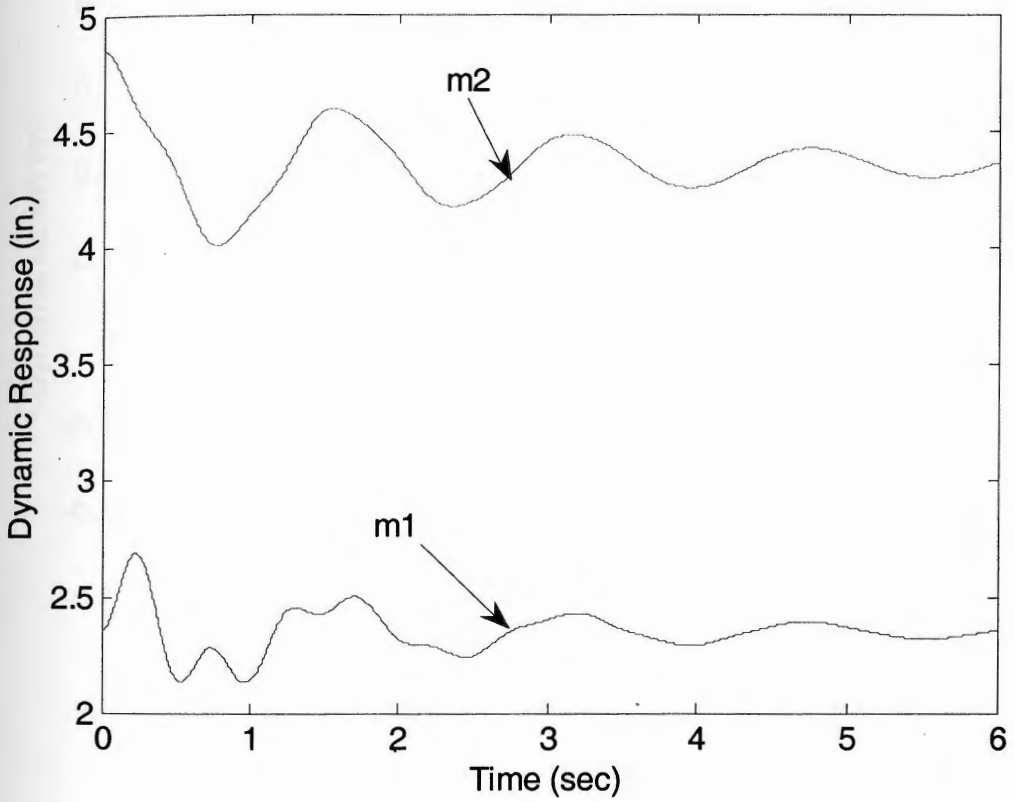

Figure 32 – Case # 1: Absolute dynamic response of mass m_1, and m_2, see Figure 30.

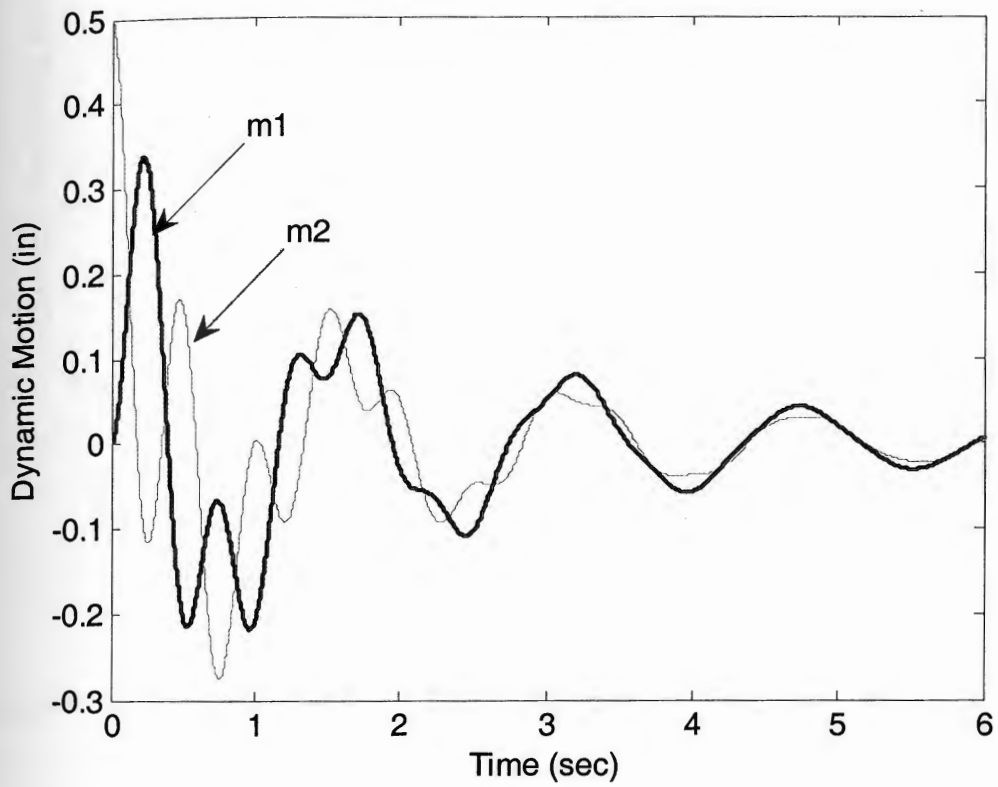

Figure 33 – Case #2 (Figure 31). The dynamic response of mass m1 and m2, see Figure 34 for the absolute response.

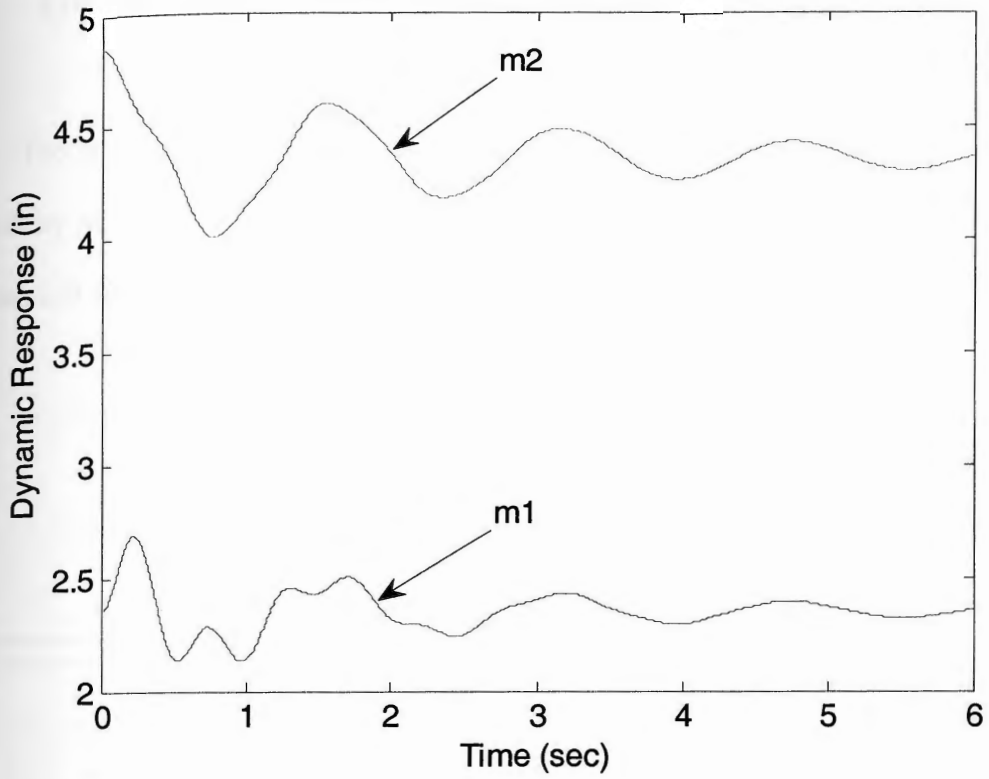

Figure 34 – Case # 2: Absolute dynamic response of mass m_1, and m_2, see Figure 31.

Equations of motion 8, and 9 are coded in m-file as shown in Appendix B. Simulations results of cases 1, and 2 are shown in Figures 32, and 33 respectively.

Figure 34, shows identical results of case 2 when appropriate changes are made to obtain absolute position of masses m1, and m2 to the corresponding results of case 1 which is shown in Figure 32.

The results of the previous simulations, which are shown in Figures 32, and 34, are also achieved using WM.

II.5 Example 3: Motion of Epicyclic (planetary) Gear System Attached to a carriage.

The goals of this example are to demonstrate both the reliability and the simplicity of the developed procedures and to investigate the motion of a mechanical system which is the building block of several proposed IPS.

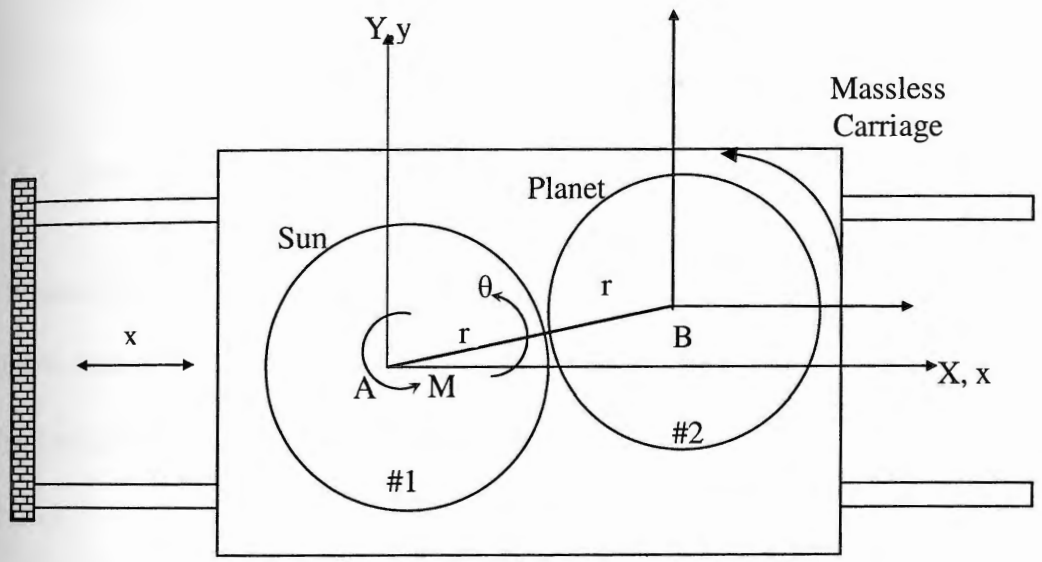

Figure 35 – shows in horizontal plan x-y, two similar gears (masses = m, radii = r, gear ratio = 1). Gear #1 (Sun gear) is fixed to the carriage (does not rotate.) A motor is mounted at the center of gear #1. The motor provides torque of M N.m., to a massless link AB, which in turn rotates in θ-coordinate.

Again, to simulate the motion of the mechanism shown in Figure 35, the following steps should be followed.

1) Development of T, V, F, and Q expressions to form the Lag expression
2) Development of equations of motion utilizing the EOMC (see example 1)
3) Converting the n-order ODE of motion system to a first order ODE utilizing code similar to TSC, see Appindex A.
4) Simulation.

II.5.1 Step 1: Developing the expression of the four parameters T, V, F, and Q

Figure 35 shows that this system has two generalized coordinates X, and θ. T kinetic energy and other parameters are shown below:

T:= [½ m_1 v_A^2] + [½ m_2 v_B^2)+ ½ I_{m2} (2 $\dot{\theta}$)^2]

V:= 0:

F:= 0:

Q_X:= 0: Q_ θ:= M:

Where

m_1 = m2 = The mass of gear #1 and #2 respectively.

v_A = $\dot{X}$ = the velocity of gear #1.

v_B = the linear velocity components of gear #2

I_{m2} = The mass moment of inertia of gear #2 with respect to the c.m 'B'

$\dot{\theta}$ = the angular velocity of the massless link AB

Gear # 2

Has angular velocity of 2 $\dot{\theta}$, which is twice the angular velocity of link AB. The linear velocity of the center of gravity of gear # 2 can be obtained by taking derivative of position r_B in complex form, as follows:

$$r_B = X + (2\,r)\,e^{i*\theta}$$

Where, X is the displacement of gear #2 in the X-coordinate, and r is the gear radius

$$v_B = \dot{X} + 2\,(dr/dt)\,e^{i*\theta} + 2\,r\,i\,(d\theta/dt)\,e^{i*\theta}$$

$$= [\dot{X} - 2\,r\,\dot{\theta}\,\sin(\theta)] + [2\,r\,\dot{\theta}\cos(\theta)]\,i$$

$$= (v_x)_B + (v_y)_B$$

II.5.2 Step 2: Developing the equations of motion

Figure 35 shows that the general coordinates are X, and θ. Therefore, in Maple software the EOMC is used twice by subsisting for the q with X, and θ respectively.

X-Coordinate Equation:

EQ1:=

$$-2m\left(\frac{\partial^2}{\partial t^2}X(t)\right) - 2mr\left(\frac{\partial^2}{\partial t^2}\theta(t)\right)\sin(\theta(t)) - 2mr\left(\frac{\partial}{\partial t}\theta(t)\right)^2\cos(\theta(t)) = 0 \qquad (10)$$

θ- Coordinate Equation:

$$EQ2:=-2m\left(\frac{\partial^2}{\partial t^2}X(t)\right)r\sin(\theta(t))+(4mr^2+4I)\left(\frac{\partial^2}{\partial t^2}\theta(t)\right)=M \qquad (11)$$

II.5.3 Step 3: Rewriting the 2nd order equations of motion for Matlab simulation

Again, simulation of the differential equations (Equations 10, and 11) in Matlab can be done after the following two steps are performed: The first step is separation of the highest derivations (i.e $\ddot{X}$, $\ddot{\theta}$). The second step, is writing the equations in an acceptable form for Matlab (see Appendix A).

First Step: Separation of the highest derivatives

The first step includes three commands to be written in Maple software. The first command substitutes Y3, and Y4 for $\ddot{X}$, and $\ddot{\theta}$ (which are the second derivatives with respect to time of θ, and X generalized coordinates) respectively. The second command pulls out each equation from the result of the previous command. The third command solves the outputs (EQ1, and EQ2) of the previous command (second command) using Cramer's rule for the Y3, and Y4.

Command 1

```
1> EQ:=subs({diff(S(t),`$`(t,2))=Y3,diff(X(t),`
   $`(t,2))=Y4},{EQ1,EQ2});
```

Command 2

```
2 > EQ1:=EQ[1];EQ2:=EQ[2];
```

Command 3

```
3 > Yt:= solve({EQ1,EQ2},{Y3,Y4});
```

$$Yt := \left\{ Y3 = \frac{1}{2} \frac{M + 2\,m\,r^2 \sin(\theta(t)) \left(\frac{\partial}{\partial t}\theta(t)\right)^2 \cos(\theta(t))}{-m\,r^2 \sin(\theta(t))^2 + 2\,m\,r^2 + 2\,I}, \right.$$

$$\left. Y4 = \frac{1}{2} \frac{r\left(\sin(\theta(t))\,M + 4\left(\frac{\partial}{\partial t}\theta(t)\right)^2 \cos(\theta(t))\,m\,r^2 + 4\,I\left(\frac{\partial}{\partial t}\theta(t)\right)^2 \cos(\theta(t))\right)}{-m\,r^2 \sin(\theta(t))^2 + 2\,m\,r^2 + 2\,I} \right\}$$

Second Step: Rewriting the equations of motion in an acceptable format for Matlab.

The second step is composed of two commands 4, and 5. Command 4 substitutes y(3), y(4) for the first derivatives of θ, and X with respect to time respectively. Command 5 substitutes y(1), and y(2) for the two generalized coordinates θ, and X respectively

Command 4

```
>P3:=
subs({diff(θ(t),t)=y(3),diff(X(t),t)=y(4)},collect(Yt[
1],{diff(θ (t),t),diff(X(t),t)})):
>P4:=
```

```
subs({diff(θ(t),t)=y(3),diff(X(t),t)=y(4)},collect(Yt[
2],{diff(θ (t),t),diff(X(t),t)})):
```

Command 5

```
> PP3:=subs({S(t)=y(1),X(t)=y(2)},P3);
```

$$PP3 := Y3 = \frac{m r^2 \sin(y(1)) \cos(y(1)) y(3)^2}{2 m r^2 + 2 I - m r^2 \sin(y(1))^2} + \frac{\frac{1}{2} M}{2 m r^2 + 2 I - m r^2 \sin(y(1))^2} \tag{10}$$

```
>PP4:=subs({S(t)=y(1),X(t)=y(2)},P4);
```

$$PP4 = Y4 = -\frac{1}{2} \frac{r(4\cos(y(1)) m r^2 + 4 I \cos(y(1))) y(3)^2}{2 m r^2 + 2 I - m r^2 \sin(y(1))^2} + \frac{\frac{1}{2} r \sin(y(1)) M}{2 m r^2 + 2 I - m r^2 \sin(y(1))^2} \tag{11}$$

Note: the outputs Y3, and Y4 are the second derivative of θ, and X respectively. In Matlab file, paste the previous two equations and substitute dy(3), and dy(4) for Y3, and Y4 respectively, see Appendix D.

The previous two Equations 10, and 11 are coded in a Matlab file (see Appendix D). This file is used to provide the simulation of the motion of the Epicyclical Gear System's model shown in Figure 35. The output simulation

results are shown in Figures 36, and 37 for generalized coordinates θ, and X respectively.

Figure 37 shows that the carriage is reciprocating between 0 to 0.6 m. Figure 38 shows the projection (AB * cos (θ)), which represents the relative motion displacement of gear #2 in the X-coordinate with respect to the c.m of gear #1. Figure 39 shows X_2, the absolute position of gear #2 in X-coordinate. Furthermore, to find the motion of the c.m of the whole system (gears #1, and Gear #2), the simple rule of $(m_1*X_1 + m_2*X_2) / (m_1 + m_2)$ is applied.

Where, m_1, and m_2 are equal mass of gears #1, and #2 respectively. In addition, X_1, and X_2 are the absolute motion displacements in X-coordinate of gears #1, and #2 which are shown in Figures 37, and, 39 respectively. Therefore, the previous rule can be simplified to become:

$(m_1*X_1 + m_2*X_2) / (m_1 + m_2) = (X_1 + X_2) / (2)$. Figure 40 shows that the motion of the c.m. of the whole system is stationary although the components of the mechanical system are in motion.

II.5.4 Step 4: Simulation of the Motion of the Epicyclic Gear System Mounted on a Carriage

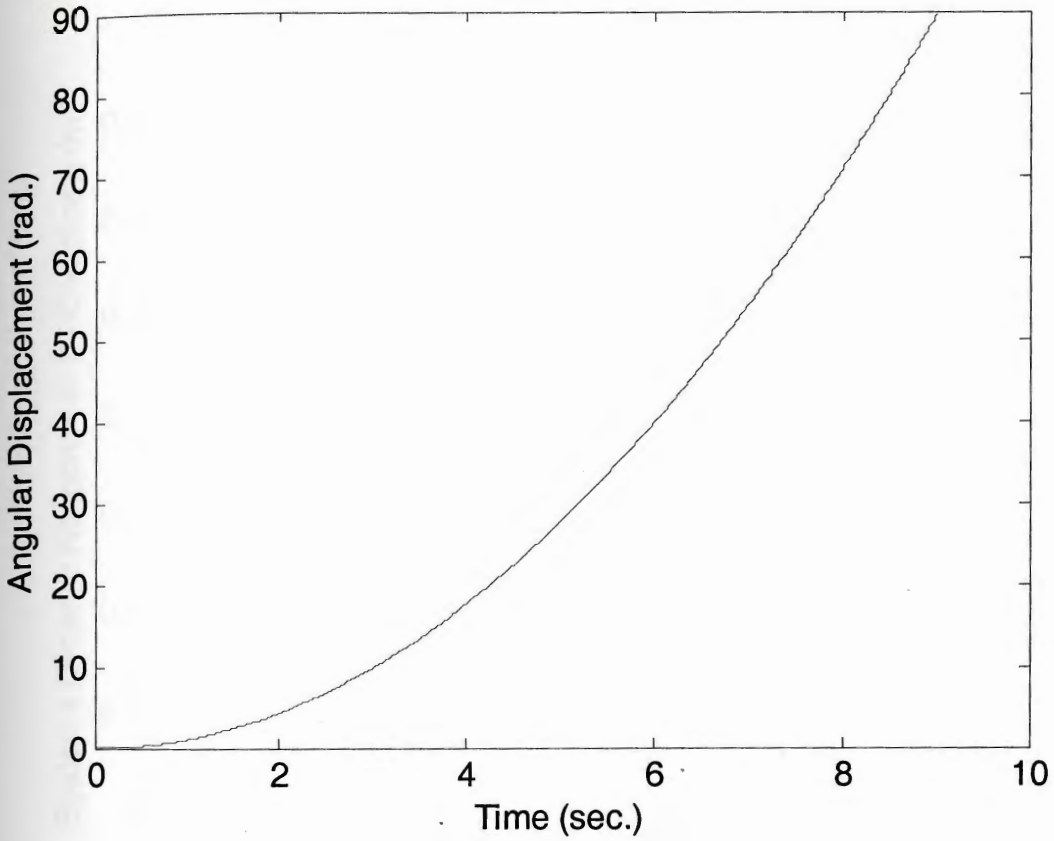

Figure 36 – Simulation of θ, the angular displacement of the massless bar AB.

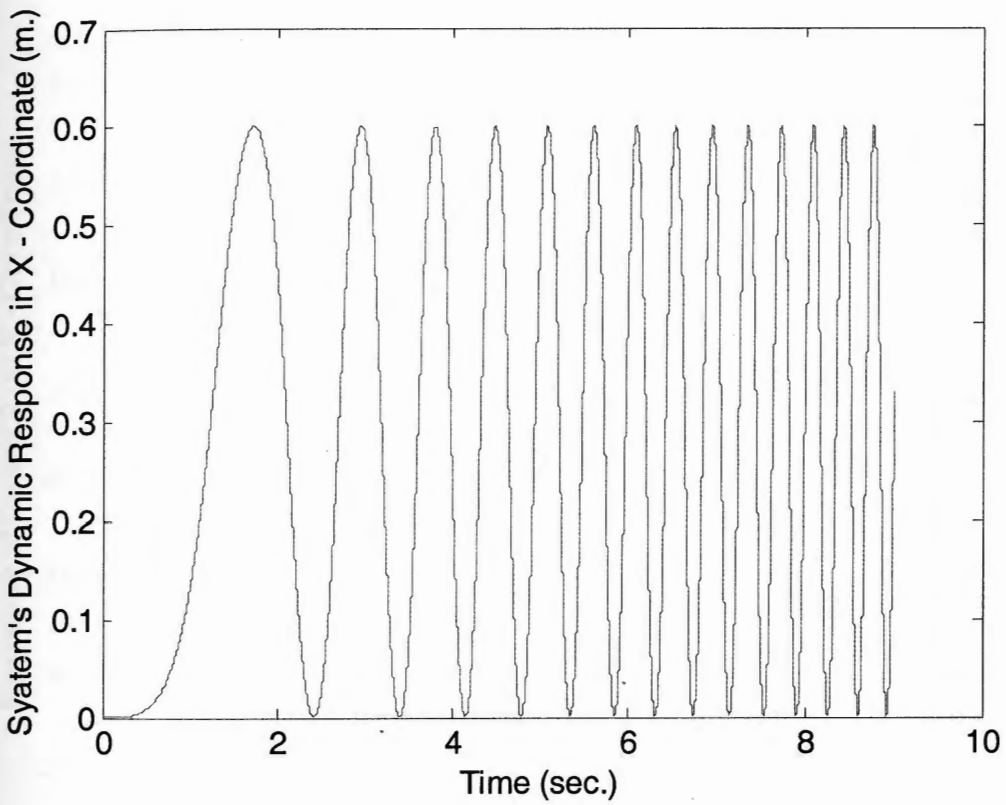

Figure 37 – Simulation of the linear motion of massless carriage in X-coordinate; response is harmonic.

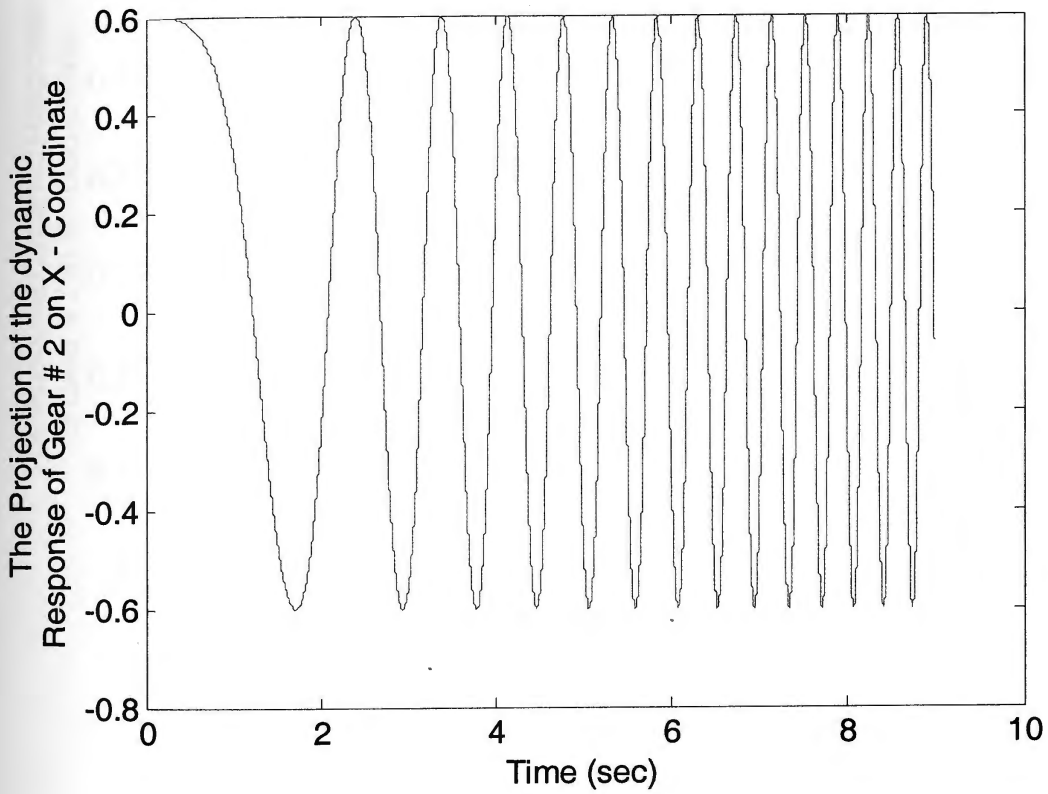

Figure 38 – Relative motion of the c.m of gear #2 in X-coordinate with respect to the c.m. of gear #1.

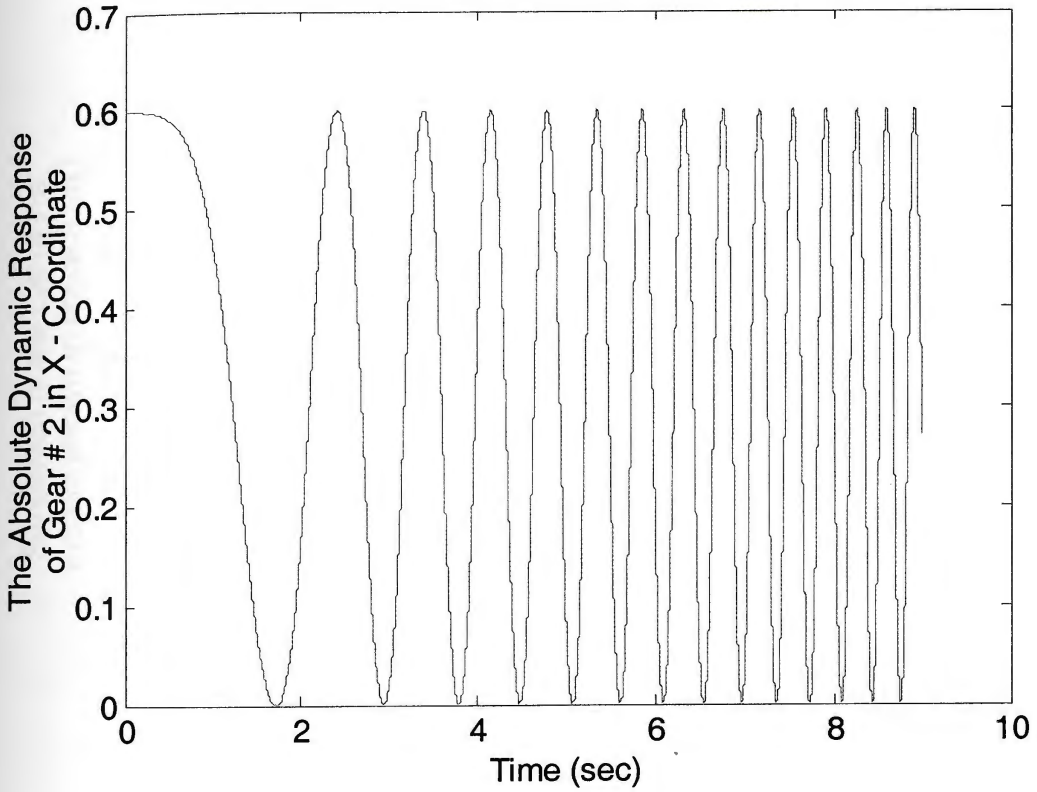

Figure 39 – Absolute position of the c.m of gear # 2.

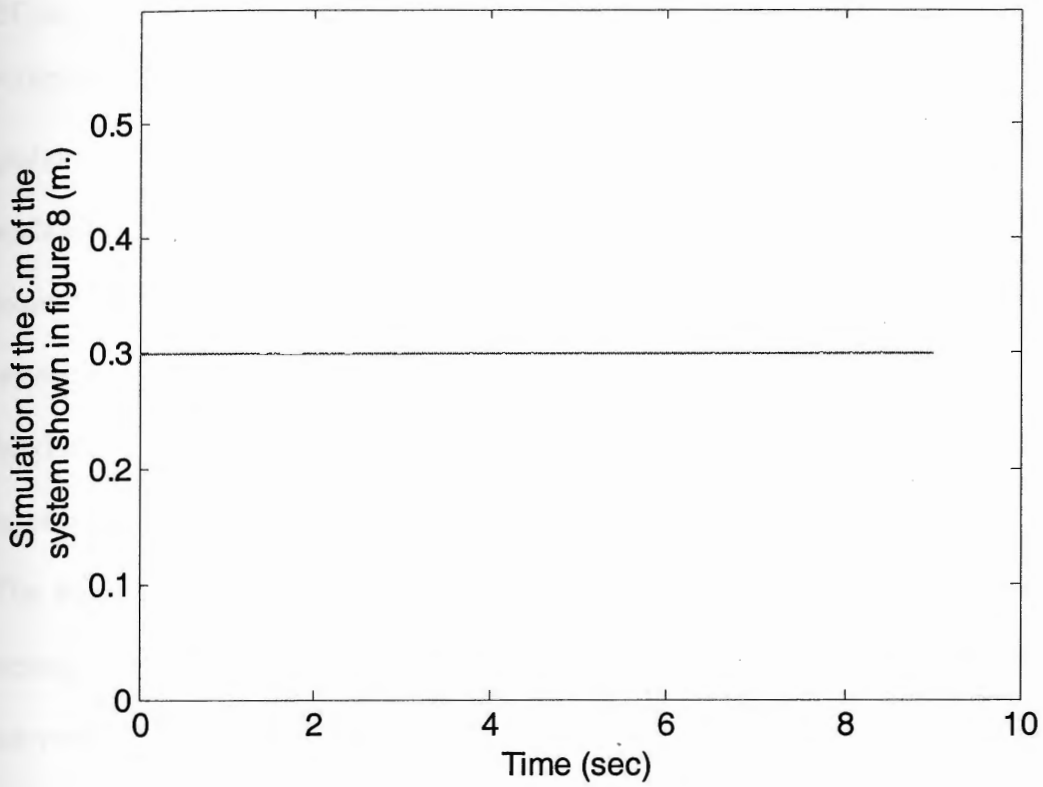

Figure 40 – Displacement of the center mass of the whole system, which is shown in Figure 35. The system c.m does not change its position during the simulation period.

II.6 Conclusions:

In this work equations of motion are automatically developed in a symbolic form. using the EOMC symbolic code. Furthermore, a simple transforming code TSC has been developed, which converts any non-linear n-order ODE system to a 1st ODE system. EOMC, and TSC together can be used as a tool to develop the equations of motion of any dynamic system in a format which can be numerically simulated in Matlab. Solver ode45 in Matlab is used, to integrate the equations of motion. This solver, which is based on the single step Runge-Kutta integration method, provides accurate simulation outputs [Tenenbaum, M., et al, 1985]. Therefore, it is concluded that EOMC, TSC, and ode45 together is a powerful and accurate tool to simulate motion of any dynamic system.

The third example shows that 'Gross Motion' is not possible for a simple mechanical device, which is the building block of many IPS. These results have been verified using WM.

Note, that the integration time step in working model and Matlab can be adjusted to provide output integration at the same period step using 'the integration time step' and the 'MaxStep' option in WM and Matlab respectively.

II.7 Future Work:

We will work with the U.S.Patent office to persuade them to reject patent applications, claiming gross linear motion based on Inertial Propulsion Systems.

II.8 References

1. Walls, A, D., Theory and Problems of Lagrangian Dynamics, McGraw-Hill, New york, 1967.
2. Greenwood, D., T., Principals of Dynamics, 2nd ed., Prentice-Hall, Englewood Cliffs, NJ, 1988.
3. Thornson, B.R. Apparatus for Developing a Propulsion Force, U.S. Patent # 4,631,971, Issued Dec. 30, 1986.
4. Saeed B., N., Introduction to Robotics Analysis, Systems, Applications, Prentice-Hall, Upper Saddle River, NJ, 2001.
5. Paul, Richard P., Robot Manipulators, Mathematics, Programming, and Control, The MIT Press, 1981.
6. Datseris, Philip, Advanced Dynamic Class Notes, 2003.
7. Shahinpoor, Mohsen, A Robot Engineering Textbook, Harpor and Raw, New York, 1987.
8. Asada, Haruhiko, J. J. E., Slotine, Robot analysis and control, John Wiley and Sons, New York, 1986.
9. Sciavicco, Lorenzo, B. Siciliano, Modeling and Control of Robot Manipulators, McGraw-Hill, New York, 1996.
10. Fu, K. S., R. C. Gonzalez, C. S.G. Lee, Robotics: Control, Sensing, Vision, and Intelligence, McGraw-Hill, 1987.

11. Featherstone, R., 'The Calculation of Robot Dynamics Using Articulated-Body Inertias," The International Journal of Robotics Research, Vol. 2, No. 1, pp. 13 – 30, Spring 1983.

12. Shahinpoor, M., "Dynamics," International Encyclopedia of Robotics: Applications and Automation, Richard C. Dorf, Editor, Johan Wiley and Sons, New York, pp. 329 – 347, 1988.

13. Vibet C., "Dynamics Modeling of Lagrangian Mechanisms from Inertial Matrix Elements," Elsevier Science, Comput. Methods Appl. Mech. Engrg. 123, pp. 317 – 326, 1995.

14. M. Richard and C. Gosselin, "A survey of Simulation programs for the Analysis of Mechanical Systems," Math. Comput. Simul. 35, pp 103 – 121, 1993.

15. K. Lilly and D. Orin, "Alternate Formula for Manipulator inertial Matrix," Int. J. Robatic Res. 10(1), pp. 64 – 74, 1991.

16. G. Chrbonneau, S. Vinarnick, P. Neel, C. Eariste and C. Vibet, "Symbolic Modeling of Controlled Mechanics," Comput. Mehtods Appl. Mech. Engrg. 98, pp. 23 – 40, 1992.

17. R. Wang and P. Woo, "Using Maple for Symbolic Computations on Robotics," Int. J. Robotics and Autom. 7(2), pp. 41 – 49, 1992.

18. Zhe Li and Sridhar Kota, "Virtual Prototyping and Motion Simulation with ADAMS," Journal of Computing and Information Science in Engineering, Vol. 1, No. 3, pp. 276 – 279, September 2001.

19. M. Tenenbaum and H. Pollard, "Ordinary Differential Equations," ISBN 0 – 486 – 64940 –7, Dover edition 1985.

CHAPTER III: MODELING THORNSON'S MECHANISM

III.1. Abstract:

In this work, Thornson inertial propulsion system (IPS) [Thornson 1986] is modeled as a rigid multibody system. The motion of this model is numerically and virtually simulated with Matlab and WM respectively.

The equations of motion code (EOMC) based on Lagrange's equation [Almesallmy et al.] is used to generate the equations of motion symbolically in Maple software. The developed equations of motion are numerically solved using Matlab software to investigate motion of the system. In addition, a virtual software 'Working Model' (WM) is also used to simulate the motion of Thornson's purposed IPS.

Both simulations (from Matlab and WM) conclude that the Thornson mechanical system cannot provide gross motion (continuous linear motion of the c.m of the system in either direction), see [Almesallmy et al.].

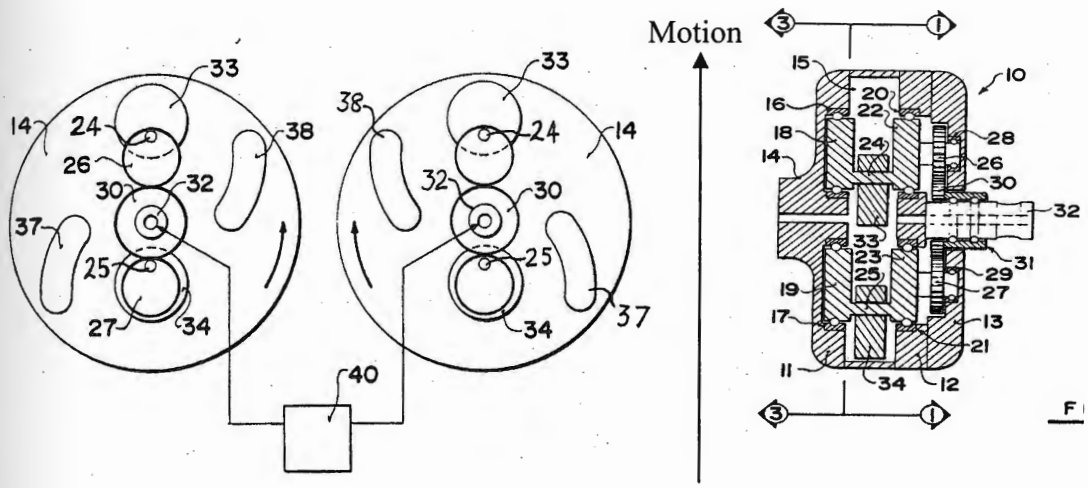

Figure 41 – Thornson Inertial Propulsion System (IPS) [1]. It is composed of two units. Each unit is composed of a sun gear 30, two planetary gears 26, and 27, and two eccentric masses 33, and 34. Each eccentric mass is attached to one of the planetary gears. In addition, two magnets 37, and 38 are attached to each unit as shown in the Figure.

III.2 Introduction

Figure 41 shows Thornson's IPS [1]. Figure 42 is a model of Thornson's mechanism. The goal of this modeling is to investigate the following two claims:

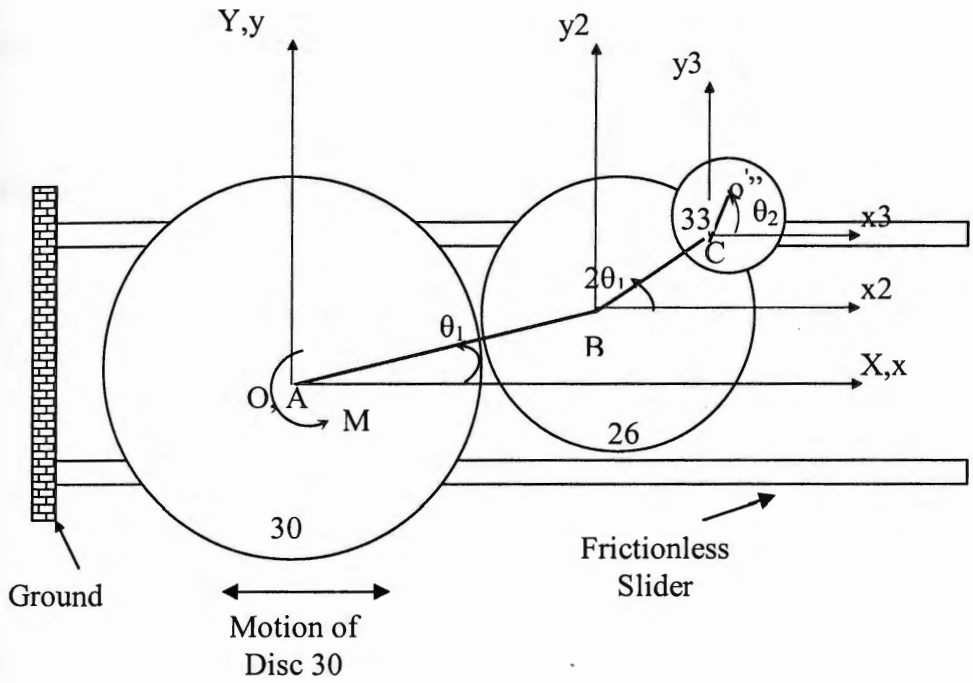

Figure 42 – models Thornson's IPS, Figure 41. From left to right, the three circles represent the stationary gears 30, the planetary gears 26, and the eccentric masses 33 in Thornson's IPS respectively, and all are mounted on frictionless slider as shown. The arrow directions show the only permitted motions of gear 30. M represents the motor torque at A. The effects of magnet 37, and 38 are modeled as initial condition. Therefore, the magnets are not shown in this Figure.

Claim 1:

Thornson [1, p.3] and Valone [3, p.1487 fig.7] claimed that the eccentric mass 33 nearly positions itself outward during 360° rotational motion of gear 26.

Claim 2:

Furthermore, Thornson [1], page 5 claimed that the magnet causes the eccentric mass 33 to have a whip-like effect, which in turn provides Thornson IPS with unidirectional gross motion.

However, to investigate the previous two claims, two submodels of Thornson's device are examined.

III.3 Submodel # 1

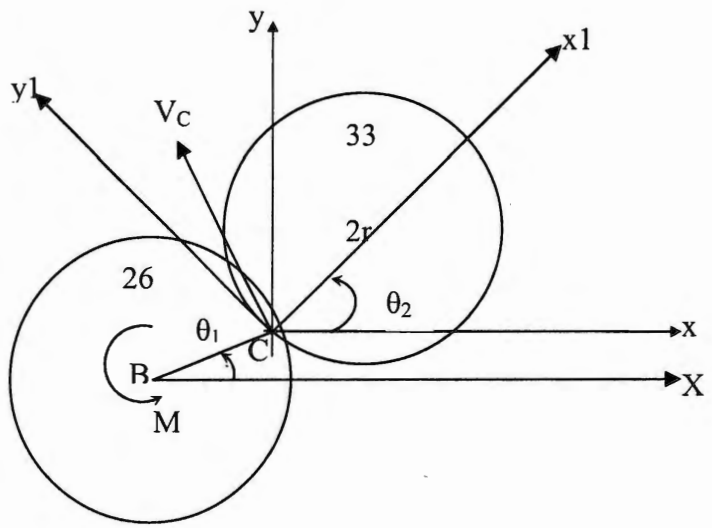

Figure 43 – A weightless disc 26 is driven with motor M, and disc 33 is mounted on disc 26 with hinge C. Disc 26 has one degree of freedom in θ_1 coordinate only.

The objective of the model shown in Figure 43 is to investigate the first claim that the eccentric mass 33 nearly positions itself outward during 360° rotational motion of gear 26. Figure 43, assumes a massless disc 26 is driven with a motor. The motor provides torque M to disc 26 at its center B. Disc 33 is mounted on disc 26 with hinge C.

This model shows that the two generalized coordinates θ_1, and θ_2 are required to describe the system's motion. However, to simulate the motion, the four steps procedures which are explained in [2] shall be applied again as follows:

III.3.1 Step # 1: Developing the expression of the four variable T, V, F, and Q

Gear 26 and the eccentric mass 33 both rotate in a horizontal plane, Figure 43. Therefore, potential energy V is zero. Also, friction between disc 26 and eccentric mass 33, is assumed negligible. Therefore, no energy dissipation exists and therefore, F is equal zero. Q is equal to M (motor torque) at coordinate θ_1, because the motor is located at the center of Disc 26, Figure 43.

Then, the four variables T, V, F, and Q for the model shown in Figure 43 are defined as follows;

$$T := \frac{1}{2} m r^2 \left(\frac{\partial}{\partial t} \theta 1(t) \right)^2 + \frac{1}{2} (I + m r^2) \left(\frac{\partial}{\partial t} \theta 2(t) \right)^2 + m r^2 \left(\frac{\partial}{\partial t} \theta 1(t) \right) \left(\frac{\partial}{\partial t} \theta 2(t) \right) \cos(\theta 2(t) - \theta 1(t))$$

V:= 0:

F:= 0:

Q_θ_1:= M: Q_θ_2:= 0:

where,

m = is the mass of the eccentric mass 33

r = is the radius of both Disc 26, and mass 33

I = is the mass moment of inertia of mass 33 with respect to an axis passing through its c.m.

θ_1 (t) = is the angular displacement in general coordinate θ_1, and it is function of time

θ_2 (t) = is the angular displacement in general coordinate θ_2, and it is function of time.

M = is the motor torque which is delivered at the c.m. of disc 26.

Note,

1. The kinetic energy T of this model is calculated for Body-fixed axes [SCHAUM's Book] for the eccentric mass 33 only, neglecting the energy of disc 26 because it is assumed massless.
2. To simulate the motion of the eccentric mass, which has free rotational motion around hinge C, one can use either Body-fixed axis or Direction-fixed axes.

III. 3.2 Step # 2: Developing the equations of motion

Figure 43 shows that θ_1, and θ_2 are two generalized coordinates, which are required to simulate the motion. In other words, the EOMC [Almesallmy, et al.] shall be employed two times to develop the two equations of motion. This can be accomplished by substituting for the q in EOMC with the coordinates θ_1, and θ_2 respectively. These two substitutions develop the following two equations of motion:

$$EQ1 := -m\,r^2\,(-\cos(\theta 2(t))\sin(\theta 1(t)) + \sin(\theta 2(t))\cos(\theta 1(t)))\left(\frac{\partial}{\partial t}\theta 2(t)\right)^2$$
$$- m\,r^2\,(-\cos(\theta 2(t))\cos(\theta 1(t)) - \sin(\theta 2(t))\sin(\theta 1(t)))\left(\frac{\partial^2}{\partial t^2}\theta 2(t)\right)$$
$$+ m\,r^2\left(\frac{\partial^2}{\partial t^2}\theta 1(t)\right) = M$$

$$EQ2 := (I + m\,r^2)\left(\frac{\partial^2}{\partial t^2}\theta 2(t)\right)$$
$$+ (m\,r^2\cos(\theta 2(t))\cos(\theta 1(t)) + m\,r^2\sin(\theta 2(t))\sin(\theta 1(t)))\left(\frac{\partial^2}{\partial t^2}\theta 1(t)\right)$$
$$- m\,r^2\cos(\theta 2(t))\sin(\theta 1(t))\left(\frac{\partial}{\partial t}\theta 1(t)\right)^2 + m\,r^2\sin(\theta 2(t))\cos(\theta 1(t))\left(\frac{\partial}{\partial t}\theta 1(t)\right)^2$$
$$= 0$$

III.3.3 Step # 3: Reforming the 2nd order equations of motion for Matlab simulation

The previous two equations of motion can be used in Matlab, but first reduction of the 2nd order differential terms to 1st order must be performed as it is explained in [Almesallmy et al.]. The developed two equations EQ1, and EQ2 are already coded here in a Matlab file as dy(3), and dy(4) respectively, see Appendix E.

III.3.4 Step # 4: Simulations

Figures 44, and 45 show the simulation of motion of disc 26, and the eccentric mass 33, respectively. Results appear to be identical but they are not. The plot in Figure 46 is calculated by subtracting the angular position (θ_1) of disc 26 (Figure 44) from the corresponding one (θ_2) of the eccentric mass 33 (Figure 45).

Figure 46 shows that the angular motion of the eccentric mass 33 w.r.t joint C looks like a damped harmonic motion during the first 10 seconds of the simulation. This apparent damping is because the system is driven with a constant torque (not constant velocity). However, Figure 46 shows that disc 33 has a substantial harmonic motion amplitude of ± 1.25 rad with respect to line BC, Figure 43, where the system starts from rest. This amplitude decreases as the motion continues but the angular magnitude of the reciprocating motion of disc 33

with respect to BC is about ± 70° after more than 10 full revolutions of disc 26, which is significant amplitude.

It is concluded that the eccentric mass 33 cannot be considered "nearly outward" as Thornson claims in his patent [Thornson 1986] and as Valone claims [Valone 1994].

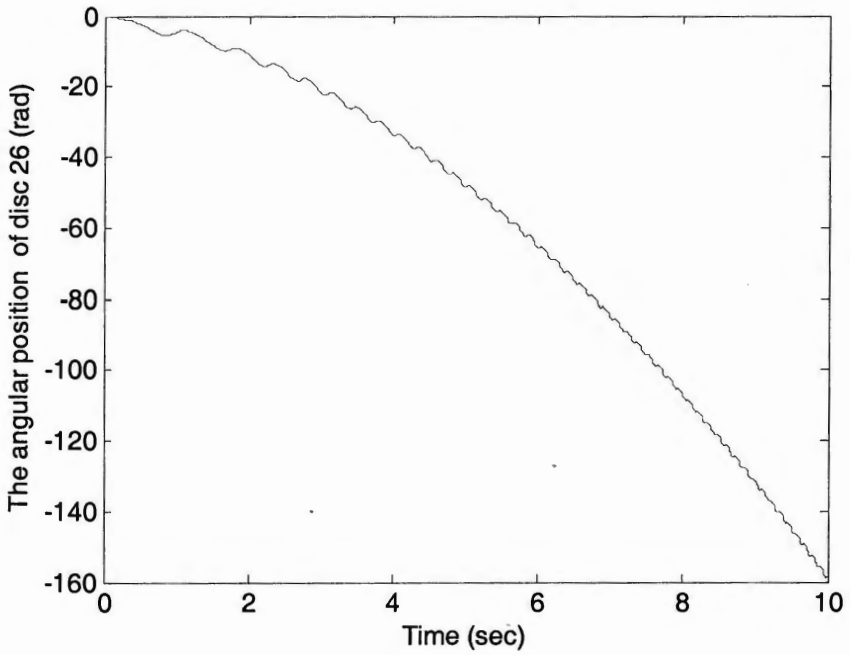

Figure 44 – shows the simulation of the angular position (θ_1) of Disc 26 w.r.t the inertial frame X-Y, see Figure 43.

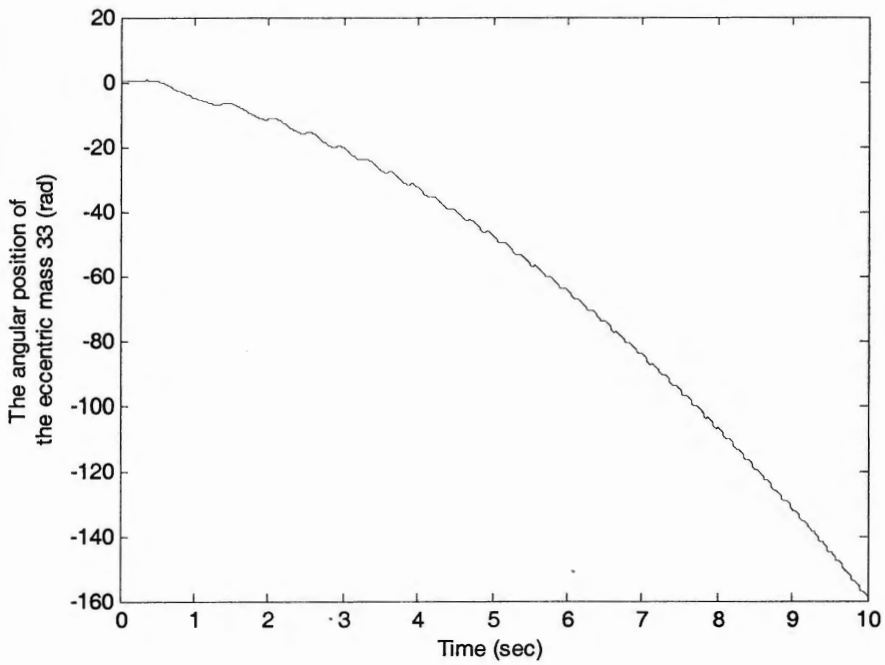

Figure 45 – Simulation of the angular position (θ_2) of the eccentric mass 33 w.r.t the inertial frame X-Y, see Figure 43.

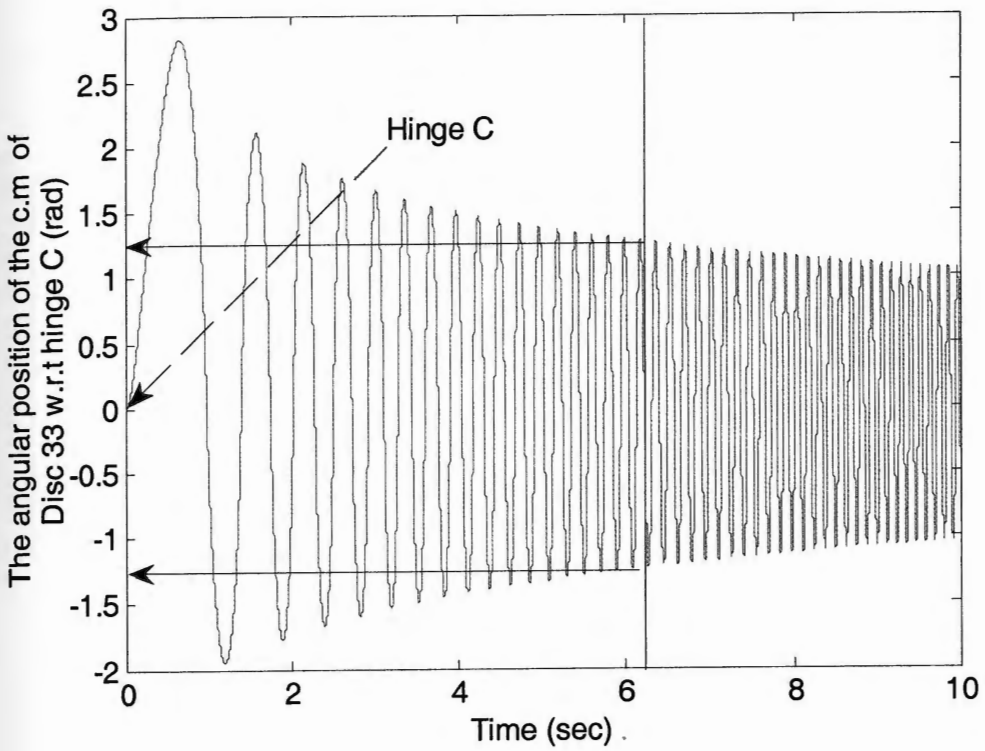

Figure 46 – This harmonic motion profile is the simulation of the angular position (θ_3) of the eccentric mass 33 with respect to line BC, Figure 43. $\theta_3 = \theta_1 - \theta_2$. Also, It shows that disc 33 is still oscillating with angular displacement of ±1.25 rad with respect to line BC, Figure 43, after 6.3 sec (time of full cycle of hinge C), Figure 47. The apparent change in frequency is because the system is driven with constant torque (not constant velocity).

III.4 Submodel #2

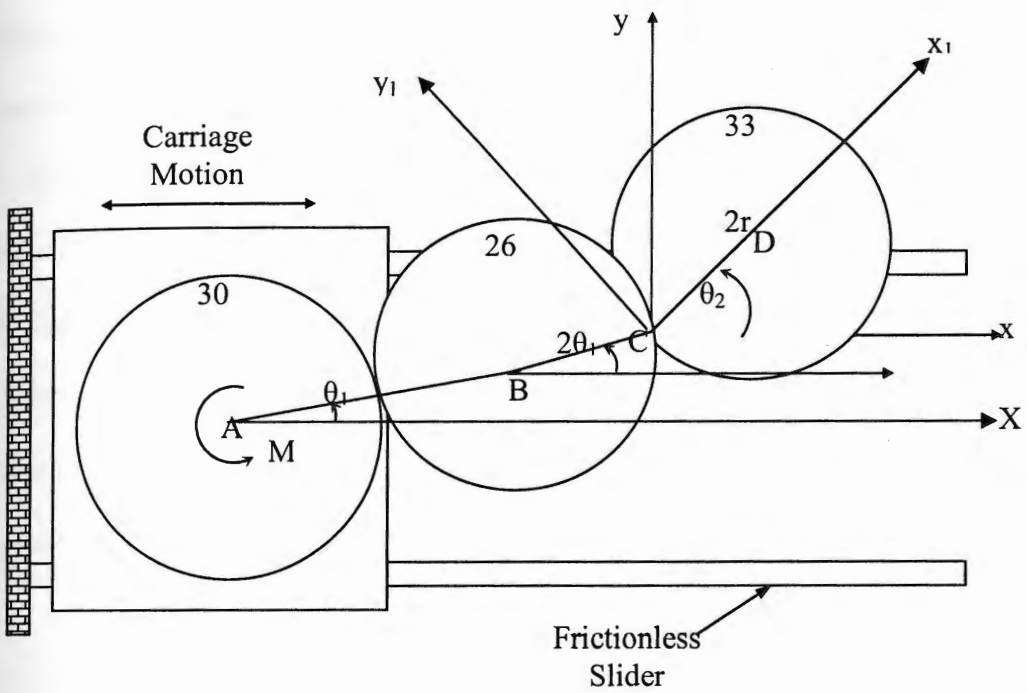

Figure 47 – shows the same model shown in Figure 42, but with an additional assumption that the three discs 30, 26, and 33 are similar. The Y axis of the inertial frame is not shown in this Figure.

The objective of the model shown in Figure 47 is to investigate the second claim by Thornson [1, p.5] that the magnets 37, and 38 shown in Figure 41 cause the eccentric mass 33 to have a whip-like effect, which in turn provides Thornson IPS with "Gross Motion." Figure 47, assumes the three bodies 30, 26, and 33 are

similar. The motor provides torque M to an arm AB, which in turn is connected to the c.m. of disc 26 at (B). Disc 26 is rotating around its c.m. (B) and with the arm AB. Disc 33 is mounted on disc 26 with hinge C and its motion in generalized coordinate, θ_2. Furthermore, the whole model can move in X-coordinate as the arrow of the carriage motion indicates.

This model shows that only three generalized coordinates, θ_1, θ_2, and X are required to describe its motion. The rotation of disc 26 around disc 30 is related to the rotational motion of the arm AB and is defined as $2^* \theta_1$, see Figure 47. Therefore, there is no need for an additional generalized coordinate. The four-step procedures, which are explained in [Almesallmy et al.] shall be applied again as shown below to develop the equations of motion.

III.4.1 Step # 1: Developing the expression of the four variable T, V, F, and Q

By investigating Thornson model, which is shown in Figure 47, one can realize that it is composed of two submodels. The first submodel is the third example in [Almesallmy et al.], where the motion was investigated for discs # 1, and # 2. The two discs 30, and 26 in Thornson are the same as discs # 1, and # 2 respectively. The second submodel is the previous one shown in Figure 43, where the motion of the eccentric mass 33 was investigated.

Therefore, to simulate Thornson motion, the two submodels are added together. This is done by adding the variables T, V, F and Q of the two

submodels to develop the equations of motion for Thornson model as shown below:

$$T = \{T\}_{sub1} + \{T\}_{sub2}$$

$$T = \{[\tfrac{1}{2} m_1 v_A{}^2] + [\tfrac{1}{2} m_2 v_B{}^2 + \tfrac{1}{2} I_{m2} (2^* \dot{\theta}_1)^2]\}_{sub1}$$

$$+$$

$$\{[1/2\ m_3\ v_D{}^2 + T_D']\}_{sub2}$$

Where,

$\{T\}_{sub1}$ = Kinetic energy of submodel 1, which is composed of the kinetic energy of discs 30, and 26, see [Almesallmy et al. 2006].

$\{T\}_{sub2}$ = Kinetic energy of submodel 2. Actually, it is the kinetic energy of the eccentric mass 33 at hinge C (and not at the c.m of the eccentric mass 33.)

v_D = The velocity of the eccentric mass 33 is derived as follows:

r_D = the position of the c.m of disc 33 at a certain time.

$$= X + 2\ r\ e^{i\theta_1} + r\ e^{i2\theta_1} + r\ e^{i\theta_2}$$

$$v_D = \dot{X} + 2\ r\ i\ \dot{\theta}_1\ e^{i\theta_1} + 2\ r\ i\ \dot{\theta}_1\ e^{i2\theta_1} + r\ i\ \dot{\theta}_2\ e^{i\theta_2}$$

$$= [\dot{X} - 2\ r\ \dot{\theta}_1\ (\sin(\theta_1) + \sin(2\theta_1) + \sin(\theta_2))] +$$

$$[2\ r\ \dot{\theta}_1\ (\cos(\theta_1) + \cos(2\theta_1) + \cos(\theta_2))]$$

$$= [(v_D)_X] + [(v_D)_Y]$$

T_D' = kinetic energy of disc 33 due to its small oscillations about hinge C and for simplicity can be ignored.

The previous added terms in T expression, express the kinetic energy of the three bodies 30, 26, and 33 respectively, see Figure 47. The first term represents the kinetic energy of disc 30. The second and third terms represent the kinetic energy of disc 26. The fourth, and fifth terms represent the kinetic energy of disc 33 which is calculated at the c.m of the disc.

Therefore, the final kinetic energy expression (T) of Thornson IPS and the other three variables V, F, Q will be as follows:

$T = \{[\frac{1}{2} m_1 v_A\text{^}2]+[\frac{1}{2} m_2 v_B\text{^}2 + \frac{1}{2} I_{m2} (2^* \dot{\theta}_1)\text{^}2]\}_{sub1} +\{[1/2\ m_3\ v_D\text{^}2]\}_{sub2}$

The previous T expression is expressed in Maple in following form:

$$T:=\frac{1}{2}m\left(\frac{\partial}{\partial t}\mathrm{X}(t)\right)^2 +\frac{1}{2}m\left(\left(\left(\frac{\partial}{\partial t}\mathrm{X}(t)\right)-2r\left(\frac{\partial}{\partial t}\theta 1(t)\right)\sin(\theta 1(t))\right)^2+4r^2\left(\frac{\partial}{\partial t}\theta 1(t)\right)^2\cos(\theta 1(t))^2\right) +2I\left(\frac{\partial}{\partial t}\theta 1(t)\right)^2+\frac{1}{2}m\left(\left(2\left(\frac{\partial}{\partial t}\theta 1(t)\right)r\left(\cos(\theta 1(t))+\cos(2\,\theta 1(t))\right)+r\left(\frac{\partial}{\partial t}\theta 2(t)\right)\cos(\theta 2(t))\right)^2+\left(-2\left(\frac{\partial}{\partial t}\theta 1(t)\right)r\left(\sin(\theta 1(t))+\sin(2\,\theta 1(t))\right)-r\left(\frac{\partial}{\partial t}\theta 2(t)\right)\sin(\theta 2(t))+\left(\frac{\partial}{\partial t}\mathrm{X}(t)\right)\right)^2\right)$$

```
V:= 0:
```

F:= 0:

Q_θ_1:= M: Q_θ_2:= 0: Q_X:= 0:

where

m1 = m, is the mass of disc 30

m2 = m, is the mass of disc 26

m3 = m, is the mass of the eccentric disc 33

r = is the radius of discs 30, 26, and the eccentric mass 33

I = is the mass moment of inertia of each of the three bodies 26, and 33 with respect to an axis passing through the c.m. of each body and perpendicular to this page.

θ_1 = is the angular position of arm AB.

θ_2 = is the angular position of the eccentric mass 33.

X = is the linear position of disc 30 in the generalized coordinate X.

$\dot{\theta}_1$ = is the angular velocity of arb AB in θ_1 - coordinate.

$\dot{\theta}_2$ = is the angular velocity of the eccentric mass 33 in θ_2-coordinate.

$\dot{X}$ = is the linear velocity of disc 30 in X-coordinate.

M = is the motor torque which is delivered to disc 26 through link AB.

III.4.2 Step # 2: Developing the equations of motion

Figure 47 shows that θ_1, θ_2, and X are the generalized coordinates, which are required to simulate the motion. In other words, the EOMC shall be employed three times to develop the equations of motion in these three coordinates. This can be accomplished by substituting for the q in EOMC with the coordinates θ_1, θ_2, and X which provides the three equations EQ1, EQ2, and EQ3 respectively:

$$EQ1 := (-4\,m\,r\sin(\theta1(t))\cos(\theta1(t)) - 4\,m\,r\sin(\theta1(t)))\left(\frac{\partial^2}{\partial t^2}\mathrm{X}(t)\right) + (4\,m\,r^2\sin(\theta1(t))\cos(\theta1(t))\sin(\theta2(t)) - 2\,m\,r^2\cos(\theta2(t)) + 2\,m\,r^2\sin(\theta1(t))\sin(\theta2(t)) + 2\,m\,r^2\cos(\theta1(t))\cos(\theta2(t)) + 4\,m\,r^2\cos(\theta1(t))^2\cos(\theta2(t)))\left(\frac{\partial^2}{\partial t^2}\theta2(t)\right) + (8\,m\,r^2\cos(\theta1(t)) + 4\,I + 12\,m\,r^2)\left(\frac{\partial^2}{\partial t^2}\theta1(t)\right) - 4\,m\,r^2\sin(\theta1(t))\left(\frac{\partial}{\partial t}\theta1(t)\right)^2 + (2\,m\,r^2\sin(\theta2(t)) + 2\,m\,r^2\sin(\theta1(t))\cos(\theta2(t)) - 2\,m\,r^2\cos(\theta1(t))\sin(\theta2(t)) - 4\,m\,r^2\cos(\theta1(t))^2\sin(\theta2(t)) + 4\,m\,r^2\cos(\theta1(t))\cos(\theta2(t))\sin(\theta1(t)))\left(\frac{\partial}{\partial t}\theta2(t)\right)^2 = M$$

$$EQ2 := -m\,r\sin(\theta2(t))\left(\frac{\partial^2}{\partial t^2}\mathrm{X}(t)\right) + m\,r^2\left(\frac{\partial^2}{\partial t^2}\theta2(t)\right) + m\,r\,(4\,r\cos(\theta1(t))^2\cos(\theta2(t)) + 2\,r\cos(\theta1(t))\cos(\theta2(t)) + 4\,r\sin(\theta1(t))\cos(\theta1(t))\sin(\theta2(t)) - 2\,r\cos(\theta2(t)) + 2\,r\sin(\theta1(t))\sin(\theta2(t)))\left(\frac{\partial^2}{\partial t^2}\theta1(t)\right) + m\,r\Bigg(-2\,r\sin(\theta1(t))\left(\frac{\partial}{\partial t}\theta1(t)\right)^2\cos(\theta2(t)) + 8\,r\cos(\theta1(t))^2\left(\frac{\partial}{\partial t}\theta1(t)\right)^2\sin(\theta2(t)) - 4\,r\left(\frac{\partial}{\partial t}\theta1(t)\right)^2\sin(\theta2(t)) + 2\,r\cos(\theta1(t))\left(\frac{\partial}{\partial t}\theta1(t)\right)^2\sin(\theta2(t)) - 8\,r\cos(\theta1(t))\cos(\theta2(t))\sin(\theta1(t))\left(\frac{\partial}{\partial t}\theta1(t)\right)^2\Bigg) = 0$$

$$EQ3 := 3\,m\left(\frac{\partial^2}{\partial t^2}\mathrm{X}(t)\right) - m\,r\left(\frac{\partial^2}{\partial t^2}\theta 2(t)\right)\sin(\theta 2(t))$$
$$- m\,(4\,r\sin(\theta 1(t)) + 4\,r\sin(\theta 1(t))\cos(\theta 1(t)))\left(\frac{\partial^2}{\partial t^2}\theta 1(t)\right) - m\Bigg($$
$$8\,r\cos(\theta 1(t))^2\left(\frac{\partial}{\partial t}\theta 1(t)\right)^2 - 4\,r\left(\frac{\partial}{\partial t}\theta 1(t)\right)^2 + 4\,r\cos(\theta 1(t))\left(\frac{\partial}{\partial t}\theta 1(t)\right)^2$$
$$+ r\left(\frac{\partial}{\partial t}\theta 2(t)\right)^2\cos(\theta 2(t))\Bigg) = 0$$

III.4.3 Step # 3: Reformulating the 2nd order equations of motion for Matlab simulation

These equations can be solved using Matlab after reduction of the 2nd order differential terms to 1st order, as explained in [2]. The developed three equations are shown as dy(4), dy(5), and dy(6) in Matlab file, Appendix F, [M Almesallmy, Dissertation].

III.4.4 Step # 4: Simulations

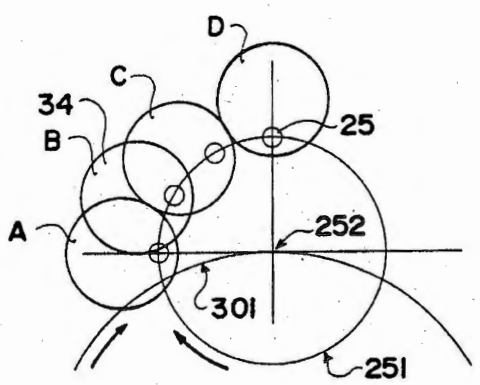

Figure 48 – Schematic showing, according to a claim by Thornson, that a magnet holds the eccentric mass 33 for ¼ revolution of the motion of hinge 25, [Thornson 1986]

The dynamic simulation of Thornson IPS (Figure 41) is composed of two stages. These two stages are needed to simulate the effects of the magnet poles 37, and 38 (see Figure 41) on the system's motion.

In spite of the magnetic force between the eccentric mass 33 and the magnet pole 37 can be expressed directly in Lagrange's equations, but the magnet effect is introduced to Lagrangian as IC^s to simulate Thornson's claim.

Thornson's claim is as follows: "Figure 48 shows that the magnet pole 37 holds the eccentric mass 33 for a period of ¼ of revolution of disc 26 or hinge C. The onset the magnet release the eccentric mass 33 till the next release the whip-like motion of mass 33 provides the mechanism with a certain magnitude of linear displacement in X–coordinate."

The first stage of the simulation is solving the previous three equations of motion for the IC^s of set A shown in Table 1 in order to develop the new IC^s of set B shown in Table 2. The IC^s of set B simulates the magnetic effects. This first stage simulates the motion behavior of Thornson IPS when there are no magnets. The second stage simulation is solving the previous three equations again but for the IC^s of set B in order to simulate the motion of Thornson IPS under the magnetic effects.

III.4.4.1 First stage, simulation for the initial conditions of set 'A'

Figure 49 shows Thornson model in its initial position. The whole model is driven with a motor of torque M, starting from rest. The three bodies (30, 26,

and 33) are assumed similar, where its masses (m), and radii (r) and the motor torque are assumed as follows:

r = 0.3 m,

m = 2.0 kg,

M = 2.0 N.m

Table 1: Initial conditions of set A	
In_θ_1 = 0 rad	In_dθ_1 = 0 rad/sec
In_ θ_2 = 0 rad	In_dθ_2 = 0 rad/sec
In_X = 0 m	In_dX = 0 m/sec

Where,

In_ θ_1, and In_ θ_2 are the initial angular positions, and In_d θ_1, and In_d θ_2 are the initial angular velocities respectively. In_X is the initial linear position, and In_dX is the initial linear velocity.

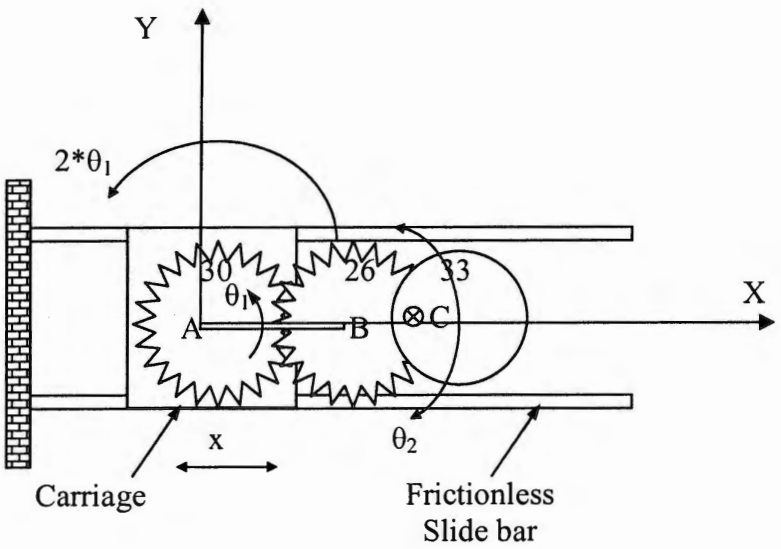

Figure 49 – shows the initial conditions of set A; where the bodies 30, 26, and the eccentric mass 33 have same radius r and oriented at zero angular position from X-coordinate ($\theta_1 = \theta_2 = 0$). Gear 30 is placed at zero linear position (X=0) where its c.m is placed at the origin of XY inertial frame. Gear 30 is fixed on the carriage and translates with it, A is the center of rotation of arm AB, which in turn rotates gear 26 around gear 30 (as indicated with arrow $2*\theta_1$), and the eccentric mass 33 is free to rotate around hinge C.

Solving the previous equations of motion for the IC^s of set A provides the motion simulation shown in Figures 50, 51, and 52. Figure 50 shows the motion of link AB in θ_1 – coordinate takes 9.4 sec to complete five full revolutions. Figures 51 and 52 show that the linear and the angular velocities of disc 30 and arm AB are zero m/sec, and - 8.5 rad/sec respectively, at 9.4 seconds.

The IC^s of set B is chosen at that instant at which arm AB completes five full rotations in θ_1-coordinate. Therefore, the IC^s of set B can be written as follows:

Table 2: The initial conditions of set B	
In_θ_1 = 0 rad	In_d θ_1 = -8.500 rad/sec
In_ θ_2 = - ½ π rad	In_d θ_2 = 0.00 rad/sec
In_X = 0.00 m	In_dX = 0.000 m/sec

Note, that the initial angular position of the eccentric mass 33 (In_ θ_2) is assumed negative 90° with respect to the positive X-coordinate, to consider Thornson claim that 'the magnet holds back the eccentric mass for a period of ¼ revolution,' see Figure 48.

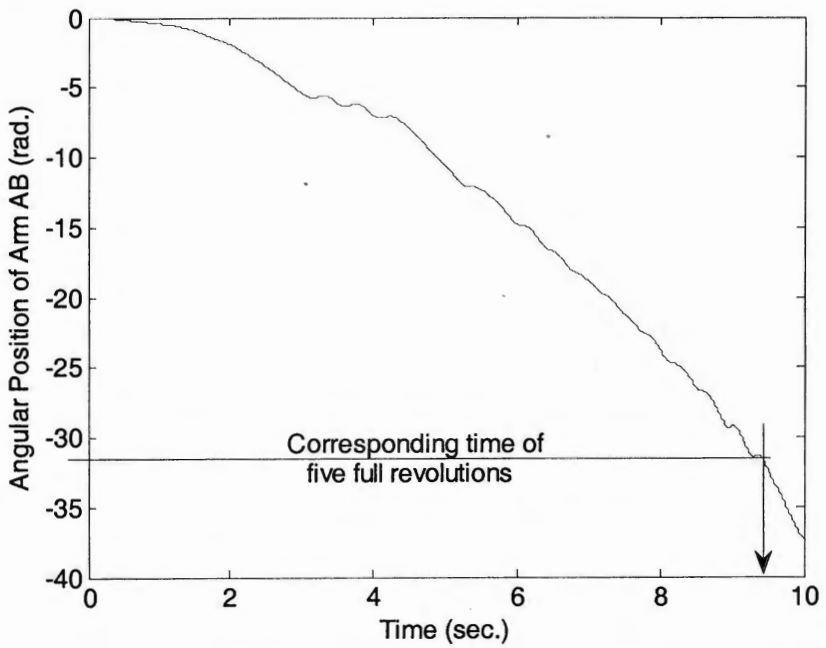

Figure 50 – Rotational position of arm AB in θ_1-coordinate, see Figure 47. It takes arm AB about 9.4 sec to complete five revolutions.

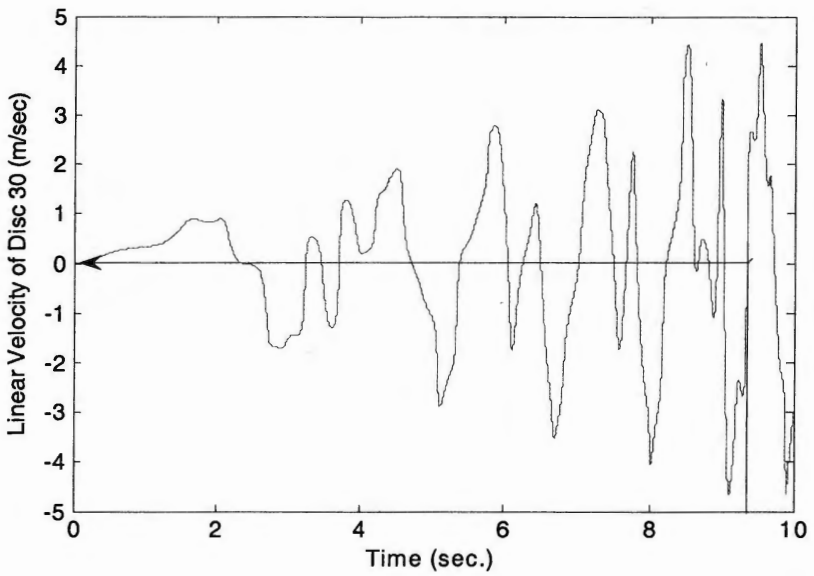

Figure 51 – Linear velocity of disc 30, $\dot{X} = 0$ m/sec (at simulation time of 9.4 sec.)

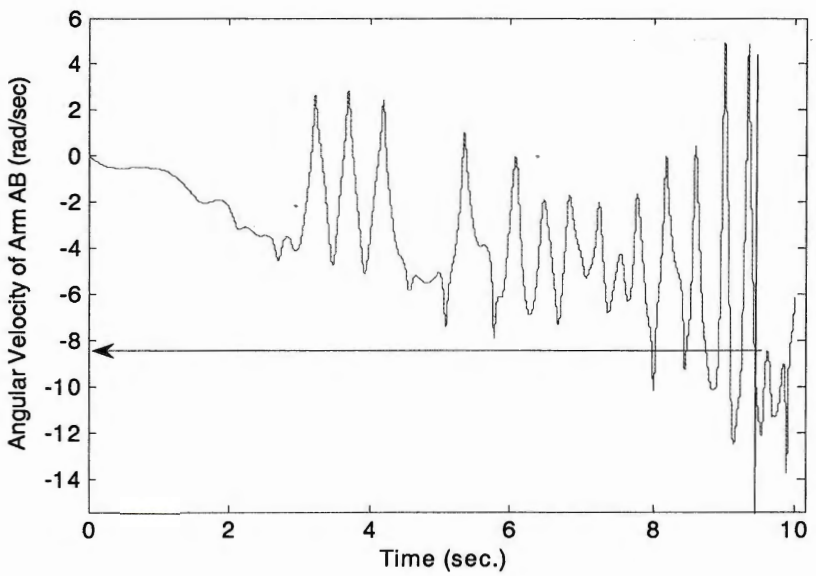

Figure 52 – Angular velocity of arm AB, $\dot{\theta}_1 = -8.5$ rad/sec (at simulation time of 9.4 sec.)

III.4.4.2 Second stage simulation for the initial conditions of set'B'

The simulation of Thornson IPS is the solution of the previous three equations of motion for the IC^s of B set. The goal of this simulation is to find the resultant displacement of body 30 at the onset that arm AB completes one full revolution. Therefore, for IC^s of sets A, and B, each of Figures 53, and 54 show the motion simulations of disc 30 and the projection of arm AB on the X-coordinate respectively.

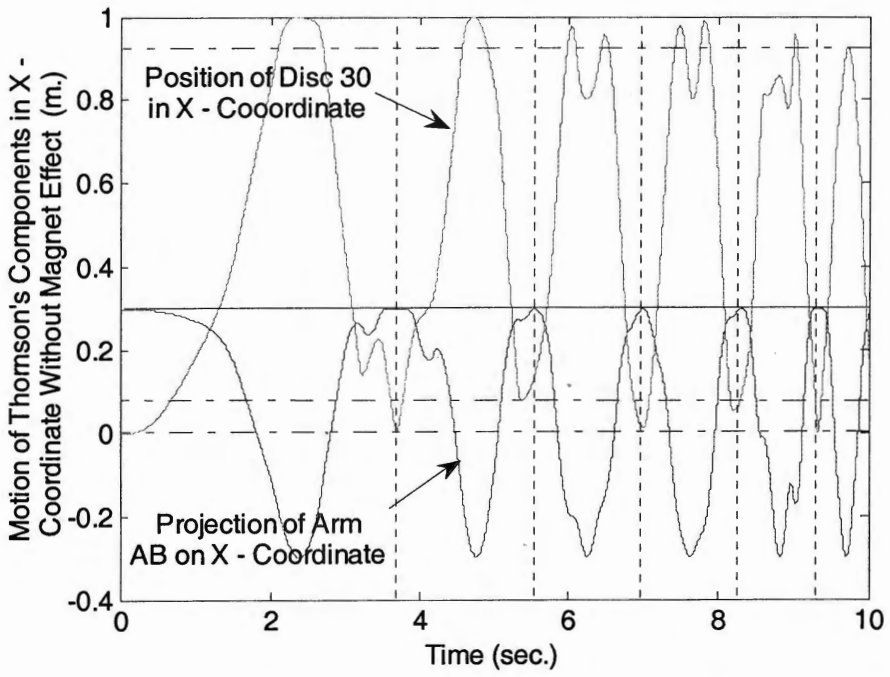

Figure 53 – For the IC^s of A set, the linear displacement of disc 30, and the projection of arm AB on the X-coordinate show that when arm AB completes one revolution disc 30 returns back to its initial position (0.0 m.)

Figure 54 shows that at the onset that arm AB completes one full revolution, disc 30 returns back to its initial position. In other words, the simulation for the IC^s set A predicts that Thornson IPS will have no gross motion.

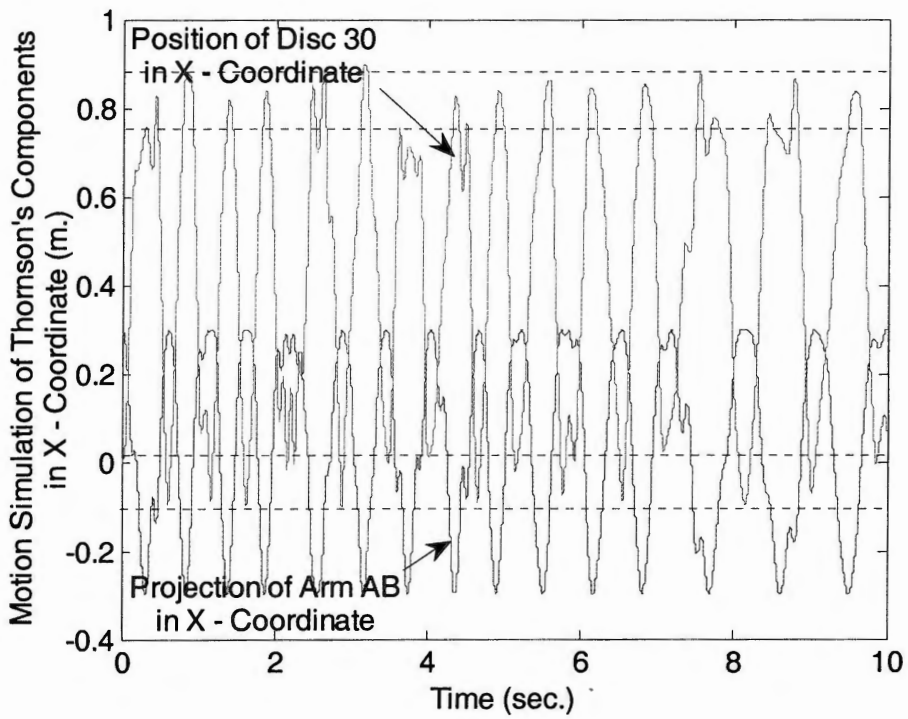

Figure 54 – For the IC^s of B set, the linear displacement of disc 30, and the projection of the c.m of arm AB on X-coordinate show the same motion behavior in Figure 54 with two differences. First, the amplitude of the motion position of disc 30 did not change but it is shifted equally at the two ends of the motion. Second, the two deviation of motion domains are also shifted equally w.r.t the motion ends with little increase. This Figure shows that the whip-like effect provides bigger harmonic amplitude but no gross motion for Thornson's IPS.

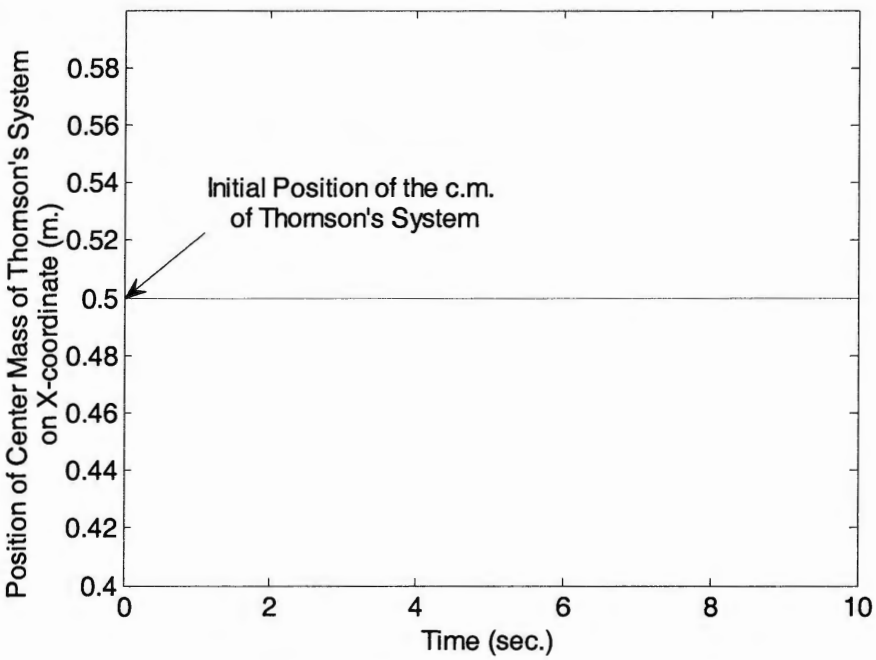

Figure 55 – X-coordinate of center mass of Thornson's system

Figure 54 shows the simulation of the motion of Thornson's IPS components in X-coordinate. Figure 54 shows that the magnet increases the frequency but it did not affect the harmonic motion amplitude of Thornson's IPS. Furthermore, figure 54 shows that in the first cycle (under initial conditions of set B) body 30 moves - 0.1 m with respect to its initial position. However, the system c.m, does not move from its initial position of 0.5 m, Figure 55. This proves that Thornson's device does not have any Gross Motion.

Therefore, it is concluded that the magnet poles 37, and 38 and the claim of the whip-like motion effect of the mass 33 will provide no gross motion for Thornson mechanism.

However, using the model shown in Figure 56, the motion simulation of Thornson IPS under the magnet effect is simulated in WM. The motion pattern of this model is tested in both 1-D and 2-D.

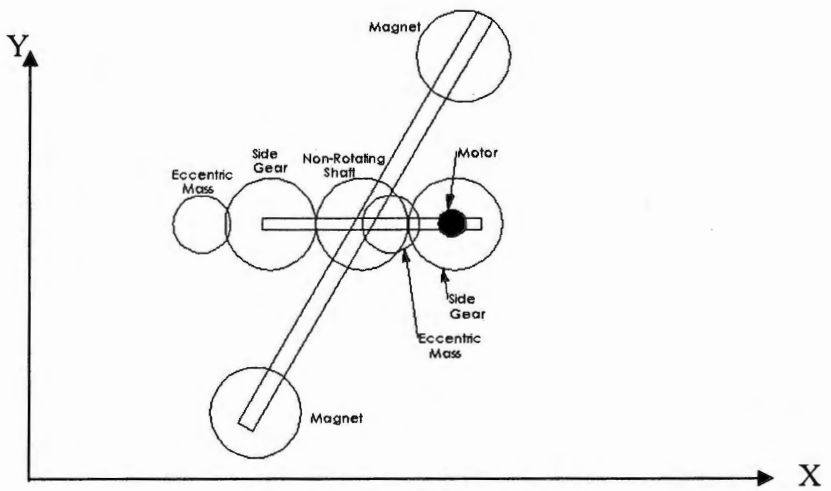

Figure 56 – Shows Thornson IPS model in WM. The model used to simulate the motion of Thornson's mechanism.

Figures 57 and 58 show the simulation of motion of the model shown in Figure 56. These Figures show that the model has a sinusoidal motion pattern in 1-D and 2-D simulation. Therefore, WM predicts that Thornson IPS will not have any unidirectional motion but a harmonic motion behavior.

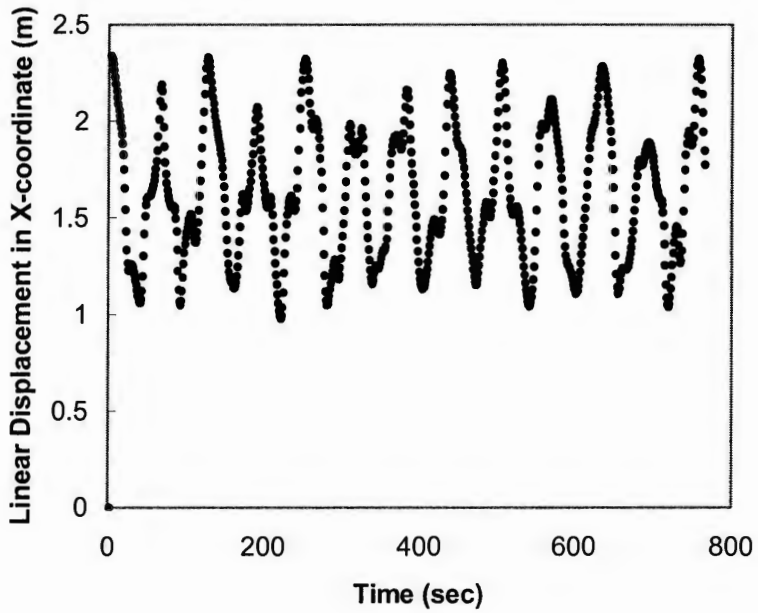

Figure 57 – 1-D simulation of motion of Thornson model, Figure 56 shows the model moves in harmonic motion in X-coordinate.

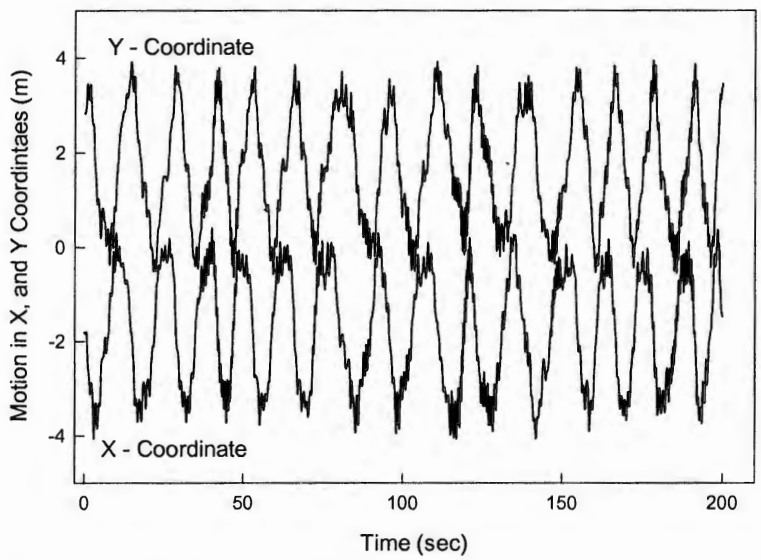

Figure 58 – 2-D simulation of motion of Thornson model, Figure 56 shows the mechanism moves in circular motion in X-Y plane.

III.5 Discussion and Conclusions:

In this work EOMC and ode 45 solver in Matlab is a good tool for developing equations of motion of complex mechanical systems.

In the Thornson's mechanism, the eccentric mass 33 cannot assume a "mostly" outward direction when magnets are not present. It is proven that the eccentric disc 33 will maintain angular motion amplitude of about ±1.25 rad. Furthermore, the Thornson device cannot provide gross motion, as the only contribution the magnet poles 37, and 38 provide is an increase in the frequency of the harmonic motion.

In summary, the conclusion of this work are as follows:

1- Maple code of eight steps code (EOMC) can be used to develop the equations of motion of any dynamic system.
2- WM is a good tool to show the motion pattern of any 2-D mechanism.
3- No motion can be achieved without an external force.
4- Thornson IPS cannot provide gross motion in the space.
5- Newton's laws are valid.
6- In mechanisms with large displacement, small oscillatory motion can be neglected for simplicity.

III.6 Future Work

Work with the U.S. Patent office to persuade them to automatically reject patent applications claiming gross linear motion based on inertial propulsion systems.

III.7 References

1. Thornson, B.R. Apparatus for Developing a Propulsion Force, U.S. Patent # 4,631,971, Issued Dec. 30, 1986.
2. M. Almesallmy and P. Datseris, "Simulation of Modeled Mechanical Systems Based on Lagrangian Mechanics," sent to ASME, Journal of Mechanical Design, 2006.
3. Valone, Thomas. "Inertial Propulsion: concept and experiment, part 2" proceedings of the intersociety Energy Conversion Engineering conference, v3, p 1484-1489, Aug. 1994.
4. M. Almesallmy, 'Experimental and Analytical Investigation of Inertial Propulsion Mechanics,' Ph.D. dissertation in MEAM, URI, 2006.
5. Dare A. Wells, 'Theory and Problems of Lagrangian Dynamics,' Schaum's Outline Series, ISBN 07 – 069258 – 0. Oct. 1967.
6. Haug, Edward 'Computer Aided Analysis and Optimization of Mechanical System Dynamics,' Computer and Systems Sciences, v 9, 700 p, 1984.
7. Sacks, E and Jaskowiez, leo, 'Model – Based Kinematic simulation,' ASME, Dynamic Systems and Control Division, v. 41, p. 83 – 91, 1992.
8. Anderson, K. S., 'Order n Formulation for Motion Simulation of General Multi – Rigid – Body Constrained System,' Computer and Structure, v. 43, n 3, p 565 – 579, May 3, 1992.

9. Anderson, K. S., 'Order n Formulation for Motion Simulation of General Multi – Rigid – Body Free System,' Computer and Structure, v. 46, n 3, p 547 – 559, Feb 3, 1993.

10. Bai, Jie and Tsuta, Toshio, 'Large Motion Response Analysis of Multi – Body Dynamics by Using Updated Lagrangian Method,' ASME, Pressure Vessels and Piping Division (publication) PVP, v. 301, p. 101 – 106, 1995.

11. Banerjee, A. K, 'Multi – Flexible Body Dynamics Capturing Motion – Induced Stiffness,' Journal of Applied Mechanics, Transactions ASME, v 58, n 3, p. 766 – 775, Sep. 1991.

12. Badreddin, Essameddin, Gambler, Adrian, 'Dynamic Modeling of MSF plants for Automatic Control and Simulation Purposes,' Desalination, v 166, n 1-3, Aug. 15, 2004.

APPENDICES

Appendix A: The Transform Symbolic Code (TSC)

It is an example of the symbolic code, which is used to transform n-order nonlinear coupled system of ODE to 1st order system. In addition this 1st order system became ready to be send to and solved numerically with Matlab.

The TSC is composed of five commands only. The reader can tailor them for any problem under investigation. For example, the equations of motion 6, 7 are used to explain the use of the TSC.

However, after equations 6 (EQ1), and 7 (EQ2) are developed, just write the following five commands in Maple software. These commands are explained afterwards.

```
1>
EQ:=subs({diff(X(t),`$`(t,2))=Y3,diff(Y(t),`$`(t,2))=Y4},{E
Q1,EQ2}):
2> EQ1:=EQ[1]; EQ2:=EQ[2];
3> Yt:= solve({EQ1,EQ2},{Y3,Y4}):
4>P3:=subs({diff(X(t),t)=y(3),diff(Y(t),t)=y(4)},collect(Yt[
1],{diff(X(t),t),diff(Y(t),t  )})):
4>P4:=subs({diff(X(t),t)=y(3),diff(Y(t),t)=y(4)},collect(Yt[
2],{diff(X(t),t),diff(Y(t),t  )})):
5> PP3:=simplify(subs({X(t)=y(1),Y(t)=y(2)},P3));
```

$$PP3 := Y4 = -(y(4)\,m1\,B + y(4)\,m2\,B + y(4)\,A\,m1 + A\,y(3)\,m1 + m1\,K2\,y(2) + m2\,K2\,y(2) - m2\,K1\,y(1))/(m2\,m1) \tag{8}$$

```
5> PP4:=simplify(subs({X(t)=y(1),Y(t)=y(2)},P4));
```

$$PP4 := Y3 = \frac{B\,y(4) + K2\,y(2) - K1\,y(1)}{m1} \tag{9}$$

Command 1 substitutes Y3, and Y4 for the second derivative w.r.t time of X, and Y respectively (note it is case sensitive). The output of command 1 put the two equation in one bract. Command #2 pulls out each equation from the result of command #1 to stand-alone. Command 3 solves the two previous equations simultaneously (using Cramer's rule) for Y3, and Y4. Commands 4 substitute for first derivative w.r.t time of X, Y (d/dt (X), and d/dt (Y)) with y(3), and y(4) respectively. Commands 5 rewrite the outputs of the previous commands in the simplest form.

Note that P3, P4, PP3, and PP4 are dummy symbols, so once equations 6, and 7 are transformed to 8, and 9 past the right hand side of PP3, and PP4 in Matlab after replacing Y3, and Y4 with dy(3), and dy(4) respectively as shown in Appendix B.

Appendix B: This Matlab file (LBMS2.m) simulated the motion of the mechanism shown in figure 30.

```
function dy = LPMS2(t,y);

L1=2.35; L2=2; K1=50; K2=50; A=1.0; B=1.0; m1=0.72; m2=1.36; X_In_Disp =2.35;

Y_In_Disp =5.35;


% L1, and L2    % are the Initial lengths of two springs before elongation in inches.

% K1, and K2    % are the springs' stiffness in Ib/in.

% A, and B;     % are the damping coefficient in Ib-sec/in.

% m1, and m2    % are the weights of the two masses

% X_In_Disp, and % initial positions of m1 in X - generalized coordinate

% Y_In_Disp     % initial positions of m2 in Y - generalized coordinate


dy = zeros(4,1);

dy(1) = y(3);   % y(1), and y(3) are the displacement and velocity of the system in     %

X – coordinate.

dy(2) = y(4);   % y(2), and y(4) are the displacement and velocity of the system in     %

Y – coordinate.

dy(3) = -(-B*y(4)+B*y(3)+K1*y(1)-K1*L1-K2*y(2)+K2*y(1)+K2*L2)/m1;

dy(4) = (-B*y(4)-y(4)*A+B*y(3)-K2*y(2)+K2*y(1)+K2*L2)/m2;


% Solve the ODE system
```

To solve the previous ODE system, write the following three commands in the Matlab command window.

```
% L1=2.35; L2=2; K1=50; K2=50; A=1.0; B=1.0; m1=0.72; m2=1.36; X_In_Disp =2.35;
% Y_In_Disp =5.35;

% options = odeset('RelTol',1e-7,'AbsTol',1e-9);

% [T,Y]=ode45(@LPMS2,[0 5],[X_In_Disp Y_In_Disp 0 0],options);
%where,
% LPMS : is the function's name.
% [0 5]: is the time range we propose for investigation.
% [X_In_Disp Y_In_Disp 0 0]: are the initial conditions of the displacements
% and of the velocities of the masses m1, and m2 in X, and Y coordinates.

% To plot the output of matrix [T,Y] in Cartesian coordinates
%==========================================================
% figure(1);plot(T,Y(:,1),'-',T,Y(:,2),'.') % <---Time versus motion
                displacements  in X, and Y coordinates respectively.
% figure(2);plot(T,Y(:,3),'-',T,Y(:,4),'.') % <---Time versus the velocities of m1,
            and m2 in X, and Y coordinates respectively.

% To Manipulate Matlab outputs within Excel Software
```

```
% write the following two commands in the Matlab command window.
% K = [T(:,1) Y(:,1) Y(:,2) Y(:,3) Y(:,4)];
% save ('DD.txt' , 'K' , '-ascii')

% To manipulate Matlab outputs data within Excel, Sigmaplot, .....etc.
% one should convert the Matlab outputs (binary) format into (ascii) format.
% Furthermore, one should save the converted data in a text file.
% However, to do so please apply the following command.
% save ('filename.txt','variable # 1', --- ,'variable # n', '-ascii')
% Note: that the filename.txt should be found in the same folder of the current
% Matlab command window.

% Example:

% K = [T(:,1) Y(:,1) Y(:,2) Y(:,3) Y(:,4)];
% save ('DD.txt' , 'K' , '-ascii')

% Now if one take a look at the current folder, the file DD.txt should be
% found.  If you want to send DD.txt file to certain folder (assume E
% folder), then substitute 'DD.txt' with 'E:\DD.txt'
```

Appendix C: This Matlab file (LBMS2.m) simulated the motion of the mechanism shown in figure 31.

Note, to simulate the model shown in figure 31, just replace the previus two equations of dy(3) and dy(4) with the following two equations.

```
dy(3) = (B*y(4)+K2*y(2)-K1*y(1))/m1;

dy(4) = -
(y(4)*m1*B+y(4)*m2*B+y(4)*A*m1+A*y(3)*m1+m1*K2*y(2)+K2*y(2)*m2-
K1*y(1)*m2)/m2/m1;
```

Appindex D: This Matlab file (HalfTh2D.m) simulates the motion of the mechanism shown in figure 35.

```
function dy = HalfTh2D(t,y)

In_S = 0; In_X = 0; dS = 0; dX = 0; r = 30/100; m1 = 2.0; m2 = 2.0; I1=1/2*m1*r^2; I2 =
1/2*m2*r^2; m = m1; I = I1; M = 2.0;

% In_S, and In_X    are the Initial conditions of the generalized
%                   coordinates S, and X in degrees and meter
%                   respectively.

% dS, and dX        are the initial conditions of first
%                   derivatives in S, and X with respect to
%                   time.
% r = 30/100 m;     is the length of arm oA in (m), see figure 35.
% I1, and I2;       are the mass moment of inertia of Discs
%                   26, and 30 around the Z-axes.
% m1 = m2 = m = 2.0 kg;  are the mass of Discs 26, and 30 in (kg)
%                        respectively.
% M = 2 N.m;        is the motor torque in Newton meter.

dy = zeros(4,1);
```

```
dy(1) = y(3);       % y(1) = Angular displacement in S - coordinate

dy(2) = y(4);       % y(2) = Linear displacement in X - coordinate


% the following are the differential equations 10, and 11.


dy(3) = -m*r^2*sin(y(1))*cos(y(1))/(m*r^2*sin(y(1))^2-2*m*r^2-2*I)*y(3)^2 -
  1/2*M/(m*r^2*sin(y(1))^2-2*m*r^2-2*I);


dy(4)          =-1/2*r*(4*m*r^2*cos(y(1))+4*I*cos(y(1)))/(m*r^2*sin(y(1))^2-2*m*r^2-
  2*I)*y(3)^2-1/2*r*sin(y(1))*M/(m*r^2*sin(y(1))^2-2*m*r^2-2*I);


% Solve the ODE system.

==================

To solve the previous ODE system, use the following three commands in the

Matlab command window

% In_S = 0; In_X = 0; dS = 0; dX = 0; r = 30/100; m1 = 2.0; m2 = 2.0;

% I1=1/2*m1*r^2; I2 = 1/2*m2*r^2; m = m1; I = I1; M = 2.0;

%options = odeset('RelTol',1e-5,'AbsTol',1e-7,'MaxStep',0.002);

%[T,Y]=ode45(@HalfTh2D,[0 9],[0.0175*In_S In_X dS dX],options);


% where:

% HalfTh2D :      is the function name.

%[0 9]:          is the time range we propose for investigation.
```

```
%[0.0175*(In_S) In_X dS dX]:  are the initial conditions in the two
%                             generalized coordinates (S and, X)

% To plot the output of matrix [T,Y] in Cartesian coordinates
%=============================================
% figure(1);plot(T,Y(:,1)) % Plot the Time versus the
% displacement in S coordinate
% figure(3);plot(T,Y(:,3)) %Plot the Time versus the
% first derivative of displacement in S coordinate or
% SUBPLOT(1,2,1);plot(T,Y(:,1),'-',T,Y(:,2),'*'),
% SUBPLOT(1,2,2);plot(T,Y(:,3),'-',T,Y(:,4),'*')

% Example: To save ascii file then load it again
%==================================
% save ('DD.txt', 'K', '-ascii');
% this is the save command, which also transform
% the data file DD from binary to ascii

% load DD.txt     (the file's name must be written with txt
%                  extension (ascii format) otherwise the file
%                  won't be recognized

% To calculate the Motion of the c.m. of the Whole system
```

```
%==========================================

% A=0.6* cos(K(:,2));  To get the projection of the c.m. of Disc 26 on
%                      the generalized X-coordinate.
% X26=A + X30;         To calculate the absolute motion of the c.m. of
%                      gear 26 in X-coordinate. where, X30 = K(:,3),
%                      which is the motion Displacement of the c.m. of
%                      Disc 30.
% X_system = (X26 + X30) / 2   To calculate the motion of the c.m of the whole
%                              system.
```

Appendix E : Simulation of the motion of a Pendulum Disc with a Driven Hinge

Dis_B_F.m File

```
%This file simulates the equations of motion, which are produced by
%Maple file 'Two_Discs_Body_Fixed.mws'

function dy = Dis_B_F(t,y)

In_S=0; In_K=0; In_dS=0; In_dK=0; r= 30/100; m3=2.0; I3=1/2*m3*r^2;
m=m3; I=I3; M=-2.0;


% In_S = 0;  is the Initial condition of the angular displacement %
        of disc 26.
% In_K = 0;  is the Initial condition of the angular displacement
%            of the eccentric mass 33.
% In_dS = 0; is the Initial condition of the first derivative of
%            the angular displacement of disc 26 w.r.t.time.
% In_dK = 0; is the Initial condition of the first derivative of
%            the angular displacement of the eccentric mass 33
%            w.r.t. time.
% r = 30/100; is the radii of both disc 26 and the eccentric mass
%             33 in m.
% m = 2.0;   is the mass of the eccentric mass 33 in kg.
% I = mass of inertia of the eccentric mass 33 at an
%     axis passing through its c.m.
% M = -2;    is the motor torque in N.m.

dy = zeros(4,1);

dy(1) = y(3); % y(1) = Angular displacement in S - coordinate
dy(2) = y(4); % y(2) = Angular displacement in K - coordinate
dy(3) = -(-2*m^2*r^4*sin(y(2))*sin(y(1))^2*cos(y(2))-...
 m^2*r^4*cos(y(1))*sin(y(1))+2*m^2*r^4*sin(y(2))^2*sin(y(1))
 *cos(y(1))+...
 m^2*r^4*cos(y(2))*sin(y(2)))/(2*sin(y(2))^2*sin(y(1))^2*m*r^2+...
 2*sin(y(2))*sin(y(1))*m*r^2*cos(y(2))*cos(y(1))-m*r^2*sin(y(1))^2- ...
 m*r^2*sin(y(2))^2-I)/m/r^2*y(3)^2-
 (I*m*r^2*sin(y(2))*cos(y(1))+...
 m^2*r^4*cos(y(1))*sin(y(2))-m^2*r^4*cos(y(2))*sin(y(1))-...
 I*m*r^2*cos(y(2))*sin(y(1)))/(2*sin(y(2))^2*sin(y(1))^2*m*r^2+...
 2*sin(y(2))*sin(y(1))*m*r^2*cos(y(2))*cos(y(1))-m*r^2*sin(y(1))^2- ...
 m*r^2*sin(y(2))^2-I)/m/r^2*y(4)^2-...
 I*M+m*r^2*M)/(2*sin(y(2))^2*sin(y(1))^2*m*r^2+...
 2*sin(y(2))*sin(y(1))*m*r^2*cos(y(2))*cos(y(1))-...
 m*r^2*sin(y(1))^2-m*r^2*sin(y(2))^2-I)/m/r^2;

dy(4) = (m*r^2*sin(y(2))*cos(y(1))-...
 m*r^2*cos(y(2))*sin(y(1)))/(2*sin(y(2))^2*sin(y(1))^2*m*r^2+...
 2*sin(y(2))*sin(y(1))*m*r^2*cos(y(2))*cos(y(1))-m*r^2*sin(y(1))^2-...
 m*r^2*sin(y(2))^2I)*y(3)^2+(2*sin(y(2))*sin(y(1))^2*m*r^2*cos(y(2))-
 ... cos(y(1))*m*r^2*sin(y(1))+sin(y(2))*m*r^2*cos(y(2))+...
 2*sin(y(2))^2*sin(y(1))*m*r^2*cos(y(1)))/(2*sin(y(2))^2*siny(1))^2*m*r
 ^2+...
```

```
      2*sin(y(2))*sin(y(1))*m*r^2*cos(y(2))*cos(y(1))-
      m*r^2*sin(y(1))^2-...
     m*r^2*sin(y(2))^2-I)*y(4)^2+(sin(y(2))*sin(y(1))*M+...
     cos(y(2))*cos(y(1))*M)/(2*sin(y(2))^2*sin(y(1))^2*m*r^2+...
      2*sin(y(2))*sin(y(1))*m*r^2*cos(y(2))*cos(y(1))-
      m*r^2*sin(y(1))^2-... m*r^2*sin(y(2))^2-I);

%To solve the ODE system apply the following command
%================================================
%options = odeset('RelTol',1e-7,'AbsTol',1e-9);
%[T,Y]=ode45(@Dis_B_F,[0 10],[0.0175*In_S 0.0175*In_K In_dS
In_dK],options);

% Dis_B_F : is the function.
%[0 10]: is the time range we propose for investigation.
%[0.0175*In_S 0.0175*In_K In_dS In_dK]: are the initial conditions.


% To plot the output of matrix [T,Y] in Cartesian coordinates
%============================================================
% figure(1);plot(T,Y(:,1),'-',T,Y(:,2),'*') % <---Time versus
%    angular displacement in S and, K coordinates respectively.
% figure(2);plot(T,Y(:,3),'-',T,Y(:,4),'*') % <---Time versus
%    angular velocity in S and, K coordinates respectively.


% Example: To save ascii file then load it again
%===============================================

%   K = [T(:,1) Y(:,1) Y(:,2) Y(:,3) Y(:,4)]; Assumed variable
%   save ('DD.txt', 'K', '-ascii'); save order from binary to
%                                   ascii

%   load DD.txt     (file must be with txt extension otherwise
%                    the file won't be recognized)
```

Appendix F : Simulation of the motion of Thornson's Mechanism

%Bfix3D.m File

```
% This file has the equations of motion, which are produced in
% Maple software to simulate the motion of Thornson's device


function dy = BFix3D(t,y)

g=9.81; In_theta1=0;In_theta2=0;In_X=0;r= 30/100; m1=2.0; m2=2.0;
m3=2.0;I1=1/2*m1*r^2;I2=1/2*m2*r^2;I3=1/2*m2*r^2;m=m1;I=I1; M=-2.0;

% g= 9.81          (32.2 ft/sc^2);%the gravitational acceleration
%                   in(m/sec^2)
% In_theta1=0;    % Initial conditions of arm AB in
%                   theta1, generalized coordinate (gc.)
% In_theta2=0;    % Initial conditions of the position of Disc
%                   26 in theta2 - gc.
% m=2.0;           % masses in (Kg),
% M=2;             % Motor torque in (N.m.)

dy = zeros(6,1);

dy(1) = y(4); % y(1) = Angular position in Theta1 - gc.
dy(2) = y(5); % y(2) = Angular position in theta2 - gc.
dy(3) = y(6); % y(3) = Linear position in X - gc.

dy(4) = -1/4*(-
 56*sin(y(1))*sin(y(2))^2*m*r^2+72*sin(y(1))^2*sin(y(2))*...
  m*r^2*cos(y(1))*cos(y(2))- 20*cos(y(2))*m*r^2*cos(y(1))*sin(y(2))+...
  128*sin(y(1))^3*cos(y(1))*sin(y(2))^2*m*r^2-
 72*sin(y(1))*sin(y(2))^2*...
 m*r^2*cos(y(1))-
 128*sin(y(2))*cos(y(2))*m*r^2*sin(y(1))^4+16*m*r^2*...
 sin(y(1))+28*m*r^2*cos(y(1))*sin(y(1))-
 64*sin(y(1))^3*m*r^2*cos(y(1))+...
  136*sin(y(1))^2*sin(y(2))*m*r^2*cos(y(2))- 24*sin(y(1))^3*m*r^2-
 20*m*...
 r^2*sin(y(2))*cos(y(2))+72*sin(y(1))^3*sin(y(2))^2*m*r^2)/( 3*m*r^
 2+...
 4*m*r^2*cos(y(1))*sin(y(2))^2+12*m*r^2*sin(y(1))^3*sin(y(2) )*cos(
 y(2))-...
 10*m*r^2*cos(y(2))*sin(y(1))*sin(y(2))-
 18*m*r^2*sin(y(1))^2*sin(y(2))^2-...
 12*m*r^2*sin(y(1))^2*cos(y(1))*sin(y(2))^2+16*m*r^2*sin(y(1 ))^3*...
 cos(y(1))*sin(y(2))*cos(y(2))-
 10*m*r^2*cos(y(1))*cos(y(2))*sin(y(1))*...
 sin(y(2))- I*sin(y(2))^2+16*m*r^2*sin(y(1))^4*sin(y(2))^2+4*m*r^2*...
 sin(y(1))^2*cos(y(1))-
 8*m*r^2*sin(y(1))^4+3*I+3*m*r^2*sin(y(2))^2+...
```

```
7*m*r^2*sin(y(1))^2)*y(4)^2-1/4*(-
4*m*r^2*sin(y(2))+8*m*r^2*sin(y(1))^2*...
sin(y(2))+2*m*r^2*sin(y(1))*cos(y(2))+8*m*r^2*cos(y(1))*cos(y(2))*...
sin(y(1))- 4*m*r^2*cos(y(1))*sin(y(2)))/(3*m*r^2+4*m*r^2*cos(y(1))*...
sin(y(2))^2+12*m*r^2*sin(y(1))^3*sin(y(2))*cos(y(2))-
10*m*r^2*cos(y(2))*...
sin(y(1))*sin(y(2))-18*m*r^2*sin(y(1))^2*sin(y(2))^2- 12*m*r^2*...
sin(y(1))^2*cos(y(1))*sin(y(2))^2+16*m*r^2*sin(y(1))^3*cos(y(1))*...
sin(y(2))*cos(y(2))-10*m*r^2*cos(y(1))*cos(y(2))*sin(y(1))*sin(y(2))-
...
I*sin(y(2))^2+16*m*r^2*sin(y(1))^4*sin(y(2))^2+4*m*r^2*sin(y(1))^2*...
cos(y(1))- 8*m*r^2*sin(y(1))^4+3*I+3*m*r^2*sin(y(2))^2+7*m*r^2*...
sin(y(1))^2)*y(5)^2-1/4*(M*sin(y(2))^2-
3*M)/(3*m*r^2+4*m*r^2*cos(y(1))*...
sin(y(2))^2+12*m*r^2*sin(y(1))^3*sin(y(2))*cos(y(2))-
10*m*r^2*cos(y(2))*...
sin(y(1))*sin(y(2))-18*m*r^2*sin(y(1))^2*sin(y(2))^2- 12*m*r^2*...
sin(y(1))^2*cos(y(1))*sin(y(2))^2+16*m*r^2*sin(y(1))^3*cos(y(1))*...
sin(y(2))*cos(y(2))-10*m*r^2*cos(y(1))*cos(y(2))*sin(y(1))*sin(y(2))-
...
I*sin(y(2))^2+16*m*r^2*sin(y(1))^4*sin(y(2))^2+4*m*r^2*sin(y(1))^2*...
cos(y(1))-
8*m*r^2*sin(y(1))^4+3*I+3*m*r^2*sin(y(2))^2+7*m*r^2*sin(y(1))^2);



dy(5) = -1/2*(44*m*r^2*cos(y(1))*sin(y(2))-48*I*cos(y(1))*cos(y(2))*...
sin(y(1))+56*cos(y(2))*m*r^2*sin(y(1))^3-
92*m*r^2*cos(y(1))*cos(y(2))*...
sin(y(1))+16*cos(y(2))*m*r^2*sin(y(1))^3*cos(y(1))-
48*m*r^2*cos(y(1))*...
sin(y(2))*sin(y(1))^2+4*I*cos(y(1))*sin(y(2))-
16*cos(y(2))*sin(y(1))^5*...
m*r^2-56*m*r^2*sin(y(1))*cos(y(2))+16*sin(y(1))^4*sin(y(2))*m*r^2*...
cos(y(1))+16*I*sin(y(2))-
32*I*sin(y(2))*sin(y(1))^2+56*m*r^2*sin(y(2))-...
12*I*sin(y(1))*cos(y(2))+16*m*r^2*sin(y(1))^4*sin(y(2))-100*m*r^2*...
sin(y(1))^2*sin(y(2)))/(3*m*r^2+4*m*r^2*cos(y(1))*sin(y(2))^2+12*m*r^2
*...
sin(y(1))^3*sin(y(2))*cos(y(2))-
10*m*r^2*cos(y(2))*sin(y(1))*sin(y(2))-...
18*m*r^2*sin(y(1))^2*sin(y(2))^2-12*m*r^2*sin(y(1))^2*cos(y(1))*...
sin(y(2))^2+16*m*r^2*sin(y(1))^3*cos(y(1))*sin(y(2))*cos(y(2))-
10*m*...
r^2*cos(y(1))*cos(y(2))*sin(y(1))*sin(y(2))-I*sin(y(2))^2+16*m*r^2*...
sin(y(1))^4*sin(y(2))^2+4*m*r^2*sin(y(1))^2*cos(y(1))-8*m*r^2*...
sin(y(1))^4+3*I+3*m*r^2*sin(y(2))^2+7*m*r^2*sin(y(1))^2)*y(4)^2-...
1/2*(-10*m*r^2*cos(y(1))*sin(y(1))-32*sin(y(1))^3*cos(y(1))*...
sin(y(2))^2*m*r^2+32*sin(y(2))*cos(y(2))*m*r^2*sin(y(1))^4+6*m*...
r^2*sin(y(2))*cos(y(2))+20*sin(y(1))*sin(y(2))^2*m*r^2*cos(y(1))+...
20*sin(y(1))*sin(y(2))^2*m*r^2+16*sin(y(1))^3*m*r^2*cos(y(1))-...
2*I*sin(y(2))*cos(y(2))-10*m*r^2*sin(y(1))-
36*sin(y(1))^2*sin(y(2))*...
m*r^2*cos(y(2))-24*sin(y(1))^3*sin(y(2))^2*m*r^2+8*cos(y(2))*m*r^2*...
cos(y(1))*sin(y(2))+12*sin(y(1))^3*m*r^2-
24*sin(y(1))^2*sin(y(2))*m*...
```

```
r^2*cos(y(1))*cos(y(2)))/(3*m*r^2+4*m*r^2*cos(y(1))*sin(y(2))^2+12*m*.
..
r^2*sin(y(1))^3*sin(y(2))*cos(y(2))-10*m*r^2*cos(y(2))*sin(y(1))*...
sin(y(2))-18*m*r^2*sin(y(1))^2*sin(y(2))^2-12*m*r^2*sin(y(1))^2*...
cos(y(1))*sin(y(2))^2+16*m*r^2*sin(y(1))^3*cos(y(1))*sin(y(2))*...
cos(y(2))-10*m*r^2*cos(y(1))*cos(y(2))*sin(y(1))*sin(y(2))-I*...
sin(y(2))^2+16*m*r^2*sin(y(1))^4*sin(y(2))^2+4*m*r^2*sin(y(1))^2*...
cos(y(1))-8*m*r^2*sin(y(1))^4+3*I+3*m*r^2*sin(y(2))^2+7*m*r^2*...
sin(y(1))^2)*y(5)^2-
1/2*(sin(y(1))*sin(y(2))*M+3*cos(y(1))*cos(y(2))*...
M-6*cos(y(2))*sin(y(1))^2*M+4*sin(y(1))*cos(y(1))*sin(y(2))*M+3*...
cos(y(2))*M)/(3*m*r^2+4*m*r^2*cos(y(1))*sin(y(2))^2+12*m*r^2*sin(y(1))
^3*...
sin(y(2))*cos(y(2))-10*m*r^2*cos(y(2))*sin(y(1))*sin(y(2))-
18*m*r^2*...
sin(y(1))^2*sin(y(2))^2-
12*m*r^2*sin(y(1))^2*cos(y(1))*sin(y(2))^2+16*...
m*r^2*sin(y(1))^3*cos(y(1))*sin(y(2))*cos(y(2))-10*m*r^2*cos(y(1))*...
cos(y(2))*sin(y(1))*sin(y(2))-I*sin(y(2))^2+16*m*r^2*sin(y(1))^4*...
sin(y(2))^2+4*m*r^2*sin(y(1))^2*cos(y(1))-
8*m*r^2*sin(y(1))^4+3*I+3*...
m*r^2*sin(y(2))^2+7*m*r^2*sin(y(1))^2);


dy(6) = 1/6*r*(-24*m*r^2+112*m*r^2*sin(y(1))^4- 80*m*r^2*sin(y(2))^2-
88*m*...
r^2*sin(y(1))^2-
52*m*r^2*cos(y(1))*sin(y(2))^2+356*m*r^2*sin(y(1))^2*...
sin(y(2))^2-288*m*r^2*sin(y(1))^4*sin(y(2))^2-64*m*r^2*sin(y(1))^2*...
cos(y(1))+48*m*r^2*cos(y(1))^2+24*m*r^2*cos(y(1))-12*I*cos(y(1))*...
sin(y(2))^2+32*I*sin(y(2))^2*sin(y(1))^2-16*I*cos(y(1))^2*sin(y(2))^2-
...
464*m*r^2*sin(y(1))^3*cos(y(1))*sin(y(2))*cos(y(2))+172*m*r^2*cos(y(1)
)*...
cos(y(2))*sin(y(1))*sin(y(2))+256*m*r^2*sin(y(1))^2*cos(y(1))*...
sin(y(2))^2-424*m*r^2*sin(y(1))^3*sin(y(2))*cos(y(2))+176*m*r^2*...
cos(y(2))*sin(y(1))*sin(y(2))+176*sin(y(1))^3*cos(y(1))^2*m*r^2*...
cos(y(2))*sin(y(2))+256*sin(y(1))^5*cos(y(1))*m*r^2*cos(y(2))*sin
  (y(2))-...
8*I*sin(y(2))^2+12*I*sin(y(2))*sin(y(1))*cos(y(2))+80*cos(y(1))^2*m*..
.
r^2*sin(y(2))^2+64*cos(y(1))^3*m*r^2*sin(y(1))^2+48*I*cos(y(1))^2+24*I
*...
cos(y(1))+48*I*sin(y(2))*cos(y(1))*cos(y(2))*sin(y(1))-
288*sin(y(1))^4*...
sin(y(2))^2*m*r^2*cos(y(1))-192*cos(y(1))^3*m*r^2*sin(y(1))^2*...
sin(y(2))^2+256*cos(y(1))^3*m*r^2*sin(y(1))^3*sin(y(2))*cos(y(2))- ...
160*cos(y(1))^3*m*r^2*cos(y(2))*sin(y(1))*sin(y(2))+112*m*r^2*...
 sin(y(1))^4*cos(y(1))+88*m*r^2*sin(y(1))^2*cos(y(1))^2+64*
cos(y(1))^3*...
m*r^2*sin(y(2))^2+272*sin(y(2))*cos(y(2))*sin(y(1))^5*m*r^2-24*I-
  240*...
sin(y(1))^2*cos(y(1))^2*m*r^2*sin(y(2))^2-
200*sin(y(1))*cos(y(1))^2*m*...
r^2*cos(y(2))*sin(y(2)))/(3*m*r^2+4*m*r^2*cos(y(1))*sin(y(2))^2+12*m*.
..
r^2*sin(y(1))^3*sin(y(2))*cos(y(2))-10*m*r^2*cos(y(2))*sin(y(1))*...
```

```
sin(y(2))-18*m*r^2*sin(y(1))^2*sin(y(2))^2-12*m*r^2*sin(y(1))^2*...
cos(y(1))*sin(y(2))^2+16*m*r^2*sin(y(1))^3*cos(y(1))*sin(y(2))*...
cos(y(2))-10*m*r^2*cos(y(1))*cos(y(2))*sin(y(1))*sin(y(2))-I*...
sin(y(2))^2+16*m*r^2*sin(y(1))^4*sin(y(2))^2+4*m*r^2*sin(y(1))^2*...
cos(y(1))-8*m*r^2*sin(y(1))^4+3*I+3*m*r^2*sin(y(2))^2+7*m*r^2*...
sin(y(1))^2)*y(4)^2+1/6*r*(24*cos(y(2))^2*m*r^2*sin(y(1))^3*sin(y(2))-
...
20*cos(y(2))^2*m*r^2*sin(y(1))*sin(y(2))+32*cos(y(2))^2*m*r^2*...
sin(y(1))^3*cos(y(1))*sin(y(2))-20*cos(y(2))^2*m*r^2*cos(y(1))*...
sin(y(1))*sin(y(2))-16*cos(y(2))*m*r^2*sin(y(1))^4-16*sin(y(1))^2*...
cos(y(1))^2*m*r^2*cos(y(2))+8*sin(y(1))*cos(y(1))^2*m*r^2*sin(y(2))-
...
12*m*r^2*cos(y(1))*cos(y(2))*sin(y(1))^2+10*m*r^2*sin(y(1))^2*...
cos(y(2))+6*I*cos(y(2))-20*sin(y(1))*sin(y(2))^3*m*r^2*cos(y(1))-...
20*sin(y(1))*sin(y(2))^3*m*r^2+24*sin(y(1))^3*sin(y(2))^3*m*r^2+26*...
m*r^2*sin(y(1))*cos(y(1))*sin(y(2))-28*sin(y(2))*sin(y(1))^3*m*r^2+...
18*m*r^2*sin(y(1))*sin(y(2))+32*sin(y(1))^3*cos(y(1))*sin(y(2))^3*m*..
.
r^2+6*m*r^2*cos(y(2))-
32*sin(y(2))*sin(y(1))^3*m*r^2*cos(y(1)))/(3*m*...
r^2+4*m*r^2*cos(y(1))*sin(y(2))^2+12*m*r^2*sin(y(1))^3*sin(y(2))*...
cos(y(2))-10*m*r^2*cos(y(2))*sin(y(1))*sin(y(2))-
18*m*r^2*sin(y(1))^2*...
sin(y(2))^2-12*m*r^2*sin(y(1))^2*cos(y(1))*sin(y(2))^2+16*m*r^2*...
sin(y(1))^3*cos(y(1))*sin(y(2))*cos(y(2))-
10*m*r^2*cos(y(1))*cos(y(2))*...
sin(y(1))*sin(y(2))-
I*sin(y(2))^2+16*m*r^2*sin(y(1))^4*sin(y(2))^2+4*...
m*r^2*sin(y(1))^2*cos(y(1))-
8*m*r^2*sin(y(1))^4+3*I+3*m*r^2*sin(y(2))^2+...
7*m*r^2*sin(y(1))^2)*y(5)^2+1/6*r*(-3*sin(y(1))*sin(y(2))^2*M-3*...
sin(y(2))*cos(y(2))*M+6*sin(y(1))*cos(y(1))*M+6*sin(y(1))*M-
6*sin(y(1))*...
cos(y(1))*sin(y(2))^2*M-
3*sin(y(2))*cos(y(1))*cos(y(2))*M+6*sin(y(2))*...
cos(y(2))*sin(y(1))^2*M)/(3*m*r^2+4*m*r^2*cos(y(1))*sin(y(2))^2+12*...
m*r^2*sin(y(1))^3*sin(y(2))*cos(y(2))-10*m*r^2*cos(y(2))*sin(y(1))*...
sin(y(2))-18*m*r^2*sin(y(1))^2*sin(y(2))^2-12*m*r^2*sin(y(1))^2*...
cos(y(1))*sin(y(2))^2+16*m*r^2*sin(y(1))^3*cos(y(1))*sin(y(2))*...
cos(y(2))-10*m*r^2*cos(y(1))*cos(y(2))*sin(y(1))*sin(y(2))-I*...
sin(y(2))^2+16*m*r^2*sin(y(1))^4*sin(y(2))^2+4*m*r^2*sin(y(1))^2*...
cos(y(1))-
8*m*r^2*sin(y(1))^4+3*I+3*m*r^2*sin(y(2))^2+7*m*r^2*sin(y(1))^2);

%To solve the ODE system for Initial Conditions (IC) apply the
following command
%=====================================================================
% IC of Set A:
%g=9.81; In_alpha=0;In_theta=0;In_phi=0;In_X=0;r= 30/100; m1=2.0;
m2=2.0;
%m3=2.0;I1=1/2*m1*r^2;I2=1/2*m2*r^2;I3=1/2*m2*r^2;m=m1;I=I1; M=-2.0;
%options = odeset('RelTol',1e-7,'AbsTol',1e-9);
%[T,Y]=ode45(@BFix3D,[0 10],[0.0175*In_theta1 0.0175*In_theta2 In_X 0 0
0 ],options);

% IC of Set B;:
```

```
%g=9.81; In_alpha=0;In_theta=0;In_phi=-90;In_X=0;r= 30/100; m1=2.0;
m2=2.0;
%m3=2.0;I1=1/2*m1*r^2;I2=1/2*m2*r^2;I3=1/2*m2*r^2;m=m1;I=I1; M=-2.0;
%options = odeset('RelTol',1e-7,'AbsTol',1e-9);
%[T,Y]=ode45(@BFix3D,[0 10],[0.0175*In_theta1 0.0175*In_theta2 In_X -
8.5 0 0 ],options);

% BFix3D : is an arbitrary function's name.
%[0 10]: is the time range we propose for investigation.

%Initial Conditions:
%====================
%[0.0175*In_theta1 0.0175*In_theta2 In_X 0 0 0 ]: are the initial
conditions
% of the three coordinates and its time derivatives (theta1, theta2,
and, X)


% To plot the output of matrix [T,Y] in Cartesian coordinates
%============================================================
% figure(1);plot(T,Y(:,1),'-',T,Y(:,2),'*') % <---Time versus y and,
theta displacements respectively.
% figure(2);plot(T,Y(:,3),'-',T,Y(:,4),'*') <---Time vs. speed in y,
and theta coordinates.
% SUBPLOT(1,2,1);plot(T,Y(:,1),'-
',T,Y(:,2),'*'),SUBPLOT(1,2,2);plot(T,Y(:,3),'-',T,Y(:,4),'*')


% Example: To save ascii file then load it again
%===============================================

%   K = [T(:,1) Y(:,1) Y(:,2) Y(:,3) Y(:,4) Y(:,5) Y(:,6)];
%   Assumed variables are :
%   Time, theta, Phi, X, d/dt(theta), d/dt(Phi), d/dt(X)

%   save ('DD.txt', 'K', '-ascii'); save order from binary to
                                ascii

%   load DD.txt  (file must be with txt extension 'ascii format'
           otherwise the file won't be recognized)


% Find Thornson's CG on the X - coordinate
%=========================================================

% H = (Y(:,3)+(Y(:,3)+0.6*cos(Y(:,1)))+Y(:,3)+0.6*cos(Y(:,1))+
%     0.3*cos(2*Y(:,1))+0.3*cos(Y(:,2)))/3;
```

BIBLIOGRAPHY

Almesallmy, M. "*Experimental and Analytical Investigation of Inertial Propulsion Mechanisms and Motion Simulation of Rigid-Multi-Body Mechanical Systems.*" Ph.D. diss., University of Rhode Island, 2006.

Almesallmy, M., and Datseris, P. "Simulation of Modeled Mechanical Systems Based on Lagrangian Mechanics." sent to *ASME, Journal of Mechanical Design*, 2006.

Anderson, K. S. "Order n Formulation for Motion Simulation of General Multi – Rigid – Body Constrained System." *Computer and Structure*, v. 43, n 3, p 565 – 579, May 3, 1992.

Anderson, K. S. "Order n Formulation for Motion Simulation of General Multi – Rigid – Body Free System." *Computer and Structure*, v. 46, n 3, p 547 – 559, Feb 3, 1993.

Asada, Haruhiko, J. J. E., Slotine. *Robot analysis and control.* John Wiley and Sons, New York, 1986.

Badreddin, Essameddin, Gambler, Adrian. "Dynamic Modeling of MSF plants for Automatic Control and Simulation Purposes." *Desalination*, v 166, n 1-3, Aug. 15, 2004.

Bai, Jie and Tsuta, Toshio. "Large Motion Response Analysis of Multi – Body Dynamics by Using Updated Lagrangian Method." ASME, *Pressure Vessels and Piping Division* (publication) PVP, v. 301, p. 101 – 106, 1995.

Banerjee, A. K. "Multi – Flexible Body Dynamics Capturing Motion – Induced Stiffness." *Journal of Applied Mechanics*, Transactions ASME, v 58, n 3, p. 766 – 775, Sep. 1991.

Bristow Jr. "Method and Apparatus for Converting Motion to Lineal Motion." *U.S. Patent # 5,156,058,* Issued Oct. 20, 1992.
http://patft.uspto.gov/netahtm/PTO/srchum.htm (accessed March 1, 2002).

Chrbonneau, G., Vinarnick, S., Neel, P., Eariste, C., and Vibet, C. "Symbolic Modeling of Controlled Mechanics." Computer Methods in Applied Mechanics and Engineering. Engrg. 98, pp. 23 – 40, 1992.

C/O Convex Group, Inc. "Physical Science." One Capital City Plaza, 3350 Peachtree Road, Suite 1500, Atlanta, GA 30326.
http://science.howstuffworks.com/gyroscope1.htm (accessed 2 February 2002).

Cook, R.L. "Device for Conversion of Centrifugal Force to Linear Force and Motion." *U.S. Patent # 4,238,968,* Issued Dec. 16, 1980.
http://patft.uspto.gov/netahtm/PTO/srchum.htm (accessed March 2, 2002).

Cuff, C. Device for Converting Rotary Motion into a Unidirectional Linear Motion, *U.S. Patent # 3,968,700*, Issued July 13, 1976. http://patft.uspto.gov/netahtm/PTO/srchum.htm (accessed March 2, 2002).

Datseris, Philip. "*Advanced Dynamic Class Notes*." *University of Rhode Island*, RI, 2003.

Dean, N.L. "System for Converting Rotary Motion into Unidirectional Motion." U.S. *Patent # 2,886,976*, Issued May 19, 1959. http://patft.uspto.gov/netahtm/PTO/srchum.htm (accessed March 4, 2002).

European Space Agency. "The Electro-Dynamic Multi-Shaker." www.estec.esa.nl. (accessed 19 November 2002).

Farrall, A.W. "Inertial Propulsion Device." *U.S. Patent # 3,266,233*, Issued Aug. 15, 1966. http://patft.uspto.gov/netahtm/PTO/srchum.htm (accessed March 4, 2002).

Featherstone, R. "The Calculation of Robot Dynamics Using Articulated-Body Inertias" *The International Journal of Robotics Research*, Vol. 2, No. 1, pp. 13 – 30, Spring 1983.

Foster, R.E. "Converting Rotary Motion Into Unidirectional Motion." *U.S. Patent # 3,653,269,* Issued May 15, 1970. http://patft.uspto.gov/netahtm/PTO/srchum.htm (accessed March 5, 2002).

Fu, K. S., Gonzalez, R. C., Lee, S. G. *Robotics: Control, Sensing, Vision, and Intelligence*. McGraw-Hill, 1987.

Geyer, H.M. "Vibration Driven Actuator." *U.S. Patent # 2,700,542*, Issued Jan. 25, 1955. http://patft.uspto.gov/netahtm/PTO/srchum.htm (accessed March 5, 2002).

Goldschmidt, R. "Propulsion of Vehicles." *U.S. Patent # 1,512,960*, Issued Oct. 14, 1924. http://patft.uspto.gov/netahtm/PTO/srchum.htm (accessed March 6, 2002).

Greenwood, D., T. *Principals of Dynamics*. 2nd ed., Prentice-Hall, Englewood Cliffs, NJ, 1988.

Halverson, E.M., et al. "Vibration Drive Vehicle." *U.S. Patent # 3,530,617*, Issued Sept. 29, 1970. http://patft.uspto.gov/netahtm/PTO/srchum.htm (accessed March 7, 2002).

Haug, Edward. "Computer Aided Analysis and Optimization of Mechanical System Dynamics." *Computer and Systems Sciences*, v 9, 700 p, 1984.

Holwerda, M. "Unidentified Flying Object with Unusual Propulsive Techniques: Generation of Antigravity by the Absorption of Gravitational Vortices." *Journal of new energy*, v 6, n 1, Summer, 2001, p 169-178.

Kagiwada, T. "Propulsion Mechanism Based on Inertial Force." *Proceedings of the IASTED International Conference on Robotics and Applications*, 2003, p 148-153.

Kammash, T., and Galbraith, D.L. "Novel Fusion Approach to Space power and propulsion." *Proceeding of the 24th Intersociety Energy Conversion Engineering Conference*, v 5, 1989, p 2531-2534.

Kellogg Jr., H.D. "Gyroscopic Inertial Space Drive." *U.S. Patent # 3,203,644*, Issued Aug. 31, 1965. http://patft.uspto.gov/netahtm/PTO/srchum.htm (accessed March 8, 2002).

Lilly, K., and Orin, D. "Alternate Formula for Manipulator inertial Matrix." *International Journal of Robotic Research.* 10(1), pp. 64 – 74, 1991.

Langman, H. "Vehicle and Steering Apparatus." *U.S. Patent # 3,006,581*, Issued Oct. 31 1961. http://patft.uspto.gov/netahtm/PTO/srchum.htm (accessed March 5, 2002).

Laskowitz, I.B. "Centrifugal Variable Thrust Mechanism." *U.S. Patent # 1,953,964*, Issued April 10, 1934. http://patft.uspto.gov/netahtm/PTO/srchum.htm (accessed March 7, 2002).

Laskowitz, I.B. "Centrifugal Variable Thrust Mechanism." *U.S. Patent # 2,009,780*, Issued July 30, 1935. http://patft.uspto.gov/netahtm/PTO/srchum.htm (accessed March 5, 2002).

Matyas, L.B. "Propulsion Apparatus." *U.S. Patent # 3,584,515*, Issued June 15, 1971. http://patft.uspto.gov/netahtm/PTO/srchum.htm (accessed March 7, 2002).

Multimedia Physics Studio. "The Truck and Ladder." http://www.glenbrook.k12.il.us/gbssci/phys/mmedia/newtlaws/il.html (accessed 1 June 2005).

Robert L. Norton. *Design of Machinery*. 2nd ed, McGraw-Hill, ISBN: 0-07-048395-7, PP. 620 – 633, 1999.

Robert L. Norton. Machine *Design*. 2nd ed. Prentice Hall, ISBN: 0-13-017706-7, PP. 328, 2000.

Novak, L.J. "Centrifugal Mechanical Device." *U.S. Patent # 3,810,394*, Issued May 15, 1974. http://patft.uspto.gov/netahtm/PTO/srchum.htm (accessed March 8, 2002).

Nowlin, A.C. "Device for Obtaining Directional Force from Rotary Motion." *U.S Patent # 2,350,248*, Issued Nov. 30, 1942. http://patft.uspto.gov/netahtm/PTO/srchum.htm (accessed March 8, 2002).

Paul, Richard P. "Robot Manipulators, Mathematics, Programming, and Control." *The MIT Press*, 1981.

Richard, M., and Gosselin, C. "A survey of Simulation programs for the Analysis of Mechanical Systems." *Mathematical Computational Simulation*. 35, pp 103 – 121, 1993.

Sacks, E and Jaskowiez, leo. "Model – Based Kinematic simulation." *ASME, Dynamic Systems and Control Division*, v. 41, p. 83 – 91, 1992.

Saeed, B.N. *Introduction to Robotics Analysis, Systems, Applications*. Prentice-Hall, Upper Saddle River, NJ, 2001.

Sciavicco, Lorenzo, B. *Siciliano, Modeling and Control of Robot Manipulators*. McGraw-Hill, New York, 1996.

Shahinpoor, Mohsen. *A Robot Engineering Textbook*. Harpor and Raw, New York, 1987.

Shahinpoor, M. *Dynamics*. International Encyclopedia of Robotics: Applications and Automation, Richard C. Dorf, Editor, Johan Wiley and Sons, New York, pp. 329 – 347, 1988.

Stock Drive Product / Sterling Instrument. "eStore." 2101 Jericho Tpke, Box 5416, New Hyde Park, NY, 11042-5416. http://www.sdp-si.com. (accessed 2 February 2002).

Tenenbaum, M., and Pollard, H. *Ordinary Differential Equations*. ISBN 0 – 486 – 64940 –7, Dover edition 1985.

Thornson, B.R. "Apparatus for Developing a Propulsion Force." *U.S. Patent # 4,631,971*, Issued Dec. 30, 1986. http://patft.uspto.gov/netahtm/PTO/srchum.htm (accessed March 8, 2002).

Valone, Thomas. "Inertial Propulsion: concept and experiment, part 1." *proceedings of the intersociety Energy Conversion Engineering conference*, Aug. 1993, v2, p 303-308.

Valone Thomas. "Inertial Propulsion: concept and experiment, part 2." *proceedings of the intersociety Energy Conversion Engineering conference,* v3, p 1484-1489, Aug. 1994.

Vibet, C. *Dynamics Modeling of Lagrangian Mechanisms from Inertial Matrix Elements*. Elsevier Science, Computer Methods in Applied Mechanics and Engineering. 123, pp. 317 – 326, 1995.

Victor, Wowk, "Machinery Vibration: Balancing." PP. 125 – 147, 1995.
Walls, A. D. *Theory and Problems of Lagrangian Dynamics*. McGraw-Hill, New york, 1967.

Wang, R., and Woo, P. "Using Maple for Symbolic Computations on Robotics." *International Journal of Robotics and Automation*. 7(2), pp. 41 – 49, 1992.

Wells, D. A. *Theory and Problems of Lagrangian Dynamics*. Schaum's Outline Series, ISBN 07 – 069258 – 0. McGraw-Hill Publishing Comp. Oct. 1967.

Wilson, J.B., "Dynamic Balancing og Rotating Machinery." PP. 144 – 180, 1967.

Young Jr., and et al. "Directional Force Generator." *U.S. Patent # 3,555,915*, Issued Jan. 19, 1971. http://patft.uspto.gov/netahtm/PTO/srchum.htm (accessed March 8, 2002).

Zhe Li, and Sridhar Kota. "Virtual Prototyping and Motion Simulation with ADAMS." *Journal of Computing and Information Science in Engineering*, Vol. 1, No. 3, pp. 276 – 279, September 2001.